NOTICE

The quality of this microform is heavily dependent upon the quality of the original thesis submitted for microfilming. Every effort has been made to ensure the highest quality of reproduction possible.

If pages are missing, contact the university which granted the degree.

Some pages may have indistinct print especially if the original pages were typed with a poor typewriter ribbon or if the university sent us an inferior photocopy.

Previously copyrighted materials (journal articles, published tests, etc.) are not filmed.

Reproduction in full or in part of this microform is governed by the Canadian Copyright Act, R.S.C. 1970, c. C-30.

AVIS

La qualité de cette microforme dépend grandement de la qualité de la thèse soumise au microfilmage. Nous avons tout fait pour assurer une qualité supérieure de reproduction.

S'il manque des pages, veuillez communiquer avec l'université qui a conféré le grade.

La qualité d'impression de certaines pages peut laisser à désirer, surtout si les pages originales ont été dactylographiées à l'aide d'un ruban usé ou si l'université nous a fait parvenir une photocopie de qualité inférieure.

Les documents qui font déjà l'objet d'un droit d'auteur (articles de revue, tests publiés, etc.) ne sont pas microfilmés.

La reproduction, même partielle, de cette microforme est soumise à la Loi canadienne sur le droit d'auteur, SRC 1970, c. C-30.

Canada

THE UNIVERSITY OF ALBERTA

MICROWAVE DIELECTRIC MEASUREMENTS

AND LAYER HEATING

BY

ROOP CHANDRA JAIN

A THESIS

SUBMITTED TO THE FACULTY OF GRADUATE STUDIES AND RESEARCH

IN PARTIAL FULFILMENT OF THE REQUIREMENTS FOR THE DEGREE

OF DOCTOR OF PHILOSOPHY

DEPARTMENT OF ELECTRICAL ENGINEERING

EDMONTON, ALBERTA

FALL 1988

Permission has been granted to the National Library of Canada to microfilm this thesis and to lend or sell copies of the film.

The author (copyright owner) has reserved other publication rights, and neither the thesis nor extensive extracts from it may be printed or otherwise reproduced without his/her written permission.

L'autorisation a été accordée à la Bibliothèque nationale du Canada de microfilmer cette thèse et de prêter ou de vendre des exemplaires du film.

L'auteur (titulaire du droit d'auteur) se réserve les autres droits de publication; ni la thèse ni de longs extraits de celle-ci ne doivent être imprimés ou autrement reproduits sans son autorisation écrite.

THE UNIVERSITY OF ALBERTA

RELEASE FORM

NAME OF AUTHOR: Roop Chandra Jain

TITLE OF THESIS: Microwave Dielectric Measurements and

Layer Heating

DEGREE: Ph.D.

YEAR THIS DEGREE GRANTED: 1988

Permission is hereby granted to THE UNIVERSITY OF ALBERTA LIBRARY to reproduce single copies of this thesis and to lend or sell such copies for private, scholarly or scientific research purposes only.

The author reserves other publication rights, and neither the thesis nor extensive extracts from it may be printed or otherwise reproduced without the author's written permission.

....
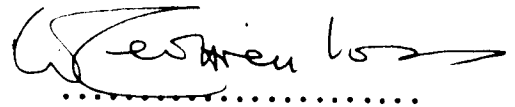(Student's signature)

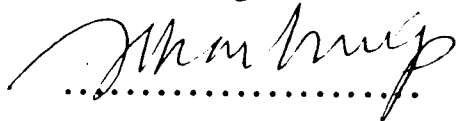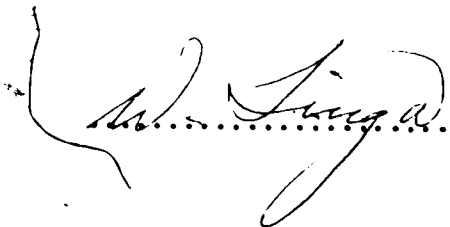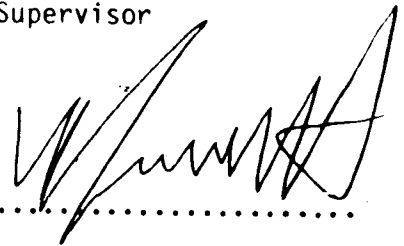Jain Street, Chauk Bazaar

Mathura, U.P.,

India

Date: 20 September 1988

THE UNIVERSITY OF ALBERTA

FACULTY OF GRADUATE STUDIES AND RESEARCH

The undersigned certify that they have read, and recommend to the Faculty of Graduate Studies and Research for acceptance, a thesis entitled **Microwave Dielectric Measurements and Layer Heating,** submitted by Roop Jain, in partial fulfillment of the requirements for the degree of Doctor of Philosophy in Electrical Engineering.

....
Supervisor

....

....

....

....
External Examiner

Date:........September 29 1988........

To my father and

the memory of my mother.

Abstract

Dielectric properties of a special category of high loss materials
- susceptors - and their microwave heating are discussed. To analyse
the data for the 2.45+0.050 GHz ISM band, a cavity perturbation method
employing a TM_{012} right circular cylindrical cavity is described.
Using the above technique, the dielectric data are obtained, 23-140°C,
on the white and yolk of chicken egg, some chloride pastes and sugar-
alcohol mixtures. The accuracy and precision of this cavity
perturbation method are estimated on the basis of the accuracy of the
dielectric constants of the calibrating liquids and the experimental
errors. The perturbation equation is also derived - for the TM_{012} mode
in an ideal circular cylindrical cavity of identical dimensions and
it is found that this equation does not hold for the actual cavity.
The dielectric data obtained from time domain measurements on some
medium and high loss liquids, which are used as calibrating liquids,
for · example ethyl acetate., methanol and pure water, are also given.
Various sources of errors in the time domain transmission methods are
analysed and discussed.

A model for the estimation of the absorption, in a microwave oven,
by a thin laminar load, is given; and the absorptions in a microwave
transparent conducting film and thin water loads are computed. The
complex dielectric constant of pure water is expressed by a
polynomial, in the frequency range 0.9 - 6GHz, from 0-60°C. Browning
tests done on foods in a microwave oven with some commercially
available edible browning agents and sugar-alcohol mixtures are
described.

Table of Contents

List of Tables

List of Figures

xiii

List of Symbols and Abbreviations

Where the same symbol denotes different quantities, the chapter to which it pertains has been indicated in brackets.

A, A_1 — power absorption per unit volume, absorption in the first layer

a — radius (inner) of the sample holder

$a_1', a_2' \cdots, a_8'$ — regression coefficients

$a_1'', a_2'' \cdots$

B, B_1 — magnetic flux density, total magnetic flux density in the cavity

b — radius (inner) of the cavity

c — phase velocity of light in vacuum

D — electric displacement density;

$d; d_1, d_2$ — dielectric layer thickness; thickness of layer 1, layer 2

E, E_1 — electric field intensity, total electric field intensity in the cavity

E_r, E_θ, E_z — electric field components in cylindrical coordinates

e — base of natural logarithm, 2.71828

FFT — Fast Fourier Transform

f — frequency (hertz)

f_c — cut-off frequency in a waveguide

f_r — resonant frequency

H, H_1 — magnetic field intensity, total magnetic field intensity in the cavity

H_r, H_θ, H_z	magnetic field components in cylindrical coordinates
J_n	Bessel's function of order n
k	wave number
ℓ	length (inner) of cavity
P	power per unit volume
$Q; Q_o, Q_L, Q_e$	quality factor of a cavity; unloaded, loaded, and external Q
R	reflection coefficient
R_s	surface resistance in ohms/square
RF	radio frequency
r	radius of an arbitrary circular cavity or a circular waveguide
r, θ, z	coordinates of an arbitrary point in cylindrical coordinate system
S_e	multiple standard error of the estimate
$S_{\epsilon'}, S_{\epsilon''}$	per cent sensitivities of ϵ' and ϵ'' for a change in phase (θ); $S_{\epsilon'} = (\frac{1}{\epsilon'} \frac{d\epsilon'}{d\theta}) \cdot 100$
T	total duration of a time window [3], temperature [4]
TM_{nmp}	transverse magnetic field mode in a cavity; n represents the number of complete cycles of variation of the axial field in θ-direction for $0 \leq \theta \leq 2\pi$; m represents the number of zeros of the axial field in the radial directions; p represents the number of zeros in the z-direction
T_1	transmission coefficient for a singly-transmitted wave
T_t	transmission coefficient for a multiply-transmitted wave
T_c	"cut-off" temperature

T_{12}	transmission coefficient from layer 1 to layer 2
t	sampling interval [3], time [4]
$\tan\delta$	loss tangent ($\varepsilon''/\varepsilon'$)
V	voltage as a function of frequency
V_c	volume of cavity
V_s	volume of sample holder
VSWR,SWR	voltage standing wave ratio in a transmission line
v	voltage as a function of time
WFM	waveform
Z_1, Z_2	wave impedance of medium 1, medium 2
α	shape parameters of the Cole-Cole Equation
β	propagation constant in vacuum
γ	complex propagation constant in a medium
Δf	shift in the resonant frequency of the cavity with the insertion of a sample
ε_o	permittivity of free space (8.854×10^{-12} farads/m)
ε^*; $\varepsilon^*(T)$, $\varepsilon^*(f,T)$	complex dielectric constant, ε^* as a function of temperature, ε^* as a function of frequency and temperature
ε'	dielectric constant (real part of ε^*)
ε''	dielectric loss factor (imaginary part of ε^*)
ε_∞	high frequency dielectric constant
ε_s	static dielectric constant
η	intrinsic impedance of a medium
θ	phase angle[3], temperature [4]

λ_g — guide wavelength

λ_o — free space wavelength

λ_c — waveguide cut-off wavelength

λ^w — wavelength in water

μ_o — permeability of free space ($4\pi \times 10^7$ henry/m)

μ^* — complex permeability

$$\mu^* = \mu' - j\mu''$$

μ' — real part of μ^*

μ'' — magnetic loss factor (imaginary part of μ^*)

ρ — reflection coefficient

σ — bulk electrical conductivity

τ — dielectric relaxation time

ω — radial or angular frequency ($2\pi f$)

CHAPTER I

Introduction

The main objective in this thesis is to investigate the dielectric and microwave heating properties of lossy dielectric materials. With a proper choice of dielectric properties, microwave differential heating in layered materials can be used to advantage, for example in the heating of prepackaged foods, susceptors [1] and interactive heaters [2,3].

Layer heating and differential heating between layers are quite complex [4]. Designing foods and their packages, for microwave heating, is one area where this is important. Research in this area is relatively new; Risman et al. have recently discussed some of these problems [5]. There is agreement on a need for more research in this area. A part of the work done for this thesis is in response to the above need.

Although microwave energy has either been proposed or used in a variety of applications such as drying of wood, paper, film, printing inks and textiles [6,7]; heating of plastics, rubbers and wood [8]; heating of tumours [9]; transmission of power [10] and powering of aircrafts [11]; etc., it is the food and beverage industry where microwave power has one of the largest applications [12] – an application which is growing at an exponential rate [1].

The first report of microwave heating of foods in cavities, in the 800-3000 MHz frequency range, appeared immediately after World War II [13,14]. In 1946 the first microwave oven for cooking purposes was

made by Raytheon Manufacturing Company and an improved model was operating in a number of restaurants by 1947 [15]. The considerable savings in cooking time and the fast heating of precooked meals, which are possible in a microwave oven, were the most attractive features which triggered a slow development for these appliances. Their large size and high cost were the main disadvantages which precluded them from being sold as home appliances. By 1956, however, microwave ovens had been reduced in size and price to the point that 2500 units were sold for home use that year in the U.S. By 1974, approximately 700,000 domestic microwave ovens were sold in the U.S. due to widespread awareness of the advantages of this applicance in society, added safety from radiation (better door seals), smaller size, longer magnetron life and lower prices [15]. Subsequent development has been fast and by the mid-eighties about 15 million ovens were sold in the world per year with a projected sale of about 21M/year in 1990, according to a survey of industry reports [16].

Along with the rising sales of ovens, sales of "microwavable" prepackaged foods also started growing exponentially in the late 70's [1]. One example of microwavable food, available in the marketplace, is a pizza-package in which the pizza is plated on a semi-transparent thin conducting film with a higher heating rate. When this package is heated in a microwave oven, the film acquires a high temperature ($>200^{\circ}$C) and acts as a conventional hot plate which convectively heats and browns one side of the pizza. Some other examples are popcorn and bags for french-fried potatoes. However, in 1986 the sales of

microwavable foods in the U.S. were only one percent of the annual food-related expenses of the population [1]. It is felt that the main reason for the relatively slow growth of microwavable foods is their inability to duplicate the characteristics of conventionally prepared foods for crisping, browning, flavour, aroma and the sizzling sound of a cooked food.

One of the ways to solve the problem of crisping and browning is by using a thermostatic susceptor in a microwave food package. Susceptors, when heated in an oven, absorb microwave energy and re-emit that energy as heat. Thus, these susceptors can serve as a conventional hot-plate inside or outside a microwave oven. To provide thermostatic (self-limiting) heating, the loss characteristics of these susceptors should ideally follow the pattern shown in Fig. 1 with a small, temperature-independent value for ϵ'. A few materials suggested for their use as susceptors are thin microwave transparent conducting films [17] and some chloride pastes [2,3]. Some sugar-alcohol mixtures, discussed in Chapter II, also have a potential for use as susceptors.

In microwave heating, heat is generated inside the material in contrast to the conventional heating where, in general, the heat is first transferred to the surface of the material - by either conduction, convection, radiation, or by a combination of any two or all of the three mechanisms - and then to the interior by thermal conduction. The microwave heat generated inside a material is proportional to power absorbed per unit volume and is given as

$$P = \omega\epsilon_0 \, \epsilon'' E^2 ,$$
(1.1)

where   P - Power absorbed per unit volume inside the material, and

E - Electric field intensity (rms) inside the material.

For a particular material geometry and at a fixed frequency, temperature, and moisture content the electric field intensity inside a small volume of a material is constant.   According to Equation 1.1, therefore, the microwave power absorbed in a material depends only upon ϵ'' of the material: in reality other parameters such as ϵ' and thermal conductivity also affect P.   For lossy materials, in general, the loss factor depends upon temperature and thus the $\epsilon''(T)$ of a load (T represents temperature) is a critical parameter in the design of a microwave heating system.   Therefore, it is essential to have data on $\epsilon''(T)$ on a load to be able to predict its microwave heating response. The measurements done on some lossy materials, and given in Chapter II, are in response to this need.

Almost all modern microwave ovens have a multimode cavity with a constant speed mode-stirrer which renders the field in the cavity homogeneous and isotropic on a time-average basis [18].   Thus for a small single-layer load, which does not excessively perturb the field pattern inside the cavity, Stratton's solution for the reflection and transmission of a plane wave normally incident on a layer of a dielectric material seems reasonable for the estimation of absorption [19]. Similarly, for a multilayer load Wait's solution could be used [20].   For loads that are not very small, compared to the cavity,

Temperature

T_c

Figure 1. Dielectric absorption characteristics of some thermostatic susceptor layers. A simple thermostatic dielectric layer requires $\frac{d\varepsilon''}{dT}$ $\geq 0(T < T_c)$, $\leq 0(T > T_c)$ with 'cut-off' temperature, T_c in the range $(100 < T_c < 300°C)$ for food heating. Examples known are Chloride Pastes for which $110 < T_c < 160°C$, Marmite™ and egg white. Essentially similar but often more effective responses occur for ferrite materials and semi-transparent metal films when used as interactive heating layers.

these models could be applicable only in an approximate sense. The measurement of $\epsilon''(T)$ and the variation of absorption in a layered material with its thickness and temperature are analysed in Chapters II and IV.

1.1 Overview of Thesis Contents

The dielectric data on eggs, chloride pastes and sugar-alcohol mixtures, obtained in a search for suitable high loss interactive microwave heating materials, are given in Sections 2.5 to 2.8. In addition, the following is included in Chapter II: a brief discussion on the loss factor, the proposed classification of high, medium and low loss materials; and a brief discussion on various techniques for dielectric measurement in frequency domain with some important references which may help in selecting the appropriate dielectric measurement technique for a given material. In Sections 2.3 to 2.5 different aspects of the measurement technique, used for all the frequency domain measurements reported in this thesis, are given. Finally, a discussion on the accuracy and precision of the dielectric measurement method are given at the end of this Chapter.

Although a cavity perturbation technique is one of the most accurate dielectric measurement techniques [21], it suffers from the defect of remaining confined to only one frequency. In an effort to determine the suitability of a time domain transmission method, for its use over a wide range of dielectric materials, measurements were done on the calibrating liquids. The results of these measurements along with the following are given in Chapter III. In Section 3.1 the

theoretical basis for the time domain transmission method is given; experimental apparatus and procedure of measurement is given in Section 3.2. This is then followed by a brief discussion on the results obtained along with the sampling requirements for TDR waveforms. In Section 3.4 a discussion is given on various sources of error in a time domain transmission method. On the basis of the theory developed in this section, an estimate is also made of the magnitude of the error in the results.

In Chapter IV a mathematical model is given to estimate the absorption in different layers of a load placed in a microwave oven. This model is useful in the design of new food packages for microwave heating. It is also shown that the model can be used for computing microwave absorption in thin conducting susceptor films in microwave food packages.

The microwave browning of foods, as well as different methods to achieve this browning, are briefly discussed in Section 5. This is followed by a discussion on the results of actual browning tests on some foods in a microwave oven using pastes and mixtures similar to those discussed in Chapter II.

In Appendix I the cavity perturbation equation for the TM_{012} mode in the idealized version of the cavity is derived. In Appendix II, mathematical models are given to compute the absorption in layered media. Fortran 77 programs are included for computing the absorption.

CHAPTER II

Dielectric Materials and Measurements

All the non-metals on this earth can be classified as dielectric materials. The Greek philosophers called these materials "insulators". However, all modern dielectrics are not insulators, for example, conducting polyacetylene and some other polymers are classified as dielectrics [22,23,24,25]. Although insulators were known to the ancient philosophers, it was Faraday who first conducted detailed scientific measurements on these materials and in 1837 for the first time, published the results of his scientific measurements and called them "dielectrics" [26]. Faraday's experiments indicated that the capacity of a condensor was dependent on the nature of the material separating the conducting surfaces. Faraday introduced the term "specific inductive capacity" for the ratio between the capacity of a condenser filled with a dielectric and the capacity of the same condenser when it is empty. This quantity is now called the relative permittivity or the dielectric constant and denoted by ϵ'.

Dielectric materials can be further classified into different categories on the basis of their characteristics as follows:

(a) Physical State - Solids, liquids, gases and vacuum.

(b) Types of material-Piezoelectric, ferroelectric, ferrimagnetic, semi-conductors, organic materials, inorganic materials, biological materials, forest products, and foods, etc.

Since our interest lies mainly in lossy materials and the measurement of their losses, all the materials are classified on the basis of their

8

dielectric losses.

When a dielectric material is placed in an electric field it shows losses. The total dielectric losses can be either due to one of the following mechanisms or any combination of them:

(i) Losses due to the conductivity;

(ii) Losses due to interfacial polarisation or Maxwell-Wagner losses; and

(iii) Losses due to other types of polarisations

For example, in a sample of commercial rubber, the observed value of dielectric loss factor (ε'') is given as:

$$\text{erved)} = \varepsilon''(\text{conductivity }) +$$

$$\varepsilon''(\text{Maxwell-Wagner}) + \varepsilon''(\text{Dipolar absorption}). \quad (2.1)$$

For most dielectric materials, ε'' is a function of temperature, frequency, moisture content and density. The loss tangent, $\tan\delta = \dfrac{\varepsilon''}{\varepsilon'}$ is a measure of the lossiness of a dielectric material. In the 1-10GHz frequency range and at room temperature the range of loss tangent is from about 1×10^{-5} for good insulators to about 5.0 for some soils. However, for polyethylene a value of loss tangent as low as 3.7×10^{-7} has been measured at 2.2K temperature and 6.5GHz [27]. This is claimed to be the lowest measured value of loss tangent. Von Hippel et al [28] have reported a value of $\tan\delta$ of 8490 at 1KHz for a sample of loamy soil having 13.77% moisture. This seems to be the highest measured value of $\tan\delta$.

On the basis of their loss tangents, all dielectric materials can be divided into three categories – low, medium and high loss

materials. As stated earlier, the loss tangent of a dielectric material varies with its temperature, frequency of operation, moisture content and amount and type of impurities, therefore, in some cases, a material may have to be classified (at different frequencies and temperatures) into different categories. In the literature, the transition points (in terms of the values of loss tangents) between medium loss and low loss materials and high loss and medium lo materials are not clearly defined.

. The American Institute of Physics Handbook [29] and von Hippel [28] define materials having loss tangents more than one as high loss materials. The rationale behind this definition seems to be the fact that when $\tan\delta > 1$, the angle δ is more than 45°, and the loss current would be more than the charging current, if this material were used in a capacitor. The above definition of high loss materials ($\tan\delta > 1$) does not agree with the values of the loss tangents for high loss materials in recent microwave journals. It seems that the above definition of high loss materials is more applicable at radio frequencies, where the values of loss tangents of the order of thousands exist for some materials (for example, sand, biological materials and foods). A proposed classification for high, medium and low loss materials in the microwave region is given below.

2.1 Proposed Classification

(i) Low Loss Materials

All the materials with their loss tangents less than or equal to 100×10^{-4} can be classified as low loss materials. Some of the materials falling in this category are: fused quartz, ice (below -12°C), polythene and PVC.

(ii) Medium Loss Materials

All the materials with their loss tangents in the range from 100×10^{-4} to 1000×10^{-4} (0.1) can be classified as medium loss materials. Some materials belonging to this category are: araldite, synthetic rubber and tufnol.

(iii) High Loss Materials

There is a lack of consensus in the definition of high loss materials. Kilp [30] mentions chlorobenzene with its loss tangent as 0.1077 as a medium loss liquid. This means that if Kilp were to define a high loss material, perhaps would have chosen 0.3 as the minimum initial value for $\tan\delta$ for this range. van Loon and Finsey [31] define chloroform with its loss tangent equal to 0.2329 as a high loss material. Zanforlin [32] mentioned ethanol ($\tan\delta = 0.3$) as a high loss liquid. Burdick et al. [33] mention 0.1 as a "large loss tangent". Dakermandji [34] defines a material with its loss tangent greater than 0.1 as a "very high loss material" Cook and Jones [35] mention a material with its $\tan\delta > 0.1004$ as a very high loss material.

On the basis of the above survey of the literature, it is suggested that all the materials with their loss tangents more than 0.1 can be classified as "high loss materials". Most of the biological and water-bearing materials fall under this category. The proposed classification is given in Table 1.

2.2 Selection of the Measurement Method

For many scientific and technological applications, dielectric data are required on a large variety of materials under different

TABLE 1

Classification of High, Medium and Low Loss Materials on the Basis of Their Loss Tangents

	High	Medium	Low
$\tan\delta$	$\tan\delta > 0.1$	$1000 \times 10^{-4} \geq$ $\tan\delta \geq 100 \times 10^{-4}$	$\tan\delta < 100 \times 10^{-4}$
Representative dielectric materials	Some soils, biological materials, moist materials (foods and pastes)	Araldite, synthetic rubber tufnol	Fused quartz, polythene, PVC

physical conditions. This would include data over a wide range of temperature low loss dielectrics for telecommunications, dielectric lenses, radomes and microwave integrated circuit (MIC) substrates, high loss pastes for the design of new food packages for microwave heating, biological materials (in vivo) for diathermy and plasmas for fusion experiments. Different materials require different techniques for their measurements. The many measurement methods are well documented in books [28,36], in conference proceedings [37] and in review papers, for example, by Magid [38], Cohn and Kelly [39], Bussey [40], and Lynch [41]. Some recent reviews on dielectric measurements have been done by Birch and Clark from 30 to 1000 GHz [42], and Afsar, Birch and Clark from 1 MHz to 1500 GHz [18]. In this thesis, the frequency range of interest is from 900 MHz to 10 GHz, which covers the three ISM frequency bands at 0.915, 2.45 and 5.80 GHz. A brief

discussion of the different measurement techniques is given below.

All the methods for measuring the complex dielectric constants of materials can be classified into the following three categories: (i) Free wave propagation, (ii) Transmission line, and (iii) Cavity.

Free wave propagation methods are essentially based on optical-type measurements and are not generally considered suitable for the frequency range under consideration. These are more suitable at mm wavelengths [43] and are discussed in detail by Musil and Zacek [44].

In the transmission line methods the dielectric material is placed in a transmission line (between outer and inner conductors of a coaxial line, or inside a waveguide). The complex dielectric constant of the material is then determined by the measurement of the input impedance of the dielectric-filled line. In one of these methods, known as Roberts and von Hippel's method [28], a waveguide is terminated by the sample in physical contact with a short circuit. This method has been used extensively in the past and is one of the recommended methods by the American Society for Testing and Materials (ASTM). Nelson [45] has made this method more convenient and versatile to use by writing a computer-program which exactly computes ε^* for high-loss as well as low-loss materials. This program is applicable to measurements made in rectangular and circular waveguides as well as coaxial lines. Corrections are also included in the program for the influence of the slot in a slotted-waveguide section, and the difference in velocity of propagation in air and in vacuum. Even if these corrections are ignored, it is claimed that the error in computed results is only 0.5% for ε' and 2-3% for ε''. The cavity methods are

discussed in Sections 2.3 to 2.5.

For about the last 15 years automatic network analysers (ANA) have also been used for measuring the reflection coefficient in a transmission line. In this method, the error from mismatches between different components of the transmission line is minimized by a standard error correction procedure [46,47]. With wide-band sweepers, and under the control of a computer, dielectric measurements can be done by ANA's over a wide range of frequencies. In this thesis, these methods have been classified in the transmission line category.

In Table 2, some dielectric measurement methods are given for different categories of materials as reported in journals. In this table all the dielectric materials are divided into different categories on the basis of their physical state. This table is expected to prove useful in selecting a dielectric measurement method for a given material. However, in the last 40 years, the total number of papers published on this subject is substantial and of these only a few, considered important, are given in this Table.

2.3 Cavity Perturbation Technique

The cavity perturbation technique was originally used by Bethe and Schwinger [77], and then by Kahan [78], and Slater [79] for the calculation of the effect on the resonant frequency of a cavity of a small deformation on its boundary. Casimir [80] applied this technique for measuring the dielectric and the magnetic properties of the materials introduced into a cavity. Since then many workers have used this technique for measuring the electrical properties of materials [52,74,81,82] including plasmas [64,65]. Perturbation techniques have been discussed in detail by Argence and Kahan [78], Lax and Button

Table 2

Suitable Dielectric Measurement Methods, 900MHz–10GHz

Dielectric Material	Methods and References		
	Transmission line	Cavity perturbation	Time domain
Solid	H[48,49,50], M[51] L[55,56]	L[52]	L[53,54][a]
Paste		H[57,58], M[57,58]	
Powder	M[53]	H[57,58], M[57,58]	
Cellular & fibrous material,e.g. RAM	H[38]		
Liquid	H[59,56,48,60]	H[52], L[52]	H[61,62], L[63]
Plasma		H[64,65]	
Biological Material (a) In vitro	H[66,67]		H[68]
(b) In vivo	H[66,47,56]		H[68]
Rock (In situ)	H[69], M[69]		H[70], M[70]
Miscellaneous	H[Foods,71,72]	M[Yarn, 73] M[Rubber, 74]	H[Fish,75] H,M[Agricultural Materials,76][b]

[a] H– High loss dielectric material, M–Medium loss, L–Low loss. Reference numbers in brackets describe the measurement technique and give results.

[b] – Description and results of time domain dielectric measurements on agricultural material – both high and medium loss – given in [76].

[83], Waldron [84] and Baden Fuller [85].

A material specimen, when introduced into a cavity, alters its characteristic parameters: the resonance frequency, f_r, and the loaded quality factor, Q_L. These changes depend upon the real and imaginary parts of the complex dielectric constant (considering either weakly magnetic substances or location into the cavity where the magnetic field is zero) and on the geometry of the sample and the cavity. For a very small specimen in an arbitrarily shaped cavity, the first-order perturbation theory gives [86]

$$\frac{\Delta f}{f_r} = -\frac{1}{2}F(\epsilon'-1) \qquad (2.2)$$

$$\Delta\left(\frac{1}{Q_L}\right) = F\epsilon'' \qquad (2.3)$$

where, Δf and $\Delta(1/Q_L)$ are changes in f_r and Q_L with the insertion of sample in the cavity. The factor F is a function of sample volume, total cavity volume, and the electric field within the sample.

In the past, most workers have preferred simple geometrical shapes such as cylindrical [81] and rectangular waveguide cavities [52], perhaps for the fact that the perturbation equations are easier to derive. However, cavities of special shape having strong fields in some regions have also been used to increase the sensitivity of the measurement; an example is the re-entrant cylindrical cavity used by is one of the most popular cavities for perturbation measurements. In this cavity, cylindrical samples are introduced along the axis of the cavity such that the length of the specimen is equal to the height of

the cavity. This geometrical arrangement has, however, the following two disadvantages [88]: (a) The fit of the sample in the cavity is critical, especially in the measurement of materials having large ϵ'. Attaining the exact fit for hard and brittle materials is a problem, because the ends of the sample rod tend to chip and crack, (b) It requires disassembling of the cavity for the insertion and correct positioning of the sample. This may lead to difficulties in reproducing the reference Q_L and the resonant frequency. To overcome the above two difficulties, Labuda and LeCraw [88] used a right circular cylindrical cavity in the TM_{012} mode. This cavity had small holes at both ends which permitted insertion of the sample without disassembling the cavity. The sample was suspended with a nylon thread such that the electric field was zero at the ends of the sample. This eliminated any error either due to the tolerance in the length, or non-uniformities at the ends of the sample. Risman [57] further modified this geometry for ease of sample insertion. Two such cavities were used in this work; Walker [89] has previously used one of these for dielectric measurements on cryoprotective agents. The field distribution and the mechanical arrangement to hold the sample in the centre of the cavity are shown in Fig. 2. As shown in the Figure, the cavity is divided into three parts and these parts fit together by lips rather than screws for easy sample insertion. The bottom plexiglass divider has a teflon cone placed in its centre, which keeps the sample holder in the centre of the cavity. The sample holder is vertically fixed through a small hole in the top plexiglass divider. For a thin sample, the total electric field is parallel to the sample and reduces to zero at both ends. In this way geometrical non-uniformities at the

ends of the sample have negligible effect on the results.

In a cavity perturbation technique there are two methods for determining the dielectric values of an unknown sample: (a) from the perturbation equation of the cavity, and (b) from the calibration of the cavity against some known materials. For all the measurements reported in this thesis the second approach has been followed. Risman [57,58] initially adopted the calibration approach which was followed by Walker [89] and later on by this author. In both the approaches the method of determining ϵ' is essentially the same: the shift in the resonant frequency (Δf) is used to compute ϵ'. In the first method the perturbation equation is used, whereas in the second a regression function is used. However, the determination of ϵ'' is different: in the first method, Q_L values of the cavity with a sample and without the sample are used, whereas in the second method a change in transmission attenuation, due to the insertion of the sample into the cavity, is used. For this cavity it seems that the determination of ϵ'' from the measurements of Q_L is not practicable for certain lossy materials; that is so on account of the interfering TM_{011} mode at 2.59 GHz which moves upwards in frequency with the insertion of a sample into the cavity and interferes with the dominant mode.

In order to compare the results obtained from the calibration method with those from the perturbation method, the perturbation equation is derived for the TM_{012} mode in an ideal circular cylindrical cavity of identical dimensions. This equation was then used to compute ϵ' and ϵ'' for some calibrating liquids of Table 3. A comparison between the computed values and those given in Table 3 is shown in Table A.1. It is seen from this table that the difference

between the theoretical and experimental values of ε^* is outside the range of errors of the measurement method. Most probably the difference is due to neglecting the effects of the construction of the cavity (three piece construction along with slots on the walls) and the arrangement for holding the sample and too much perturbation of the resonant frequency (7% for water).

2.4 Calibrating of the Cavity

Risman [57,58] originally used a TM_{012} cavity shown in Fig. 2 for the dielectric measurements; an exact copy of Risman's cavity has been used in this work. He calibrated his cavity with the first five liquids of Table 3, as he knew the dielectric data on these liquids to a high level of confidence. Later on Walker [89] calibrated a similar cavity with all the seven liquids of Table 3 using pyrex glass vials of 4.9mm diameter (internal) and 93.10mm length and obtained the following relations:

$$\varepsilon' = -0.7294+0.3347(\Delta f)-1.8085\times10^{-3}(\Delta f)^2+0.9650\times10^{-5}(\Delta f)^3$$

$$(2.4)$$

$$\log \varepsilon''(25)=0.2202 + 0.2898\log(\varepsilon'-1)$$

$$+ 0.9960\times10^{-1}\{\log(\varepsilon'-1)\}^2$$

$$+ 0.3125\times10^{-1}\{\log(\varepsilon'-1)\}^3$$

$$(2.5)$$

and $\varepsilon'' = $ Antilog $(\frac{\Delta T}{20} + \log\varepsilon''(25)-1.25)$

$$(2.6)$$

(b)

(a)

REMOVABLE TOP

PLEXIGLASS DISC

SAMPLE

TEFLON CONE

COUPLING LOOP
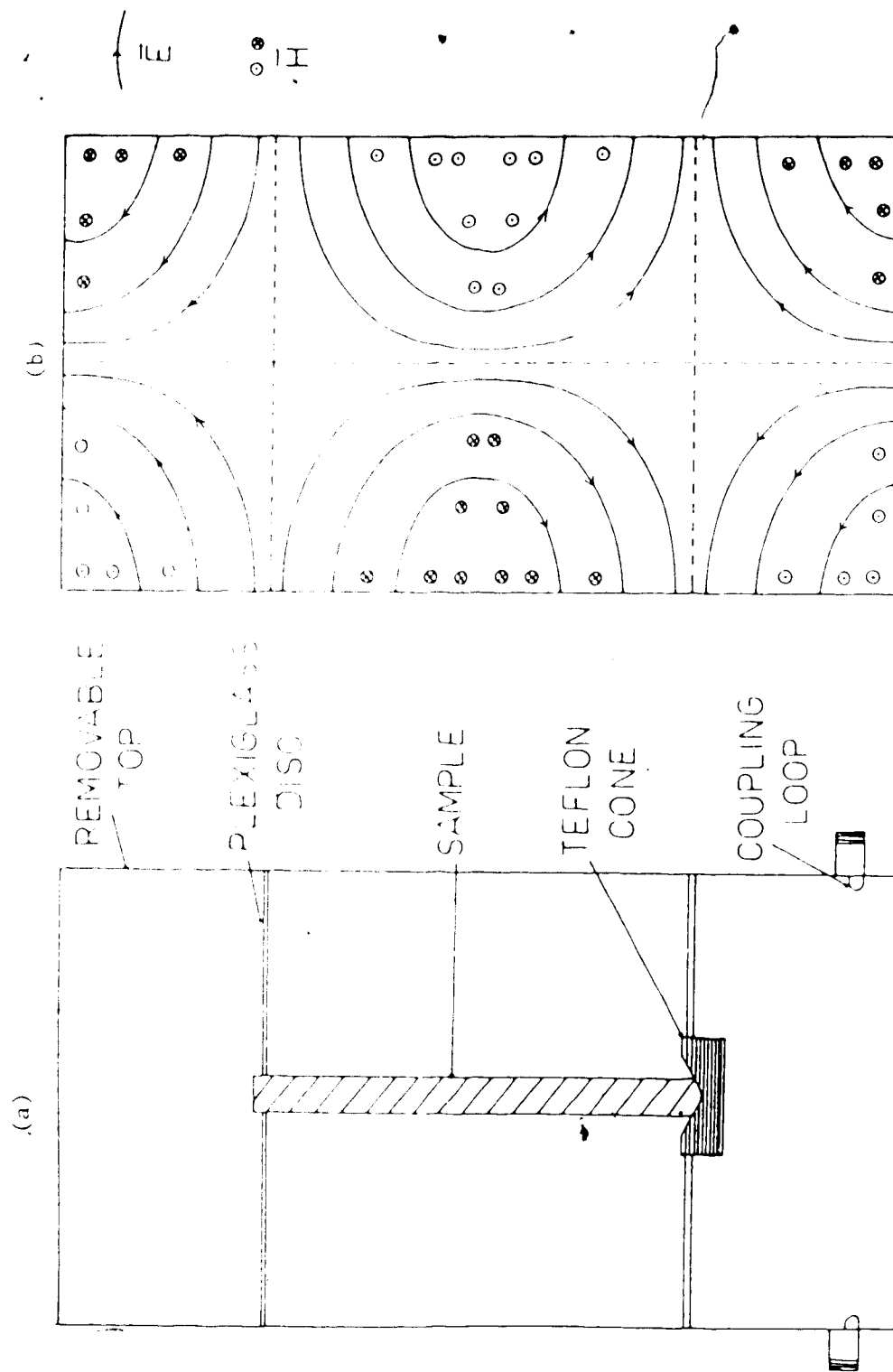
Fig. 2. Circular Cylindrical Cavity and its Field Configuration. (a) Cavity arrangement. (b) Field configuration (TM_{012}).

where Δf is the frequency shift in MHz and ΔT is the difference in transmission attenuation in dBs due to the insertion of the sample into the cavity in the standard vials. $\varepsilon''(25)$ is an arbitrary parameter which is the ε'' of a hypothetical dielectric material having ε' equal to that of the unknown material but transmission attenuation (ΔT) equal to 25dB. For this cavity, ΔT is a function of both ε' and ε'', i.e., for a given ΔT, ε'' depends upon the ε' of the sample. The term $\log(25)$ appearing in Equation (2.6) attaches a weight to ε'' according to the value of ε' of the sample. The method of measurement is described below.

2.5 Measurement Method Used

The measurement procedure consists of placing the sample in the cavity and measuring the changes in resonant frequency (Δf) about the empty sample holder resonant frequency (f_r) and the transmission attenuation (ΔT) at resonance, relative to the empty (low-loss) sample holder. The two-step method is also shown in Fig. 3. Step 1 determines the shift $f_r - f$; step 2 determines T and refines the measurement of f to +/- 1MHz. After the determination of f and T, ε' and ε'' are computed from Equations 2.4 - 2.6. For measurements above room temperature, the cavity is inserted into a temperature-controlled oven.

Sample handling and temperature measurements (with needle thermocouples) are simple with liquids and thin pastes. Samples can be quickly inserted or removed from the cavity without changing the unloaded Q. Considerable care is required with materials which undergo volume and state-changes, with temperature. This can be a serious

sample holders and leave no room for the expansion of the material with temperature. With the vials open·at one end above the "active" volume of the cavity (E ₊parallel to the sample reduces to zero at the plexiglass disc) small expansions and contractions of a material can be managed, although considerable patience is required; trial runs are needed in some cases to ensure that the right amount of material is uniformly present at a given temperature, without air voids. The material is constrained by virtue of the small opening (4.9mm) relative to the length of the vial (9.3 cm). The rate of change of temperature of the sample has to be slow to achieve a uniform density. Each temperature run ($22 - 140^{o}C$) reported in this thesis took 1.5 +/- 0.25 h. In spite of these factors there are two advantages of this cavity method: first, it is possible to achieve uniform samples and, secondly, the measurements are then made at the natural density of the material at the particular temperature.

In order to find suitable high loss materials for their use in microwave heating, the dielectric constants of the constituents of eggs, some sugar-alcohol mixtures and chloride pastes were measured in this cavity. The dielectric data on these materials are given in the following sections. At the end of this chapter, the accuracy and the precision of the data obtained from this cavity is discussed.

2.6 Dielectric Data On Eggs

2.6.1 Chemical Composition and Sample Preparation

The constituents of an egg (both yolk and white) are complex dielectric mixtures. The dielectric properties of these mixtures vary with the grade of the eggs, freshness and even with the diet of a hen [90]. Typically an egg contains 65% white and 35% yolk, by volume.
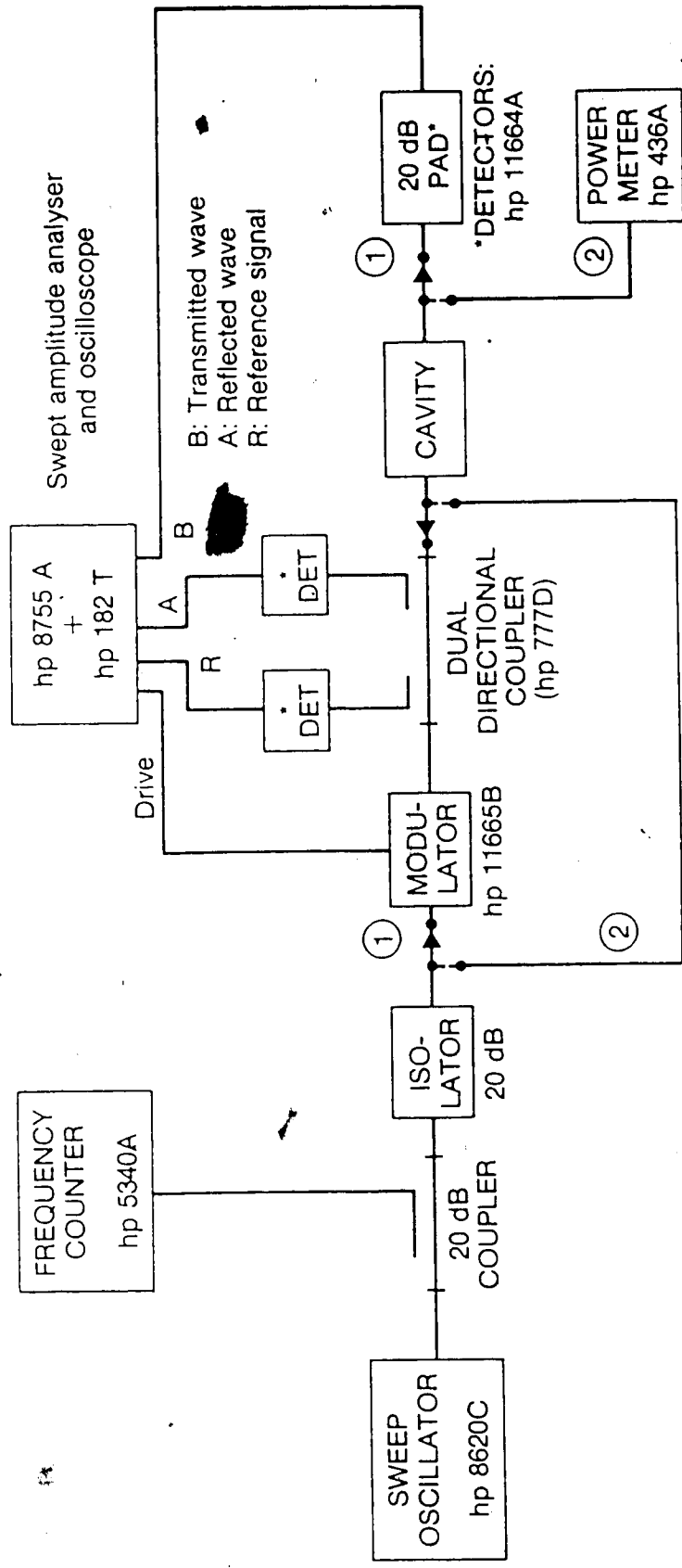
Figure 3: Measurement of Δf and ΔT. The block diagram shows the required connections. Step 1 determines the shift Δf, Step 2 determines ΔT and refines the measurement of Δf.

Table 3

Cavity Calibration Liquids, 2.9 GHz and 20-23°C[a]

Substance	Values used ϵ'	ϵ''
Methanol (Anechemia 99.8% pure; <0.2% H_2O)	22.0	13.0[b]
Distilled Water	78.0	11.0[b]
Methanol (60%) and Distilled water (40%)	46.0	17.0[b]
Acetone (10%), methanol (20%) and benzene (70%)	7.30	1.60[b]
Methanol (6%), benzene (94%)	2.98	0.18[b]
Additional liquids: Monochlorobenzene	5.54	0.67
Ethyl acetate	6.40	0.34

[a] Cavity f_r = 2.92GHz, Δf_{max} = -208MHz

[b] Risman's values [57]

Water is the chief constituent of egg white (typically 88%) followed by protein (typically 11%). The remainder are a trace of fat with minerals and sugars (glucose, etc). Ovalbumin, a glycoprotein, is the chief protein constituent. Oromucin, a mucoprotein, is responsible for the thickness of the white: a 4 to 1 range in oromucin content occurs naturally. The albumen content is even more variable. The total range is from 1 (minimum for the inner thin white) to 80% (for thick white).

The total solids content of egg yolk is about 50%. The major constituents of the yolk solids are proteins and lipids. The fatty acid content depends on the diet of the hen. Half of the water content of yolk is free; the rest is bound to protein and lipoproteins.

Dielectric data for egg constituents have been reported by Westphal [91], Norris and Brant [92] and Rzepecka [52]. Rzepecka's data, at 2450 MHz and 15 − 60°C, is the most extensive but there is no agreement between these writers. Egg variability and unspecified sample preparation may be one reason; heating time (moisture and oil content) may be another factor. For this work, five batches of Canadian Grade A eggs [90] were purchased over a 6 month period; 3 from each batch were used for permittivity measurements. All eggs were kept refrigerated (+7°C) and used after 6 +/- 2 days of purchase. White and yolk were separated and measurements began within 1 hour of separation. The thick albumen (typically 25% of the white by volume) was not used; the remainder of the white was gently mixed as fairly as possible for sample preparation. Egg yolks were gently mixed and samples prepared. Additional eggs from the batches were used for density measurements. Powdered yolk was obtained by cooking and then hot-air drying, with the density measured at the time of the dielectric measurements. Other

eggs from the batches were used for void observations and other related measurements. This convinced us that we had fairly sampled and prepared the same material (in appearance) from eggs laid over a 6-month period.

2.6.2 Results and Discussion

The data obtained are shown in Figs. 4 and 5. The arrows indicate the direction of temperature change. Least-squares fitted straight lines relate to the data points marked; the spread is considered typical. The values are given on the graphs to define the typical $\varepsilon^*(T)$ relationships. Variability (the range of all values recorded) are shown at 23 and 80°C. A sample standard deviation is also shown for egg yolk at 23°C for the measurements taken on the temperature runs: these illustrate precision with a limited natural variability - values which arose from eggs coming from one batch. For egg white samples, it was determined, in separate experiments, that the water loss was <1%, with a volume expansion of about 5% when heated slowly in the vials, in water, to 90°C and held at that temperature for 10 minutes. Voids in the vials were small. Under the same conditions egg yolk was reduced in weight by about 10% with a small (<10%) loss in volume. Insertion of the material in the vials required care for all measurements. The specific gravity of the dried yolk was found to be 0.91 +/- 0.01,

The dielectric constant of the thin egg white, Fig. 4(a), is less than water but follows a similar negative temperature coefficient. The bars show the adjusted range of values obtained (maximum recorded + maximum estimated experimental error to minimum recorded - maximum experimental error). The mid range value is 65.5 (23°C). The line shown is fitted to a temperature run and the markers (+, etc) relate to

the line. The range is also shown at 80°C. Once the material is cooked the variability is much less; it was not measured in detail. The data for the dielectric loss factor in Fig. 4(b) show a greater adjusted range (9.5 to 17.5, 23°C). The loss factor increases with temperature (with a wide range of initial possible values) up to 100°C and then drops rapidly. Above 100°C the dielectric constant drops rapidly as the water becomes bound in the solid material.

Egg white may be a dielectrically - ideal food surface browning agent. In fact, the temperature response of the dielectric loss factor follows that of a susceptor material (see Fig. 1) [2]; were it possible to shift ϵ''_{max} from 100 to about 160°C the browning potential would be enhanced. The lower curves, in Figs. 4(a) and 4(b), show the effect of temperature on the cooked material. At constant-weight these curves are "reversible"; that is, they apply to an increase or decrease in temperature.

The egg yolk data (Figs. 5(a) and 5(b)) show that both ϵ' and ϵ'' have negative temperature coefficients except in the dried state (then both are small and positive). Tanδ is large and is similar for both constituents but in terms of what may be an important heating property with egg white, tanδ does not reveal the transition at 100°C.

2.7 Dielectric Data on Chloride Pastes and Microwave Browning Agents

Chloride pastes are among the new interactive (susceptor) heating materials being used in or proposed for microwave food packages. [1,17,93]. These pastes, which have been called chemical susceptors [3], heat rapidly into the range 140°-200°C and then dry, providing a controlled "hot plate" for foods packaged with them. Examples are

packages for pizza and fried potatoes. These pastes represent one family of suceptor materials whose dielectric properties have not been reported, although the trend of the loss factor (ϵ'') can be deduced from the carefully reported microwave heating experiments in the patent literature [2,3].

The dielectric measurements were, therefore, made on two $CaCl_2$ pastes. These were then compared with data on some of their nearest edible counterparts, all of which are (or have been suggested as) microwave browning agents [94]. These materials are Marmite^{TM}, a stiff savoury paste of yeast, vegetables and salt, which turns light brown if cooked [95]; Cross & Blackwell Browning^{TM} [96]; and Kitchen Bouquet^{TM}, a dark meat and gravy sauce [97]. The latter two are liquids rather than pastes.

2.7.1 Sample Preparation

Two calcium chloride pastes were made with a consistency similar to those described in the patent literature for interactive heating elements [2]. Data are given in Fig. 6. The pastes were packed into the 4.9mm (internal diameter) thin-walled pyrex vials used in the perturbation-cavity. It is believed that the internal pressure with heating, the expansion and the loss of water, are similar by virtue of the relative geometries of the vial and the vented plastic bags used, or proposed, in practice. The samples were heated and stabilized slowly in the cavity placed within a temperature controlled oven; although this is quite different from the rapid heating that occurs in a microwave oven, it should still be representative of the material's condition at each temperature under microwave heating. If samples did not maintain a visually uniform density they were not used. Dry value measurements were made by the same method, but the technique

is not particularly accurate or precise for small ϵ' ($1\sim2.5$) and ϵ'' ($<$ 0.1). In some cases (see graphs) dry samples were obtained by rapid heating in a microwave oven and were then reheated in the cavity for the dielectric measurement. The other materials were handled in the same fashion in order to make the results comparable.

2.7.2 Results and Discussion

The dielectric data for the materials measured are shown in Figs. 6 - 9. The nearest linear or quadratic curve was computed for the measured values recorded; the equations are given on each figure, which also (in the legend) include the physical parameters of the samples used.

It is apparent from the results why $CaCl_2$ pastes make suitable interactive heating elements: the maximum temperature for water release (about $150^\circ C$) is known to be greater than that for NaCl [2,3] with a consequently larger $\epsilon''_{max}(T)$; further at the cut-off temperature (T_c) the value of ϵ'' for the dry material is significant – high enough, in fact, to maintain energy absorption (and thus the "hot plate" effect) into the critical food browning range – which, for rapid browning, is $>$ $160^\circ C$. Certainly the higher the temperature the faster the browning. [94]. For simple layer and multilayer model calculations, similar to those shown to be approximately true for water layers in microwave ovens [4], it is suggested that ϵ' be taken as 10 ($25 < T < 150^\circ C$) and ϵ'' as $2 + 0.15T$ over the same range: these are the "trend" values. However, it should be noted that ϵ'' is greater for the drier (stiffer) $CaCl_2$ paste, thus higher values may be possible with mixture optimization. The dielectric properties of these materials do not appear to be well understood and data on any chloride-paste could not

be found for a comparison.

Marmite^{TM}, rich in NaCl, behaves in a similar fashion (Fig. 7), but with a lower cut-off temperature (T_c); it has useful heating properties and browns foods by virtue of its "susceptibility" with the added effect of a staining action. This means that an edible chloride-yeast susceptor (or browning agent) is possible.

Crosse & Blackwell (Microwave) Browning^{TM} (Fig. 8) also has similar properties, particularly $\varepsilon''(T)$, but the maximum temperature for water release is only about $110^{\circ}C$. Also, it is not thick enough to create a "food layer", for interactive heating, in practice. The value of $d\varepsilon''/dT$ is, quite different from similar weak NaCl solutions over the same temperature range [98,99] suggesting again the need for a careful evaluation of chloride-yeast mixtures. Kitchen Bouquet^{TM} (Fig. 9) has quite different dielectric properties, ones which are similar to water and weak NaCl solutions.

2.8 Dielectric Data on Sugar Alcohol Mixtures

Some mixtures of alcohol and sugar show synergistic dielectric absorption at room temperature and 1 - 3 GHz [100]. However, data are not available in the literature at higher tempertures [101,102]. Measuremnts were, therefore, done on these materials in search for more effective "edible susceptors" or surface-activators for heating microwave foods with the dielectric-temperature characteristics discussed in Chapter I and shown in Fig. 1. The dielectric data [25-100$^{\circ}C$, 2.9 GHz] on some sugar alcohol mixtures are given in this section in Figs. 10 - 13. Except for the sugar and water mixtures, the variation of loss factor with temperature is similar, in nature for all the solutions and mixtures; it increases up to a certain

temperature – called the "cut-off temperature (T_c)" – before falling sharply. This shows that these mixtures have a potential for use as browning agents (Chapter V).

2.8.1 Sample Preparation

Three mixtures of icing sugar [103], distilled water and ethanol, with the following constitution were made. Ethanol was 98% pure, reagent grade. The sugar water mixture was a saturated solution at room temperature: at a higher concentration, sugar settled to the bottom and maintaining a uniform density in the sample holder was difficult. The sugar and ethanol mixture was a thick paste; and sugar, water, and ethanol mixture was a thick solution. The concentrations and densities of these solutions and paste are given in Figs. 10-13. Sample holders open at one end were used, even then the measurements could be made only up to the boiling points of these mixtures.

2.8.2 Results and Discussion

For sugar and distilled water mixtures, ε'' remains constant whereas ε' increases with temperature - Fig. 11. When heated beyond the boiling point of the mixture, the water evaporates and a thick paste, with some bound water, remains in the sample holder. The dotted curves given below the solid ones are for those thick pastes. Simple expressions for $\varepsilon^*(T)$ are also given in these figures for calculating absorption and transmission through a layer of this mixture with microwave heating. The heating results for the sugar-water mixture, at $25^{\circ}C$, matched ε' very closely, ε'' not so closely - with those given by Roebuck [101] for a sucrose mixture of identical concentration at $25^{\circ}C$ and 3 GHz. (For comparison, Roebuck's values are also shown on Fig.

11). The value of ε'' for our mixture seems to differ from that of Roebuck [101] due to the composition of the sugar used [103]. For other mixtures, no previous data could be found in the literature. The results shown in the other figures are explained in the captions.

On the basis of the information derived from the above results, Sections 2.7 and 2.8, and from a general survey of the dielectric data [104,105] some mixtures were synthesized in an effort to make an "edible" browning agent. The composition of these mixtures and surface browning done with these are discussed in Chapter V.

The accuracy and precision of the dielectric measurement method are discussesd in the next section. An analysis of the deviation of the data obtained about a mean value indicates the degree of precision. Accuracy is more difficult to estimate. The most convincing way of demonstrating accuracy is to measure, in the same system, the dielectric properties of known dielectric materials. The accuracy and the precision of the cavity perturbation method, of Sections 2.3 - 2.5, are discussed in the following section.

2.9 Accuracy and Precision of the Method

2.9.1   Accuracy

In a calibration method, the accuracy of a dielectric measurement depends upon the accuracy of the dielectric values of the calibrating liquids. Risman [57] has stated that the materials, other than water, given at serial numbers 1,3,4 and 5 in Table 3 were measured in the Physics Laboratory of the RVO T.N.O. in the Hague by courtesy of Dr. De Loor, using a method described by Poley [106]. For water, Risman [57] has stated: "The values of water were taken from the literature and corrections were made to $f = 2.8GHz$ and $+20^{o}C$." He

also measured water in a TM_{010} cavity and checked his experimental results with those calculated from the perturbation formula for that cavity. Risman has stated that a comparison of all the three values of ε^*, obtained as above, satisfied him of the accuracy of water's ε^* as $(78 - j11)$ at 2.8 GHz and $20^{\circ}C$.

In view of Risman's above statement regarding water's dielectric values it is considered desirable to estimate its dielectric values at 2.8GHz, $20^{\circ}C$ from a separate source. Water is chosen for the analysis, because this is the only substance in Table 3 for which maximum data are available in the literature.

A mathematical relation, based on a dielectric theory, does not exist to calculate $\varepsilon^*(f,T)$ for pure water. It is known that pure water does not obey Debye's theory for dielectrics [107]. Sheppard, Jordan and Grant [108] and Sheppard and Grant [109], after analysing their dielectric data on water, have suggested that water obeys the Cole-Cole equation. Based on a statistical analysis, Hasted [110] has given the parameters of the Cole-Cole equation, which are used to determine $\varepsilon^*(f,T)$ for water as described following the next paragraph.

The observation that the dispersion of water is better characterized by a small departure from Debye behaviour has also been confirmed by others such as Schwan et al. [111] and Afsar et al. [112]. Thus, a small departure from the Debye behaviour now appears to be accepted but the form of dispersion with which to replace it is not obvious [113]. There are two schools of thought: one contends that the dispersion of water can be modelled by superimposing two Debye processes of equal amplitude with their relaxation times separated by a

factor of two whereas the other rejects this model [109,113]. It should be possible to calculate $\epsilon^*(f)$ for water theoretically, when these subtleties regarding the dielectric dispersion of water are clarified.

Under these circumstances the only way to check the possible range for $\epsilon^*(f,T)$ for water at a given temperature and frequency is from a statistical analysis of the available experimental data. Accordingly, a polynomial was obtained from the parameters given in Table 4, which are from Hasted [110]. Hasted obtained these parameters from a regression analysis of the experimental data of Collie, Hasted and Ritson [114], Saxton and Lane [115], Grant, Buchanan and Cook [107], Cook [116], Hasted and El Sabbeh [117], Buchanan and Grant [118], Sandus and Lubitz [119] and Hasted [120] at more than 40 frequencies (from 0.50 to 900 GHz) and from 0-75°C.

From Stogryn's analysis [121] for the complex dielectric constant of saline water, it is expected that for pure water a third-order polynomial of the following form is also required:

$$\epsilon^*(f,T) = \epsilon'(f,T) - j\epsilon''(f,T), \qquad (2.7)$$

$$\epsilon'(f,T) = a'_1 + a'_2 f + a'_3 T$$

$$+ a'_4 f^2 + a'_5 T^2 + a'_6 fT \qquad (2.8)$$

$$+ a'_7 f^2 T + a'_8 fT^2 + \ldots$$

$$\epsilon''(f,T) = a''_1 + \ldots , \text{etc.} \qquad (2.9)$$

Where a'_1, a''_1, etc., are to be determined. To find the above relationship, $*(f,T)$ is computed at 0, 20, 40 and $60^{o}C$ at the unit frequencies from the Cole-Cole equation and the parameters, given in Table 4. The static dielectric constant, $_s(T)$, was obtained from the Malmberg and Maryott relation [121], also given in Table 4; this is accepted as the most accurate relationship available [110]. The values of $*(f,T)$ so obtained are given in Column A of Table 5. The values found by regression analysis are given in Column B. The regression coefficients of the least-squared fitted polynomials for 0, 20, 40 and $60^{o}C$ are also shown in Table 5. It is found that the two independent variables, f and T, are interacting in their effect on ; thus the polynomial form of Equations (2.8 - 2.9) is required with f, T and fT terms. The results of a multiple regression analysis are shown in Column C of Table 5; the coefficients in this case are given in Table 6.

The coefficients of determination, R^2, which are the measure of the variations in the experimental data explained by the multiple regression models [122], are 0.99 for both ' and ". This is the reason for the choice of this model for $*(f,T)$. The computer programs have been checked with an example given by Devore [122]. In Table 7, experimental values at 2.8 GHz, given by Risman [123], and the regressed values obtained from Equations (2.8 - 2.9) are shown, together with values calculated from Hasted's data [110].

It is seen from Table 7 that the experimental value of ', used for the calibration of the cavity, is very close to that obtained from the multiple regression analysis: the difference is only 0.53%. For " the experimental value differs as much as 20% from that obtained from

multiple regression. However, it seems that the actual value of ε'' at 2.8GHz, 20°C is near 11.0 as deduced below.

In Table 8 experimental values of ε'' are given at 3GHz and 20-25°C from four different sources. The values differ considerably; the divergence can be ascribed to the accuracy and precision of different methods used to obtain the data. As shown in this Table, the most probable range for ε'' is 12 ± 1 at 3GHz and 11.50 ± 1 at 2.8GHz. It is, therefore, reasonable to believe that the value of ε' for water in Table 2 is within $\pm1\%$ of the actual value, and that of ε'' within $\pm5\%$ (taking $\varepsilon''=11.5$). Since Risman checked the dielectric values of other calibrating liquids in the same way as that of water (by using a TM_{010} cavity), it is accepted that in the worst case ε' and ε'' in Table 3 are within $\pm5\%$ of their actual values.

Thus, this method will give about $\pm5\%$ accurate results, for a sample which has its dielectric values close to a calibration liquid. For materials with their dielectric values different than the calibration liquids results within $\pm10\%$ were obtained (more error in ε'') ; a few examples are N/10 NaCl solution (75.9-j18.1) and N-butyl alcohol (3.5-j1.64). For others such as ethylene glycol (12.0-j12.0) the measured values were up to $+20\%$ of those in the literature. However, this comparison itself is inaccurate, because the reference dielectric values are mostly at 3 GHz and never at the resonant frequency of this cavity.

The two sources of error-that from an uncertainty in the dielectric values of the calibrating liquids and that from the calibration procedure - are independent random errors. The total error, therefore, is the quadrature sum of individual errors [124]. If

the error due to calibration procedure is taken as $\pm 10\%$, the total error E_1 is

$$E_1 = \sqrt{(10)^2 + (5)^2} \qquad (2.10)$$

or, $\qquad E_1 = \pm 11.18\%$

This is the upper bound of error in an extreme case. For materials with their dielectric values near calibrating liquids total estimated error, E_2, is

$$E_2 = \sqrt{(5)^2 + (5)^2} \qquad (2.11)$$

or, $\qquad E_2 = \pm 7.07\%$

2.9.2 Precision

The precision of the cavity is estimated to be $\pm 2\%$ for lossy materials. This is illustrated by considering the measurement errors in the case of egg white at $24^\circ C$ in the 4.9mm diameter vial, shown in Table 9. The frequency counter has a resolution of 0.1KHz. As the frequency shift is used to calculate ε', this effect is negligible. For all the measurements, it was always possible to determine the peak transmission of the frequency response to ± 1 MHz with $\Delta f \leq 200$ MHz. The power meter used to measure the transmission through the cavity was calibrated against its internal standard before each series of temperature measurements. The calibration removes the effect of small impedance mismatches of the sensor and its RF losses. The error on the

measurements is then theoretically the uncertainty of the power meter itself, which, according to the manufacturer, is +/- 0.07 dB (relative). The cumulative effect is illustrated in Table 9: if the assumptions are true a precision of +/- 2% on ϵ", +/- 1% on ϵ' when ϵ' is 70, ϵ"=16 is expected. For 16.5-j8.3 a similar calculation gives +/-1.7% for ϵ". At the lower end of the calibration range, i.e., for ϵ'=6, ϵ"=0.4, the precision is ±0.8% for ϵ".

When the dielectric data is required over a wide band of frequencies, a cavity perturbation method serves only a limited purpose. Other frequency domain methods are also not very convenient and time-efficient. For example, to determie the optimum frequency for the design of an applicator for hyperthermia, we may require the dielectric data on a tumor from 13 MHz to 5.88 GHz in the ISM band [10,125]. Similarly, for the determination of the optimum frequency range for selective dielectric heating of insects, control of stored-grain insects, dielectric data on insects, agricultural products were needed in a wide frequency range. For these and other applications of this nature, the time domain methods, discussed in Chapter III, provide a convenient alternative.

Table 4

Relaxation Parameters for Water[a]

T(^{o}C)	ε_∞[b]	$\tau(10^{-11}$s)	$\alpha 10^{-3}$
0	4.46	1.79	14
10	4.10	1.26	14
20	4.23	0.93	13
30	4.20	0.72	12
40	4.16	0.58	9
50	4.13	0.48	13
60	4.21	0.39	11
75	4.49	0.32	--

in: $\varepsilon^*(\omega) = \varepsilon_\infty + (\varepsilon_s - \varepsilon_\infty)/(1+(j\omega\tau)^{1-\iota})$

where: $\varepsilon_s = 87.740 - 0.40008T + 9.398 \times 10^{-4}T^2 - 1.410 \times 10^{-6}T^3$ [121],

τ is the relaxation time and ι is the shape parameter of the Cole-Cole equation.

---

[a] Numerical values from Hasted [110].

[b] The average value of ε_∞ is 4.25; the experimental accuracy of the values of ε_∞ in the table is typically $\pm$ 0.16 [110].

Table 5. Calculated Values of the Dielectric Constant of Water, 0.9-6 GHz, 10-80°C

T °C	ε' A	ε' B	ε' C[d]	δ(nm)[b]	ε" A	ε" B	ε" C[d]	D:integer values[c] ε'	ε"
0.915 GHz									
0	86.62	86.60	86.79	38.70	8.71	8.80	9.08	87	9
20	79.78	79.83	79.61	77.15	4.19	3.92	3.99	80	4
40	73.04	72.99	72.96	130.45	2.37	2.64	1.64	73	3
60	66.75	66.77	66.75	202.76	1.46	1.37	2.01	67	1
2.45 GHz									
0	81.26	81.13	81.16	5.73	24.41	21.60	20.95	81	22
20	78.29	78.61	77.94	11.00	10.8	10.28	11.73	79	10
40	72.49	72.12	72.98	18.50	6.23	6.79	5.99	72	7
60	66.51	66.63	66.29	28.63	3.85	3.66	3.73	67	4
80	----	58.42[e] (61.8)[g]	----		----	2.65[f] (2.8)[g]	----	58	3
100	----	48.98[e] (56.9)[g]	----		----	1.75[f] (2.1)[g]	----	49	2
3.0 GHz									
0	78.56	78.38	78.76		25.19	25.39	24.54	78	25
20	77.49	78.04	77.09		13.09	12.51	14.10	78	13
40	72.20	71.65	72.86		7.58	8.17	7.40	72	8
60	66.38	66.56	66.08		4.70	4.51	4.46	67	5
5.88 GHz									
0	62.34	61.92	62.83	1.24	37.44	37.52	37.63	62	38
20	71.12	72.98	70.39	2.09	23.03	22.78	23.01	73	23
40	69.94	68.68	71.12	3.40	14.06	14.31	13.53	69	14
60	65.37	65.79	65.03	5.15	8.86	8.78	9.22	66	9

0.915 GHz
$\bar{a}'_1 = 86.6375$ $\bar{a}''_1 = 8.62051$
$\bar{a}'_3 = -0.35238$ $\bar{a}''_3 = -0.25323$
$\bar{a}'_5 = 0.00034$ $\bar{a}''_5 = -0.00226$[d]

2.45 GHz
$\bar{a}'_1 = 81.38498$ $\bar{a}''_1 = 21.22351$
$\bar{a}'_3 = -0.13899$ $\bar{a}''_3 = -0.59358$
$\bar{a}'_5 = -0.00185$ $\bar{a}''_5 = 0.00512$

3.0 GHz
$\bar{a}'_1 = 78.74449$ $\bar{a}''_1 = 24.99203$
$\bar{a}'_3 = -0.03103$ $\bar{a}''_3 = -0.68005$
$\bar{a}'_5 = -0.00297$ $\bar{a}''_5 = -0.00576$

5.88 GHz
$\bar{a}'_1 = 62.75847$ $\bar{a}''_1 = 37.35652$
$\bar{a}'_3 = 0.55967$ $\bar{a}''_3 = -0.81893$
$\bar{a}'_5 = -0.00872$ $\bar{a}''_5 = 0.00576$

a ε* values in column C from multiple regression analysis; see Table 6 for regression coefficients. Values in column A from the Cole-Cole equation and parameters given in Table 4.

b Depth at which power is one half of its surface value.

c Integer - value estimates.

d For Column B at each frequency, $\varepsilon'(1) = \bar{a}'_1 + \bar{a}'_3 I + \bar{a}'_5 I^2$ where $\bar{a}'_1$ refers to ε', $\bar{a}''_1$ to ε", etc.

e From the regression model, $\varepsilon'(1) = \bar{a}'_1 + \bar{a}'_3 I + \bar{a}'_5 I^2$.

f Predicted from the rate of change of slope, $d\varepsilon''/dI$.

g From Debye's first order approximation of dielectric dispersion, and from the data measured at 2.8 GHz by Kisman [123].

Table 6

The Multiple Regression Analysis Third Order Polynomial for

ϵ' and ϵ'' for Water

$$\epsilon^* = a_1 + a_2 f + a_3 T + a_4 f^2 + a_5 T^2 + a_6 fT + a_7 f^2 T + a_8 fT^2$$

Regression Coefficients	For ϵ':	For ϵ'':
a_1	90.38934	0.70905
a_2	− 2.53070	9.67392
a_3	− 0.51207	-0.16301
a_4	− 0.33793	-0.57724
a_5	0.00237	0.00285
a_6	0.14718	-0.18456
a_7	0.00565	0.01122
a_8	− 0.00185	0.00061
$S_e{}^a$	0.82	0.76
R^2	0.99	0.99

[a] S_e is the multiple standard error of the estimate, as defined in [122]

[b] R^2 is the coefficient of multiple determination, as defined in [122]

Table 7

Comparison between Experimental and Regressed

Values of ϵ^* for Water at 2.8 GHz

	ϵ'			ϵ''		
$T^{o}C$	Experimental [123]	Hasted [110]	Multiple	Experimental [123]	Hasted [110]	Multiple
0	83.0	79.57	79.65	21.0	23.87	23.27
10	79.7	79.61	78.82	15.0	17.01	17.81
20	78.0	77.80	77.41	11.0	12.28	13.26
30	74.5	75.18	75.45	8.4	9.19	9.62
40	71.9	72.31	72.91	6.6	7.09	6.90
50	69.3	69.30	69.82	5.1	5.67	5.09
60	66.7	66.43	66.16	4.3	4.39	4.19

Table 8

Experimental Values of ε'' for Water, 20–25°C

| Temp. (°C) | ε'' (Experimental) | | ε'' (Estimated)[a] | |
	Freq. (GHz)	Value	Freq. (GHz)	Value
20	3	13.05 [110]	2.8	12.24
20	3	13.0 [107]	2.8	12.20
25	3	12.04 [28]	2.8	11.29
25	3	11.0 [111]	2.8	10.32
			2.8	11.51[b]

[a] Estimated from the Cole-Cole equation

(6.19% less than at 3 GHz)

[b] Average of the four estimated values

Table 9

Possible Error in ϵ^* for Egg White from Measurement

Uncertainities at 24°C, Sample Holder Diameter, 4.9 mm.

Δf (MHz)		ΔT (dB)		ϵ'		ϵ''	
Measured value	Range[a] ± dΔf	Measured value	Range ± dΔT	Measured value	Range (% error)	Measured value	Range (% error)
198.867	197.867	22.35	22.28	69.75	69.01(1.06)	15.85	15.56(1.83)
	199.867		22.42		70.51(1.09)		16.15(1.89)

[a] dΔf: uncertainty in placing resonant frequency marker; dΔT is due to the uncertainty of power meter.

(a)

16.5

140

120

CUOKED
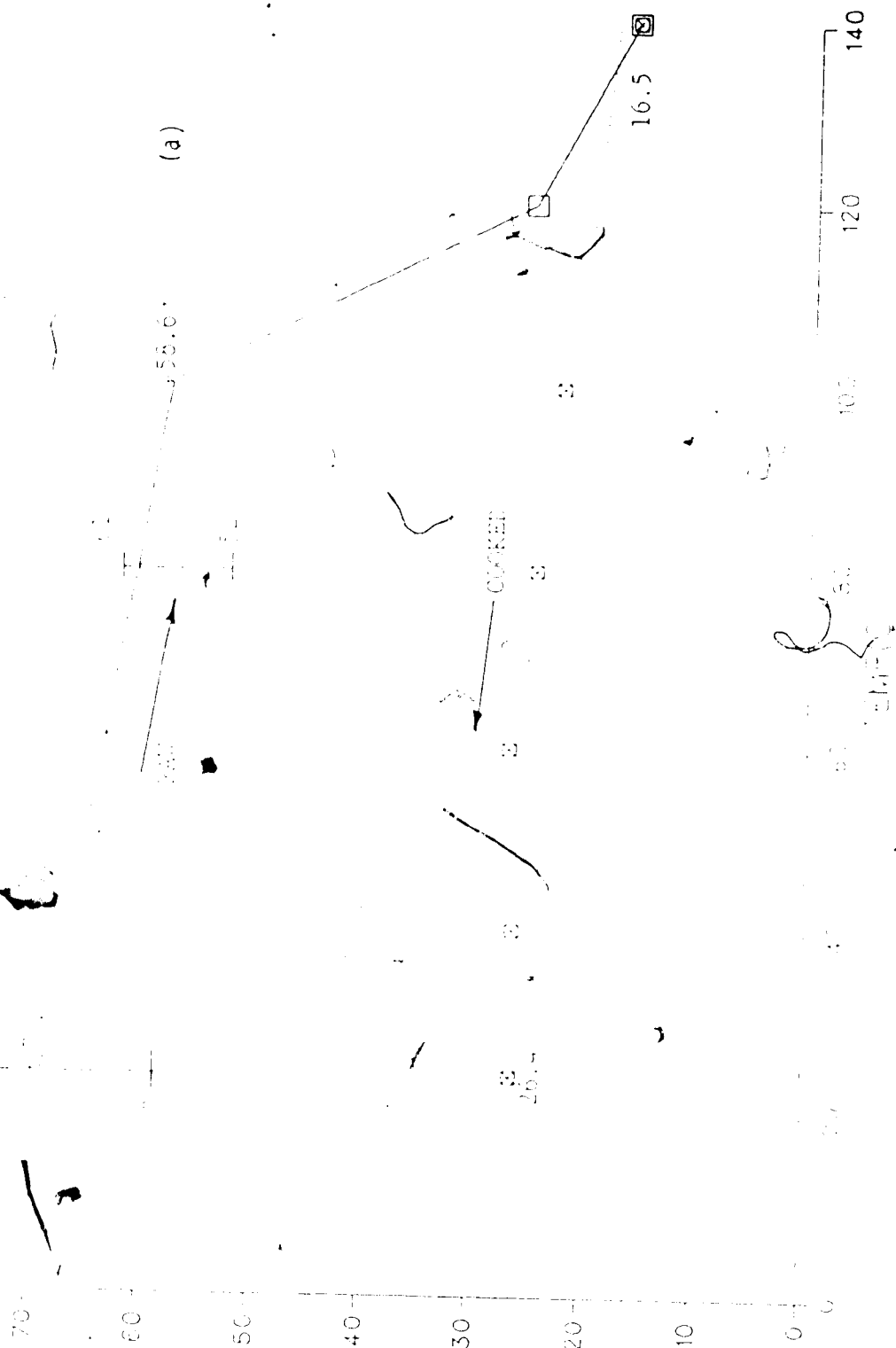
Figure 4(a). Dielectric constant vs. temperature for thin egg white at 2.9 GHz. The arrows indicate the direction of temperature change. Lines are least-square fits to the data points shown; dashed bars show the range of values recorded during work(material variability).
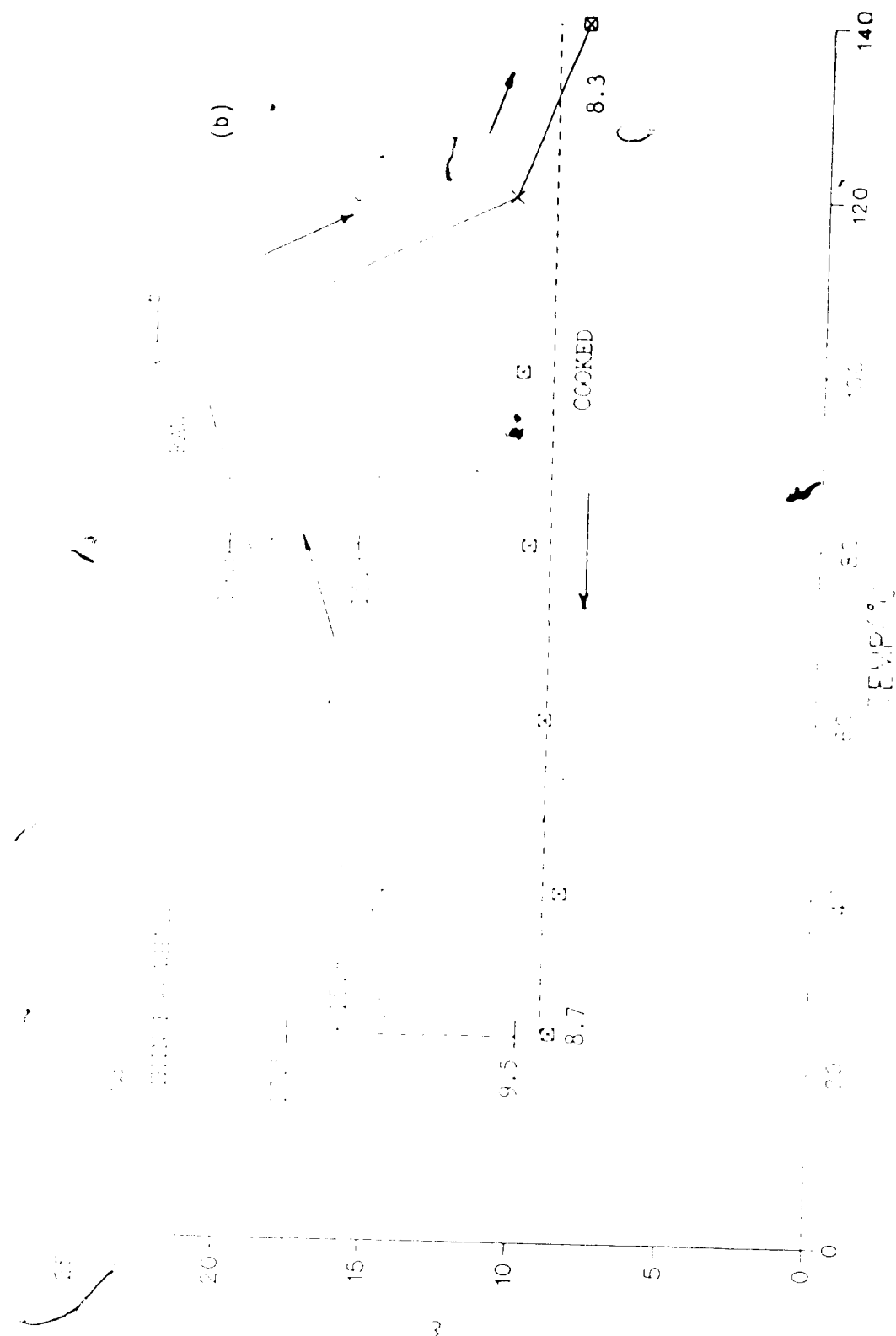
Figure 4(b). Dielectric loss factor vs. temperature for thin egg white at 2.9 GHz. **The arrows indicate the direction of temperature change. Lines are least-square fits to the data points shown; dashed bars show the range of values recorded during the work(material variability).**

Figure 4(c). Dielectric loss tangent vs. temperature for thin egg white at 2.9 GHz. The arrows indicate the direction of temperature change. Lines are least-square fits to the data points shown.
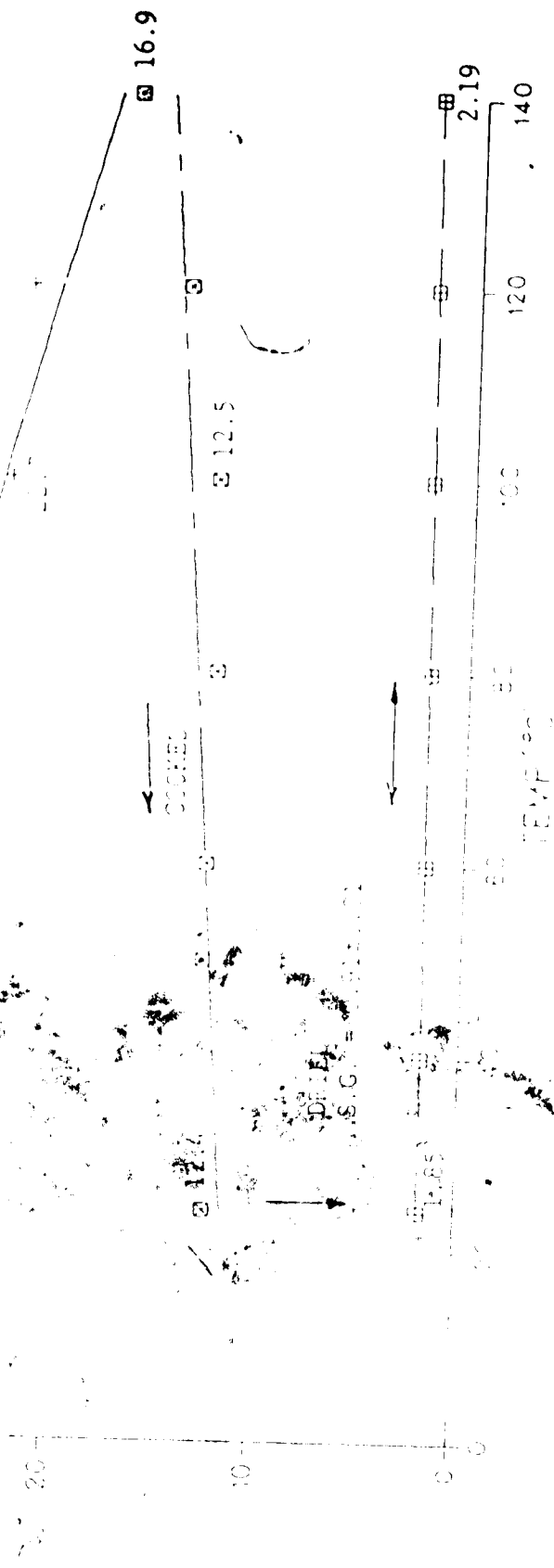
Figure 5(a). Dielectric constant vs. temperature for egg yolk at 2.9 GHz. Data presentation as for Fig. 4(a). Inner bars(solid): ± one sample standard deviation(n=6) for one batch of eggs; outer bars(dashed) show the range of values recorded during the work(material variability).

(b)

6.9

0.16

140

Figure 5(b). Dielectric loss factor vs. temperature for egg-white at 2.9 GHz. Data presentation as for Fig. 4(b). Inner bars(solid): ± one sample standard deviation(n=6) for one batch of eggs; outer bars(dashed) show the range of values recorded during the work(material variability).
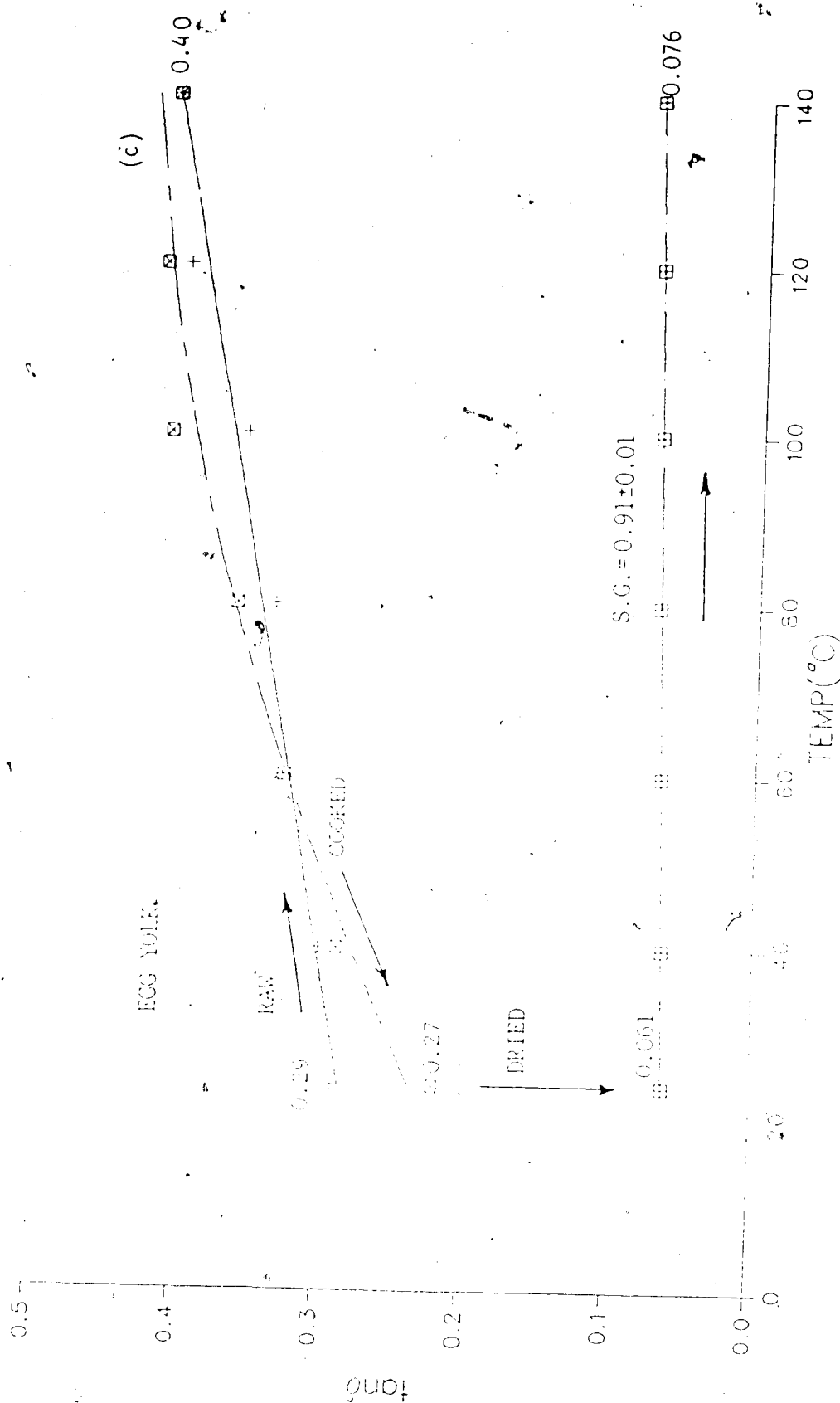
Figure 5(c). Dielectric loss tangent vs. temperature for egg yolk at 2.9 GHz. Data presentation as for Fig. 4(c).
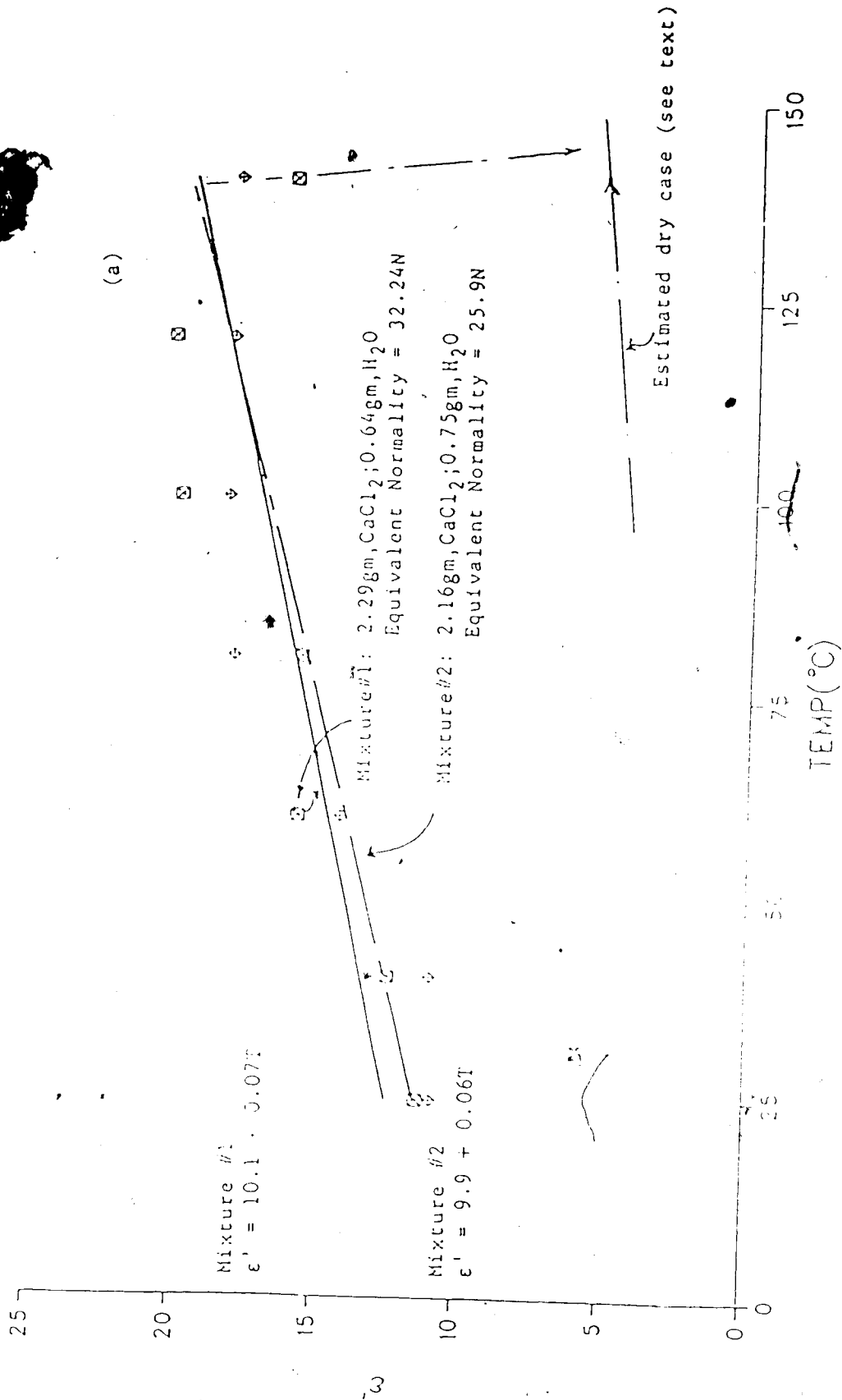
Figure 6(a). Dielectric constant vs. temperature for two (typical susceptor) pastes of CaCl₂ in distilled water at 2.9 GHz. The arrows indicate the direction of temperature change. Extreme-right-hand arrows show the observed trend for T > 140°C. Dry powder values are also shown.
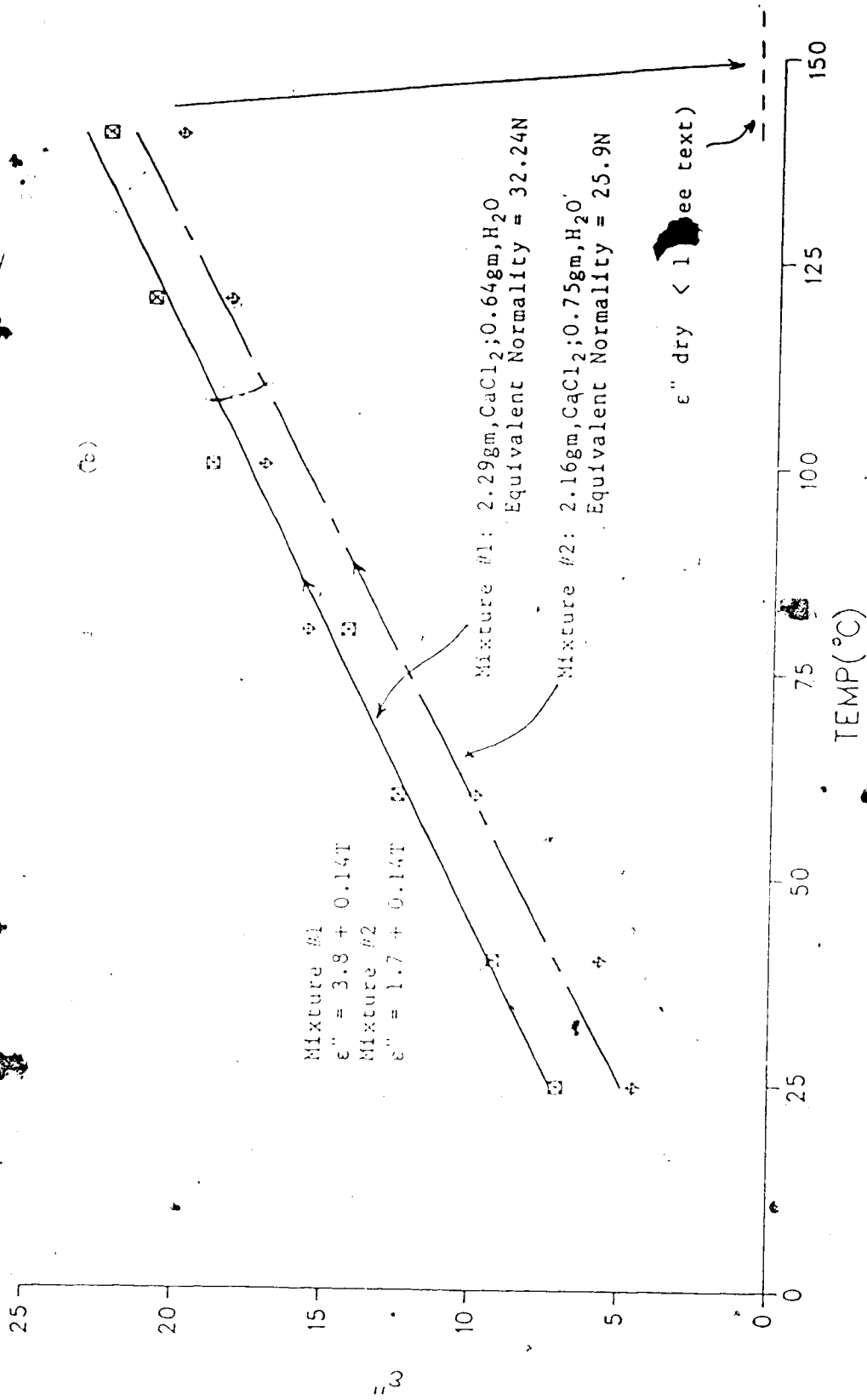
Figure 6(b). Dielectric loss factor vs. temperature for two (typical susceptor) pastes of $CaCl_2$ in distilled water at 2.9 GHz. The arrows indicate the direction of temperature change. Extreme-right-hand arrows show the observed trend for $T > 140°C$. Dry powder values are also shown.

Mixture #1
$\varepsilon'' = 3.8 + 0.14T$
Mixture #2
$\varepsilon'' = 1.7 + 0.14T$

Mixture #1: 2.29gm,$CaCl_2$;0.64gm,H_2O
Equivalent Normality = 32.24N

Mixture #2: 2.16gm,$CaCl_2$;0.75gm,H_2O
Equivalent Normality = 25.9N

ε'' dry < 1 (see text)

TEMP(°C)

52

(a)

$\epsilon' = 18.6 - 0.063T + 0.0006T^2$

$\epsilon' = 1.3 + 0.013T$

TEMP(°C)

20

10

0

ϵ'
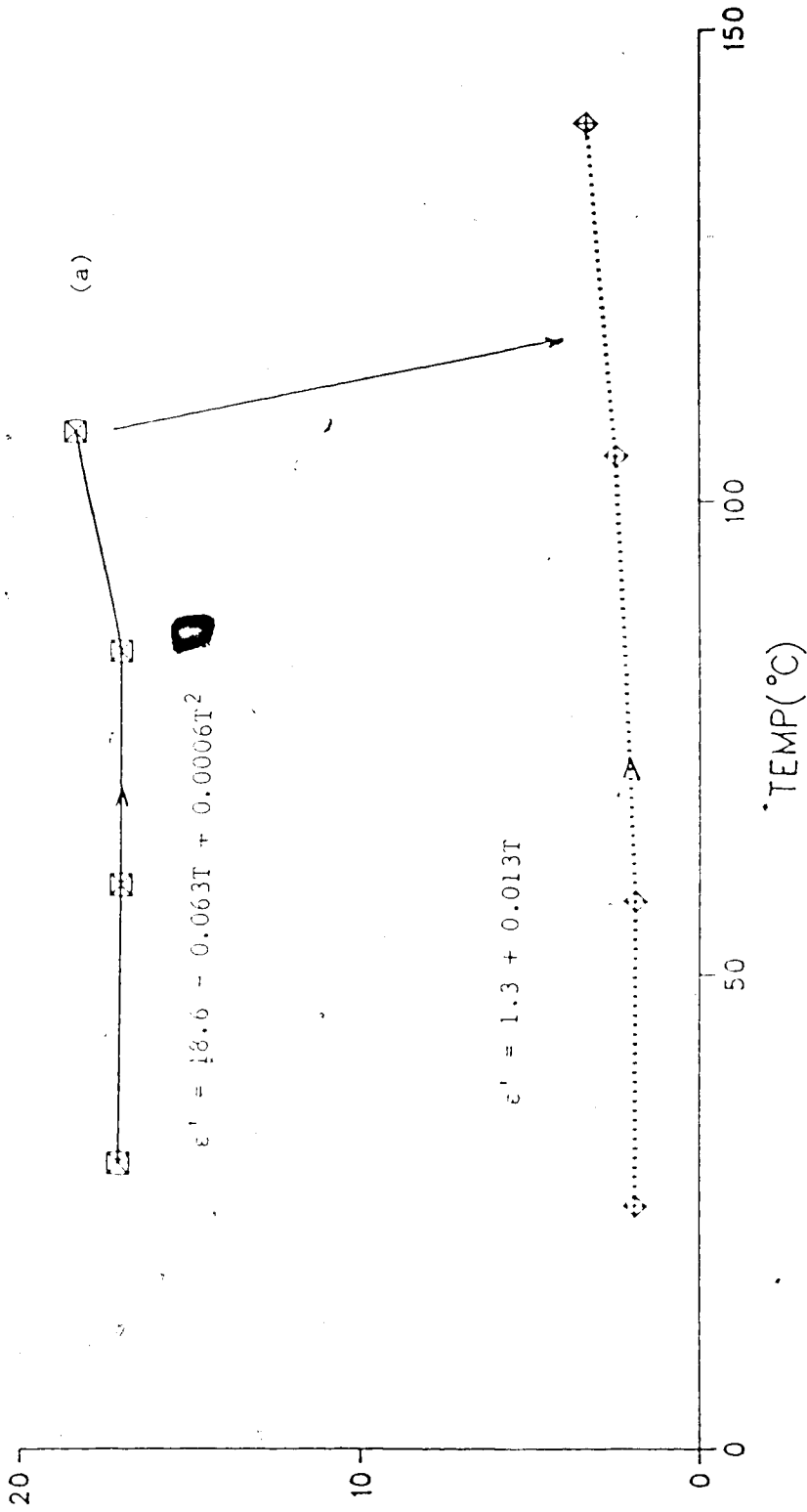
Figure 7(a). Dielectric constant vs. temperature for a commercial Marmite™ paste at 2.9 GHz. Notation as in Figure 6. The dotted curves are for the powder (specific gravity = 0.645) obtained after heating Marmite in a 700 W microwave oven for 1 minute.

(b)

$\varepsilon'' = 3.8 + 0.045T$

TEMP(°C)

ε''
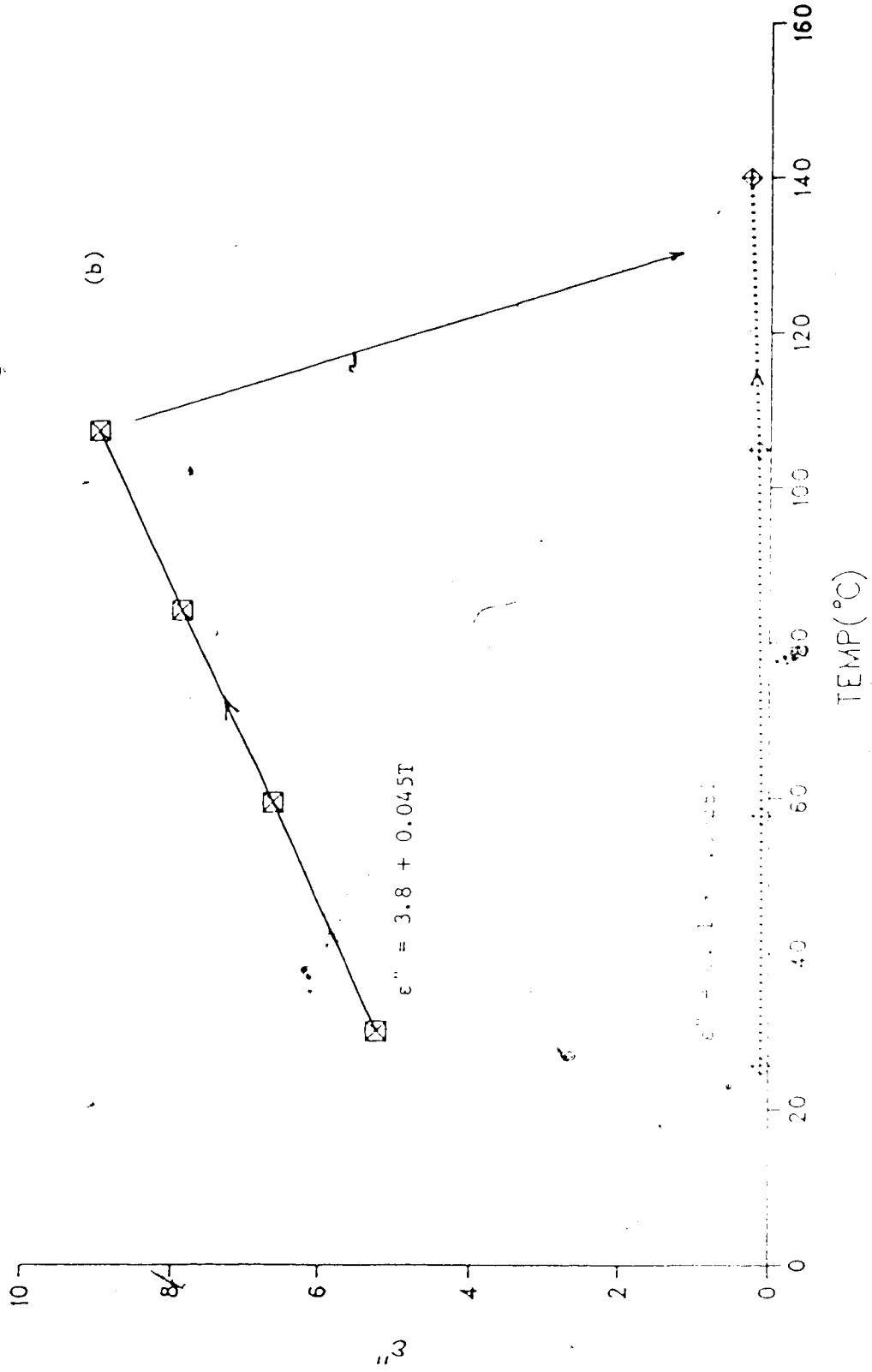
Figure 7(b). Dielectric loss factor vs. temperature for a commercial Marmite[TM] paste at 2.9 GHz. Notation as in Figure 6. The dotted curves are for the powder (specific gravity = 0.645) obtained after heating Marmite in a 700 W microwave oven for 1 minute.

(a)

TEMP(°C)

ε'
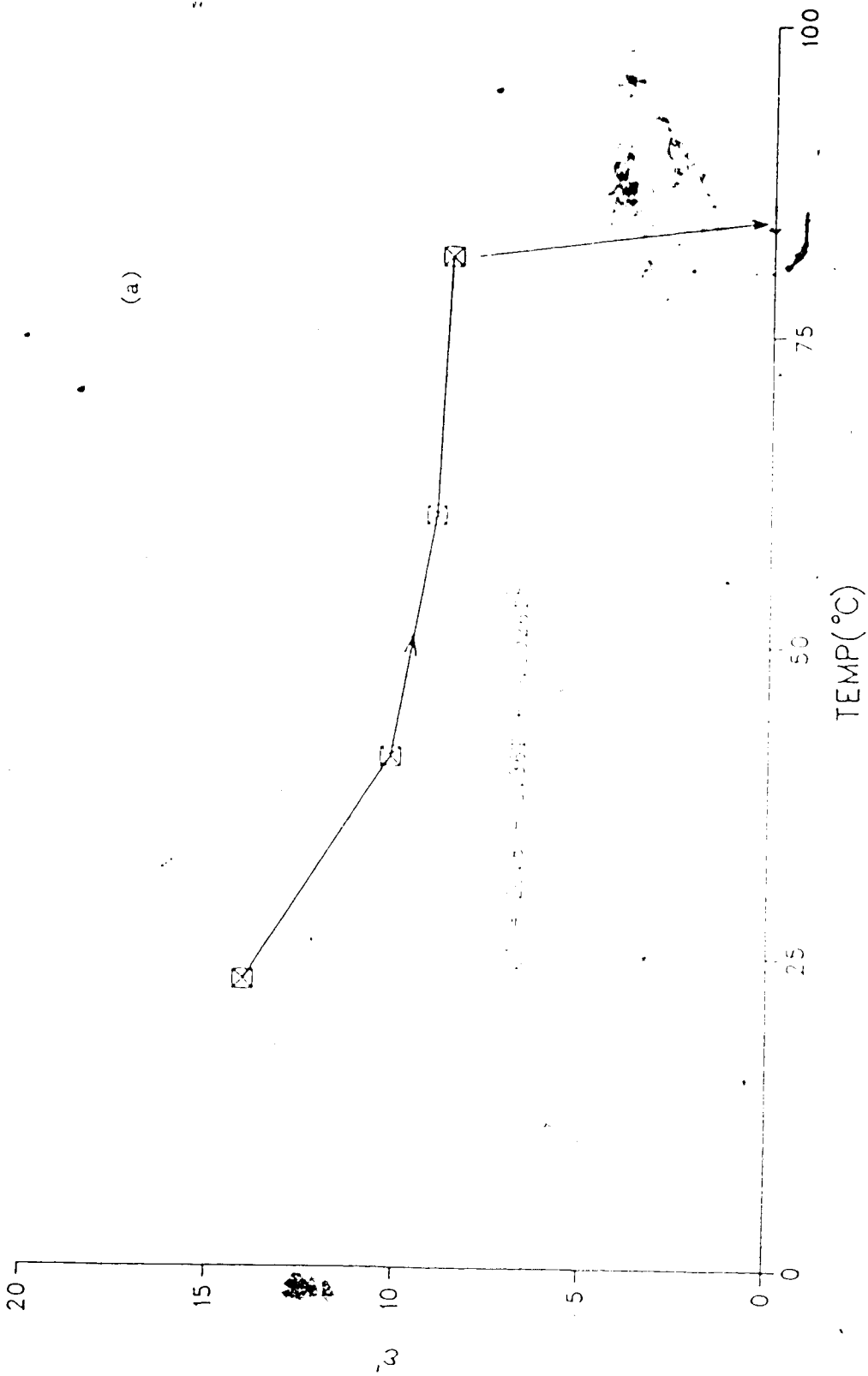
Figure 8(a). Dielectric constant vs. temperature for a Crosse and Blackwell Browning^{TM} at 2.9 GHz. Notation as in Fig. 6.

(b)

$\epsilon'' = 7.2 - 0.057T + 0.0012T^2$

TEMP(°C)

25   50   75   100

15   10   5   0

ϵ''

Figure 8(b). Dielectric loss factor vs. temperature for a Crosse and Blackwell Browning™ at 2.9 GHz. Notation as in Fig. 6.
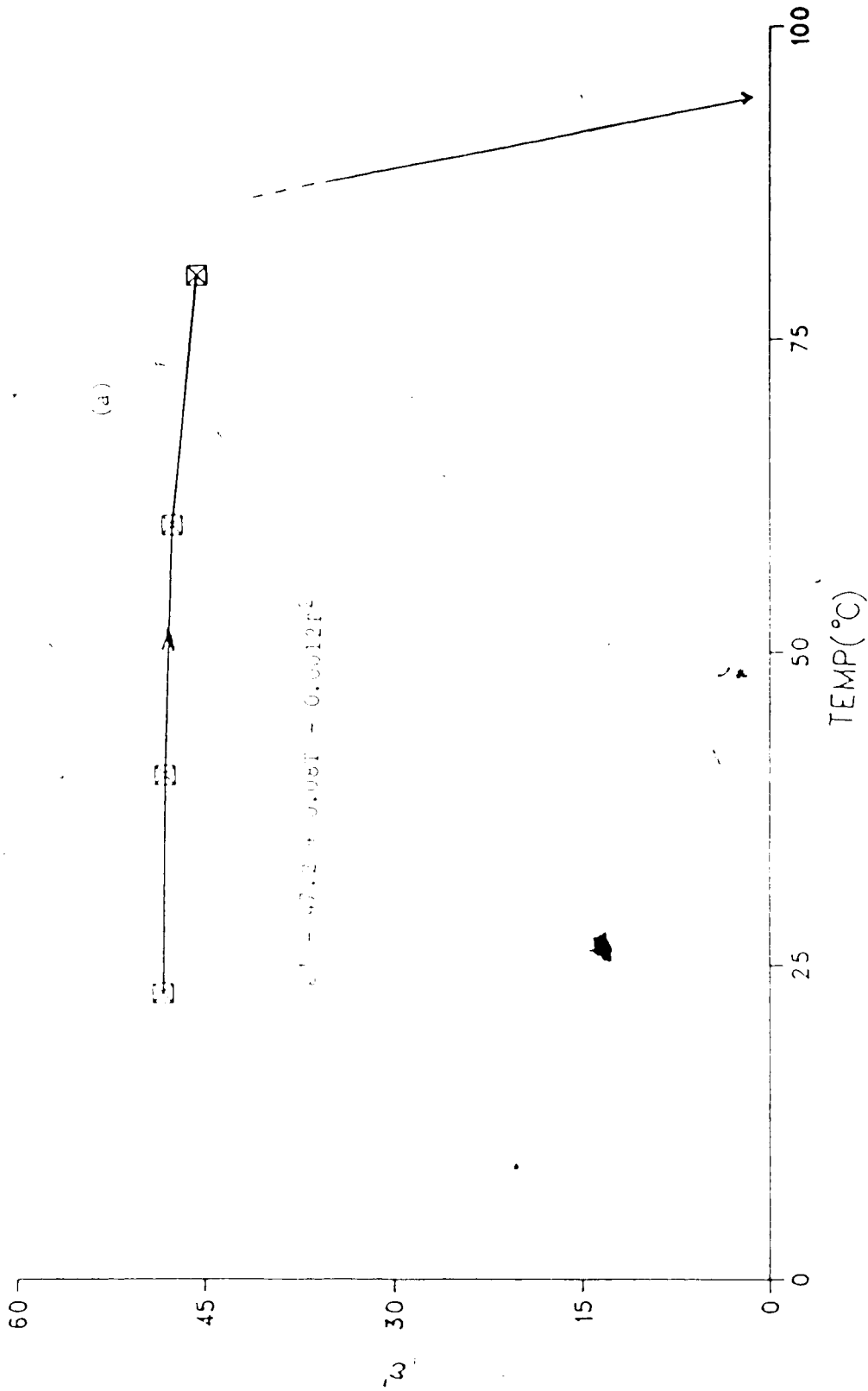
Figure 9(a). Dielectric constant vs. temperature for Kitchen Bouquet[TM] (a meat and gravy sauce) at 2.9 GHz. Notation same as in Fig. 6

$\epsilon'' = 20.5 - 0.21T + 0.0014T^2$

TEMP($^{\circ}$C)

Figure 9(b). Dielectric loss factor vs. temperature for Kitchen Bouquet™ (a meat and gravy sauce) at 2.9 GHz. Notation same as in Fig. 6

(a)

A to B:

$\epsilon' = 1.11 + 0.17T - 0.0016T^2$

B to C:

$\epsilon' = 0.73 + 0.0081T$

$\epsilon' = 0.96 + 0.018T$

TEMP(°C)

ϵ'
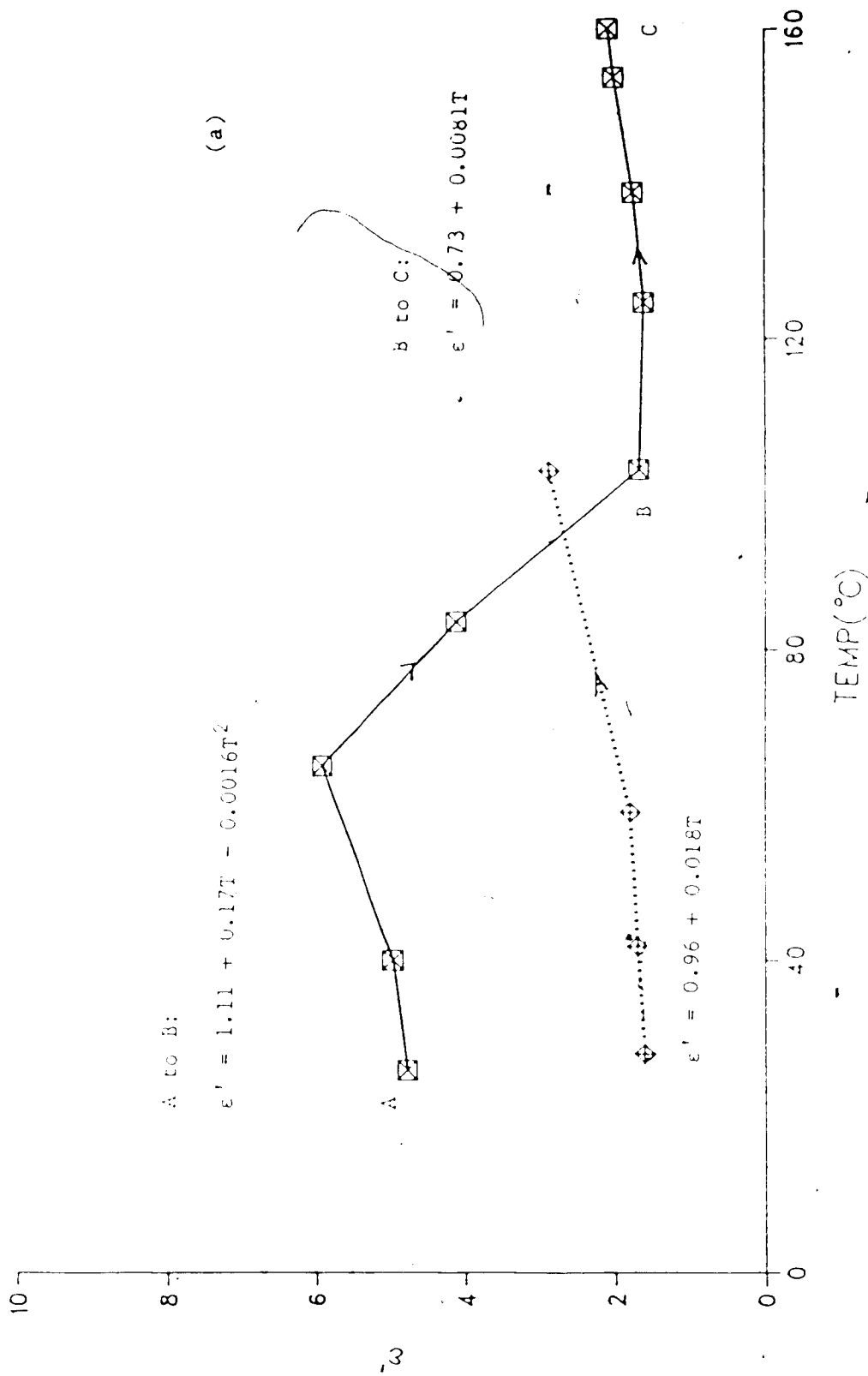
Figure 10(a). Dielectric constant vs. temperature for a thick paste of sugar and ethanol at 2.9 GHz, constituents in percent by weight: sugar, 71.3%; ethanol, 28.7%; specific gravity =1.412. Dotted curve for the powder obtained after heating the above solution in a 700W microwave oven for 5minutes. The arrows indicate the direction of temperature change.

(b)

B to C:

$\varepsilon'' = 0.018 + 0.00072T$

A to B:

$\varepsilon'' = 0.55 + 0.027T - 0.00032T^2$

$\varepsilon'' = 0.035 + 0.0011T$
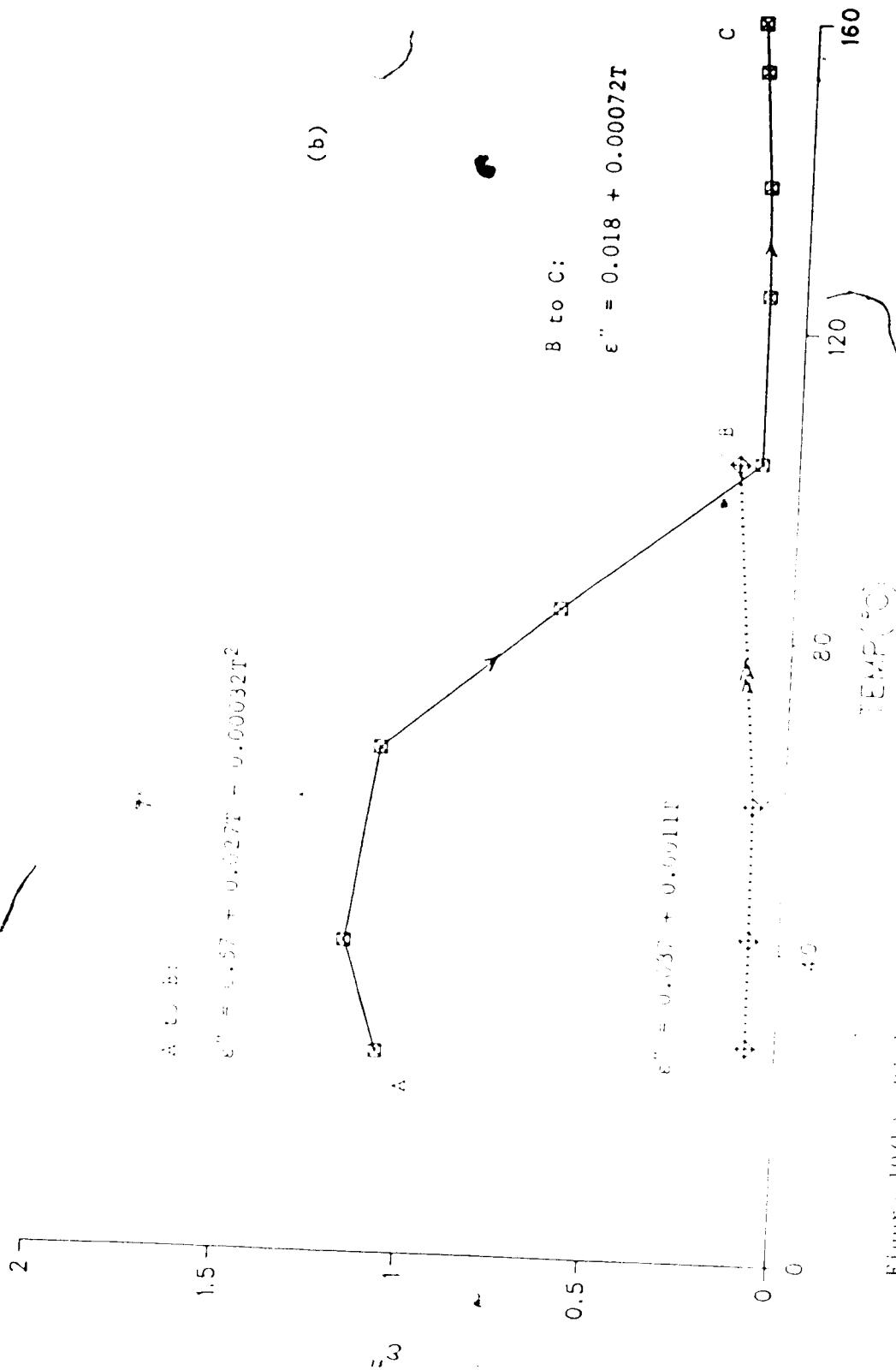
Figure 10(b). Dielectric loss factor vs. temperature for a thick paste of sugar and ethanol at 2.9 GHz, constituents in percent by weight: sugar, 71.3%; ethanol, 28.7%; specific gravity ~1.412. Dotted curve for the powder obtained after heating the above solution in a 700W microwave oven for 5 minutes. The arrows indicate the direction of temperature change.
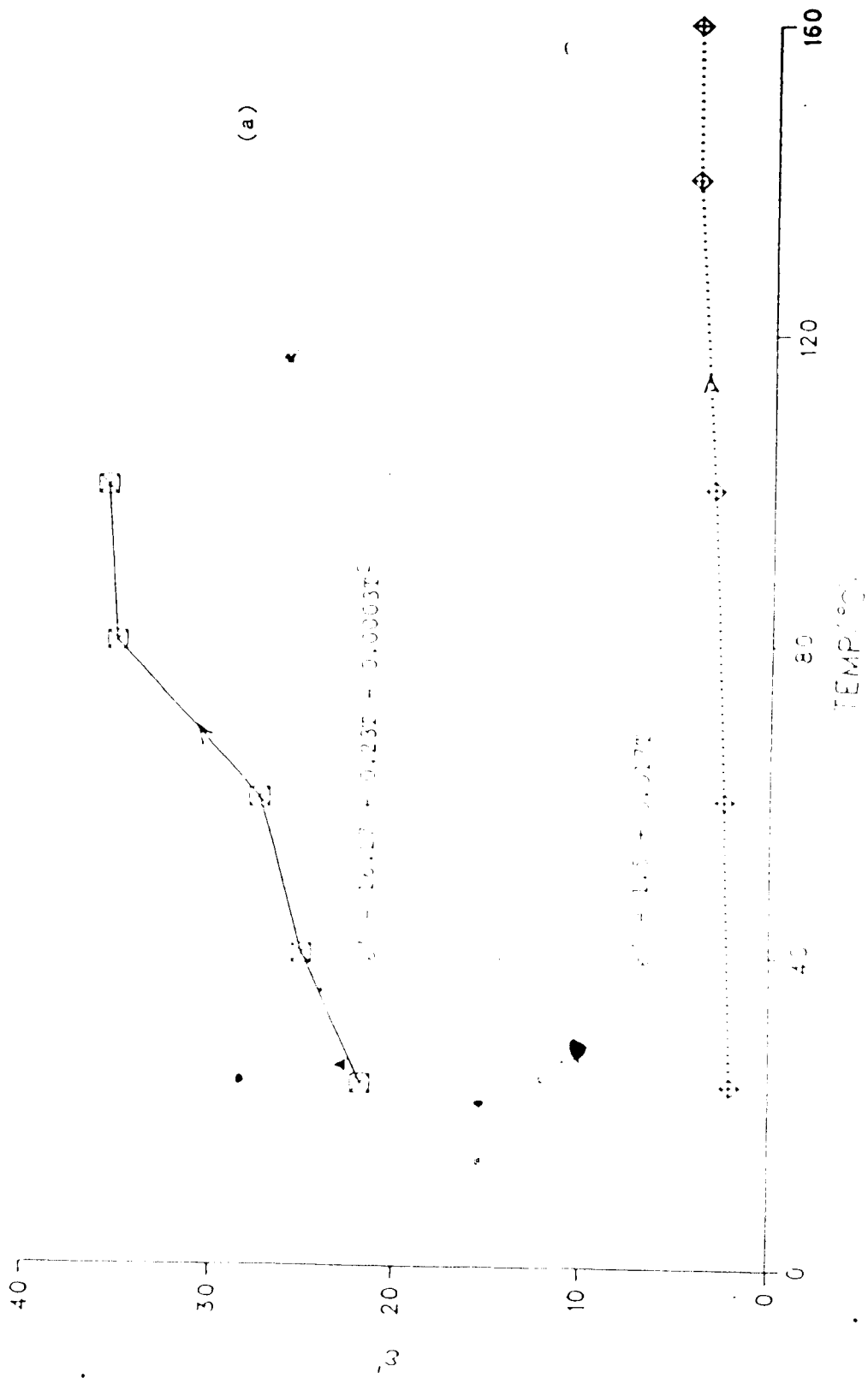
Figure 11(a). Dielectric constant vs. temperature for a thick solution of sugar and distilled water at 2.9 GHz in percent by weight: sugar, 66.6%; distilled water, 33.4%; specific gravity = 1.480. The dotted curves are for the powder (specific gravity = 0.775) obtained after heating the above solution in a 700W microwave oven for 5 minutes.
▲ Roebuck's values for a sucrose mixture of identical concentration at 3.0 GHz and 25°C.

61

Figure 11(b). Dielectric loss factor vs. temperature for a thin solution of sugar and distilled water at 2.9 GHz, in percent by weight: sugar, 66.6%; distilled water, 33.4%; specific gravity = 1.450. The dotted curves are for the powder (specific gravity = 0.775) obtained after heating the above solution in a 700 W microwave oven for 5 minutes. Roebuck's values for a sucrose mixture of identical concentration at 3.0 GHz and 25°C.
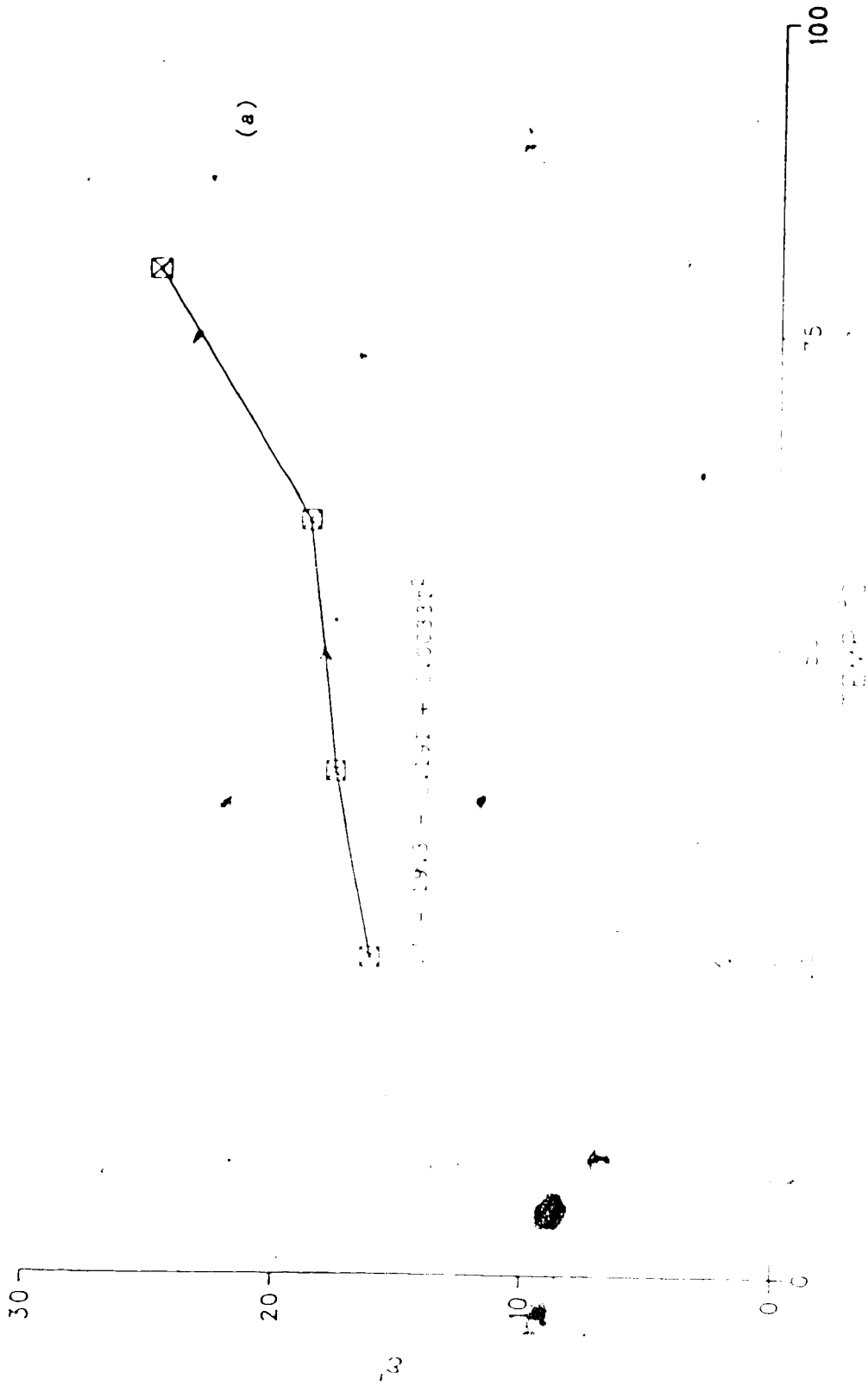
Figure 1? (a). Dielectric constant vs. temperature for a solution of sugar, distilled water and ethanol at 2.9 GHz. constituents in percent by weight: 30 sugar, 36.5 distilled water, and 28.5 ethanol.

(b)

$\varepsilon'' = 8.1 + 0.028T$

TEMP(°C)

ε''

0   25   50   75   100

0   5   10   15

Figure 12 (b). Dielectric data for a solution of sugar, distilled water and ethanol at 2.9 constituents in percent by weight: 36% sugar, 35.5% distilled water, and 28.5% ethanol.

$\varepsilon' = 1.8 + 0.24T - 0.0006T^2$

(a)

TEMP(°C)
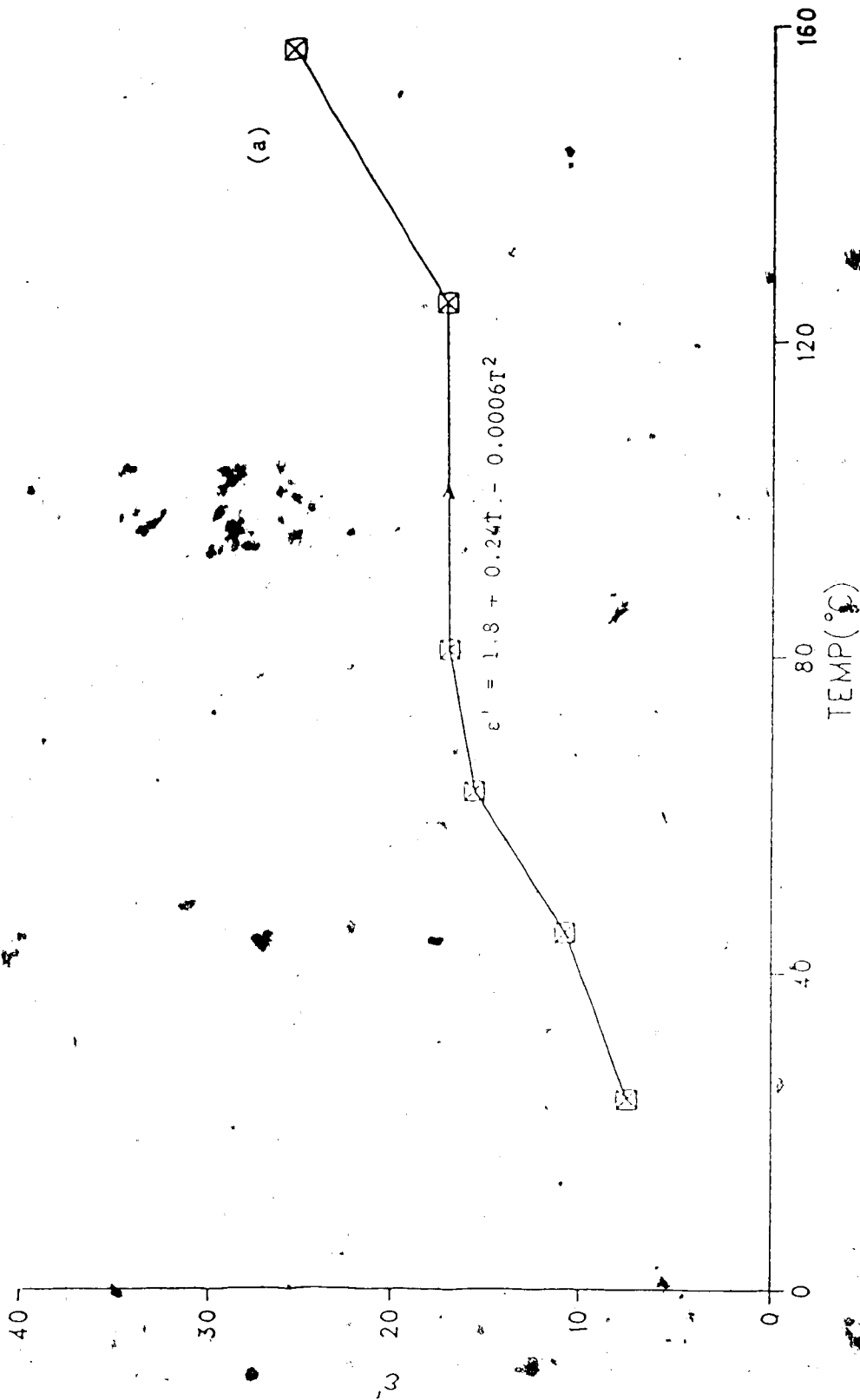
Figure 13 (a). Dielectric constant vs. temperature for a thick mixture of honey (10 ml), glycerin (10 ml) and sodium chloride (1 g) at 2.9 GHz.

$$\varepsilon'' = -1.3 + 0.15T - 0.00056T^2$$

(b)

TEMP(°C)
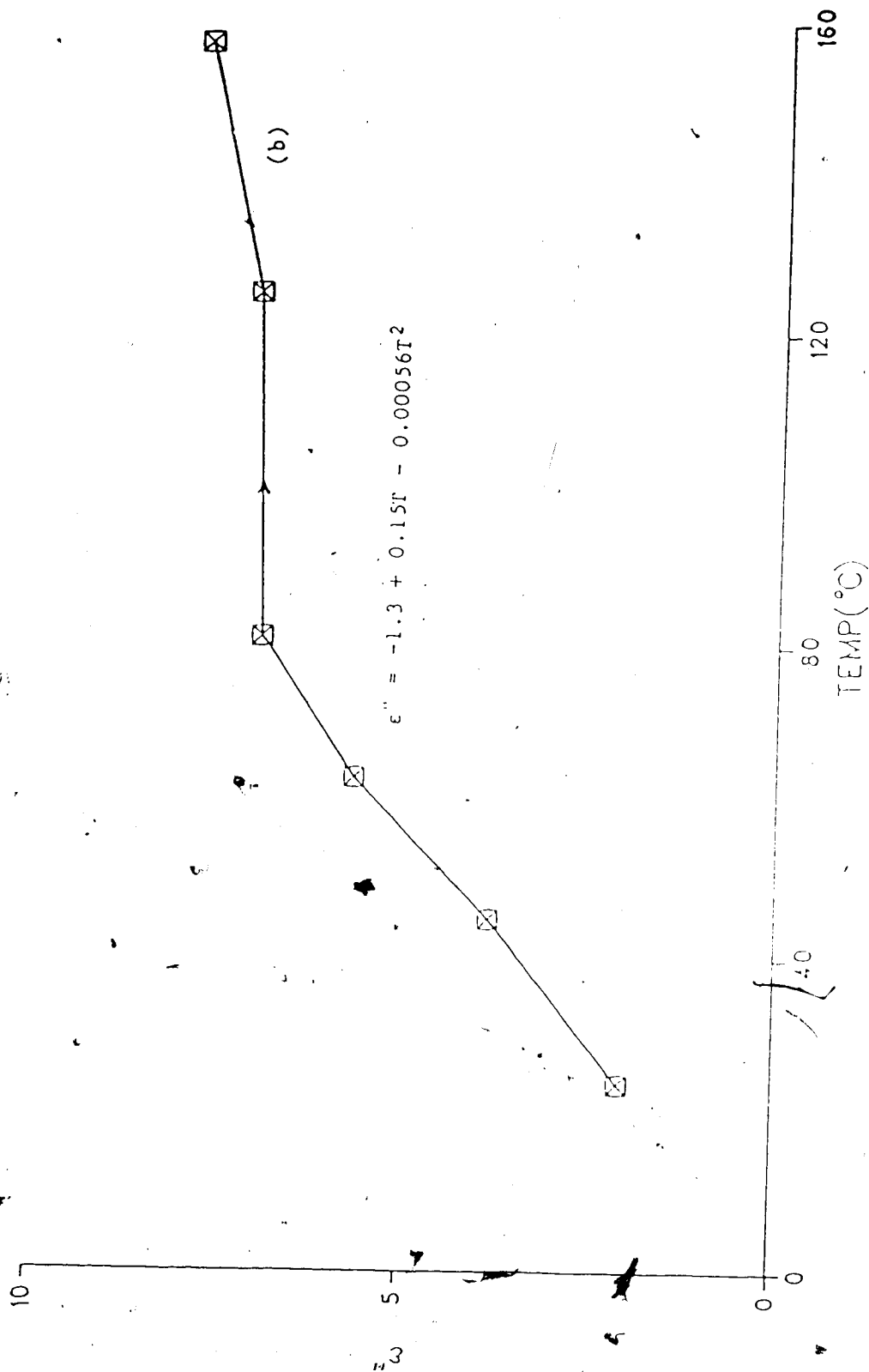
Figure 13 (b). Dielectric loss factor vs. temperature for a thick mixture of honey (10 mL), glycerin (10 mL) and sodium chloride (1 g) at 2.9GHz.

CHAPTER III

Time Domain Methods

Time domain methods for dielectric measurements offer three distinct advantages over frequency domain methods. First, time domain methods are inherently of wide bandwidth as compared to the traditional frequency domain methods (waveguide and cavity perturbation methods). For example, in the waveguide technique, at least four waveguide systems are needed to measure dielectric properties over 1 to 10 GHz, along with samples of different shapes and sizes compatible with the waveguide dimensions for different bands (L-,S-,C- and X-bands). Second, the time required for performing a time domain measurement valid over a wide range of frequencies is considerably less than that required for multiple frequency domain measurements. Thus time domain methods are more suitable for materials whose characteristics may not remain constant over a period of time, such as some biological materials. Third, the instrumentation required for time domain methods requires less capital investment as compared to an automated network analyzer.

Time domain methods for dielectric measurements can be divided into two broad categories: reflection methods and transmission methods. Initially, reflection methods were used in electrical engineering for the testing of transmission lines and these techniques are called "Time Domain Reflectometry" (TDR) [126,127]. Later, transmission methods were used by Sugget [128] and van Gemert [129] for dielectric measurements. Both the reflection and transmission techniques are collectively known as "Time Domain Spectroscopy" (TDS).

For dielectric measurements, most workers have preferred.

67

reflection methods to transmission methods. A comprehensive review of different variations on the time domain reflection and transmission methods has been given by van Gemert [129]. Of the few who have used the transmission method only Gestblom [130] has given quantitative experimental results. The dielectric constants for six liquids are measured using all of the three variations for the transmission method described by van Gemert [129], and the results are compared with the published data [57,89].

3.1 THEORY

In time domain methods, a steplike waveform (resembling an ideal step) is propagated in a low-loss coaxial line containing a section filled with the unknown dielectric sample. For a lossless line, the shape of the input step waveform, $v_i(t)$, remains unchanged as long as the characteristic impedance of the line remains constant with respect to the location along the line. Accordingly, when the step waveform meets the section filled with the dielectric material, the waveform is partially reflected $[v_{r1}(t)]$ and partially transmitted $[v_{t1}(t)]$, where $v_{r1}(t)$ and $v_{t1}(t)$ are respectively the amplitudes of the first reflected and transmitted waves. The waveshape of these reflected and transmitted waves can be analyzed to provide values for the dielectric constant of the material over a wide range of frequencies.

The Single Reflection Method (SRM) is based on a study of the first reflected pulse, $v_{r1}(t)$. The equation for the reflection coefficient in the frequency domain is

$$\rho(j\omega) = \frac{F[v_{r1}(t)]}{F[v_i(t)]} \ , \qquad (3.1)$$

where $F[v_{rl}(t)]$ and $F[v_i(t)]$ are respectively the Fourier transforms of the time domain waveforms (WFMs) $v_{rl}(t)$ and $v_i(t)$ and ω is the angular frequency of measurement. From transmission line theory, the reflection coefficient at the air-dielectric interface is given as

$$\rho(j\omega) = \frac{1-\sqrt{\varepsilon^*(j\omega)}}{1+\sqrt{\varepsilon^*(j\omega)}} \qquad (3.2)$$

where $\varepsilon^*(j\omega)$, the complex dielectric constant of the dielectric sample be obtained from Equations 3.1 and 3.2.

The Single Transmission Method (STM) is based on a study of the first transmitted pulse, $v_{t1}(t)$. The equations for the transmission coefficient in the frequency domain are:

$$T_1(j\omega) = \frac{F[v_{t1}(t)]}{F[v_i(t)]} \qquad (3.3)$$

and

$$T_1(j\omega) = \frac{4\sqrt{\varepsilon^*(j\omega)}}{[1+\sqrt{\varepsilon^*(j\omega)}]^2} \exp\frac{-j\omega\ell}{c}\{\varepsilon^*(j\omega)-1\} \qquad (3.4)$$

where ℓ is the length of the dielectric sample and c is the velocity of light in free space. Gestblom [130] has described Equation 3.4. Note that $\varepsilon^*(j\omega)$ can be determined from an implicit solution of Equations 3.3 and 3.4.

The Multiple Transmission Method (MTM) is based on the comparison of the totally transmitted signal, $v_t(t)$ with the incident signal $v_i(t)$. The total transmission coefficient at a frequency ω through a

sample of length ℓ is given by [130]

$$T_t(j\omega) = \frac{F[v_t(t)]}{F[v_i(t)]}$$

(3.5)

and

$$T_t(j\omega) = \frac{(1-\rho^2)\exp\left\{\frac{-j\omega\ell}{c}\sqrt{\varepsilon^*(j\omega)}\right\}}{1-\rho^2\exp\left\{\frac{-2j\omega\ell\sqrt{\varepsilon^*(j\omega)}}{c}\right\}}$$

(3.6)

Again, note that $\varepsilon^*(j\omega)$ can be determined from an implicit solution of Equations 3.5 and 3.6.

In the above analysis, the effect of connectors at the ends of the sample has been neglected. Although precision 7-mm connectors were used, (connectors C_1 and C_2 in Fig. 14), these do have a finite reflection coefficient which tends to increase with use. Strictly speaking, therefore, the transfer function of a sample holder is made up of three components as shown in Fig. 14; H_{C_1} and H_{C_2} are the transfer functions of the connectors and H is the transfer function of the section filled with dielectric material. $V_i(j\omega)$ is the Fourier transform of the incident waveform and $V_0(j\omega)$ is the Fourier transform of the waveform at the far end of the sample holder. If two sample holders of lengths ℓ_1 and ℓ_2 are chosen, and the ratio of the transform of transmitted WFM's through two samples of different length are studied then the method is called the ratio method [131]. If $V_{01}(j\omega)$ and $V_{02}(j\omega)$ are the Fourier transforms of the first transmitted waveforms, $v_{t1}(t)$ and $v_{t2}(t)$, at the far end of the sample holders of lengths ℓ_1 and ℓ_2, the equations for the singly-transmitted wave are

$$\frac{V_{01}(j\omega)}{V_i(j\omega)} = H_{c_1}(j\omega)H_{\ell_1}(j\omega)H_{c_2}(j\omega) \tag{3.7}$$

$$\frac{V_{02}(j\omega)}{V_i(j\omega)} = H_{c_1}(j\omega)H_{\ell_2}(j\omega)H_{c_2}(j\omega) \tag{3.8}$$

and

$$\frac{V_{01}(j\omega)}{V_{02}(j\omega)} = \frac{H_{\ell_1}(j\omega)}{H_{\ell_2}(j\omega)} = \exp\frac{-j\omega(\ell_1-\ell_2)\sqrt{\varepsilon^*(j\omega)}}{c} \tag{3.9}$$

Since $v_{t1}(t)$ and $v_{t2}(t)$ are the initial transmitted waves through the sample holders of lengths ℓ_1 and ℓ_2

$$\frac{V_{01}(j\omega)}{V_{02}(j\omega)} = \frac{F[v_{t1}(t)]}{F[v_{t2}(t)]} \tag{3.10}$$

where again it is noted that $\varepsilon^*(j\omega)$ can be computed by an implicit solution of Equations 3.9 and 3.10.

Theoretically the ratio method should give more accurate results than STM or MTM, because for the forward travelling wave the effect of the discontinuities at the interface of the coaxial cable and the connectors of the sample holder is removed. Although this method was first suggested by Loeb [131], not many results obtained using this method appear to have been published. Some experimental results, using this method, are presented in this thesis.

A problem inherent in the time domain method using steplike excitation arises when transforming the time domain data to the frequency domain. This problem is defined in Figure 15 [132]. The

time domain method provides a limited-duration time domain data set shown in Figure 15(a). Taking the FFT of this data set gives the spectrum for the periodic version of Figure 15(a) namely of Figure 15(b) and not the spectrum for the steplike TDR signal shown in Figure 15(c). There are two approaches to deal with the above problem: (a) Use of window functions, (b) Other techniques. Harris [133] has given an excellent review on the use of window functions. However, window functions are not suitable for TDR type signals as these attach weights to the data points depending upon their position in the observation window. Another review on alternative spectral estimation techniques has been given by Kay and Marple [134], where the authors have given techniques used in radar, sonar and geoseismological applications.

For TDR signals, Samulon's [135], and Nicholson's method [136] have been used. A discussion on these methods is given by Waldmeyer [137], and Shaarawi [138]. For this work, the Extended Function Fast Fourier Transform (EF-FFT) method proposed by Cormack and Binder [132] has been used. With the help of an example, these authors have proved that the EF-FFT technique gives results closer to reality than those obtained from the use of either Nicholson's method [136] or the Hanning window.

3.2 EXPERIMENTAL APPARATUS AND PROCEDURE

The experimental apparatus is shown in Fig. 16. It consists of a Tektronix 7854 oscilloscope, 7S12 TDR/Sampler Plug-in, S-52 Pulse Generator Head and a S-4 Sampling Head; both have a rise time of 25ps or less. Thus the rise time of the pulse at the output of the sampler is 35 ps or less. The sample holder containing the dielectric liquid being measured is connected between the pulse generator and the

sampling head. Both coaxial and stripline geometries were used; both provide TEM propagation. Four coaxial-line sample holders (mechanically identical to HP precision line model 11566A) of lengths 17, 9, 6 and 3.5 cm were used. The strip line sample holder was 1 cm long. Precision 7-mm connectors were used at the ends of the sample holders. The plastic beads in these connectors provided a leak-tight seal at each end for all organic liquids except those such as monochlorobenzene which dissolved these beads. These liquids could have been used if the plastic beads had been replaced with a ceramic material. Different sample holder lengths were required to maximize measurement accuracy for different liquids at different frequencies. For example, for lossy liquids (like methanol) accurate results around 10GHz were obtained using a 1cm sample holder whereas at 3GHz a longer sample holder such as 3.5 cm was needed.

The measurement procedure is simple and straightforward. Initially the empty sample holder is connected to the TDR and the desired waveform - either first transmitted wave or the multiply transmitted wave - is stored in the oscilloscope, and called the input waveform (IN WFM). The material to be measured is then poured into the sample holder and again the transmitted waveform through the sample holder is stored in the oscilloscope. This is called the output waveform (OUT WFM). The system transfer function is thus given as F[(OUT WFM)]/F[(IN WFM)] where F denotes the Fast Fourier Transform operator. Each stored waveform consists of an array of 1024 waveform values, each value corresponding to the waveform amplitude at one of the 1024 equally spaced points along the time axis of the display. To reduce the effect of random noise, signal averaging over 1000 traces
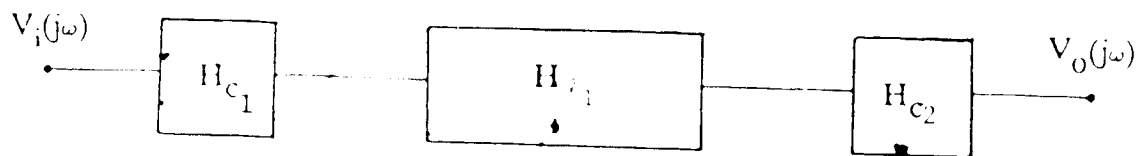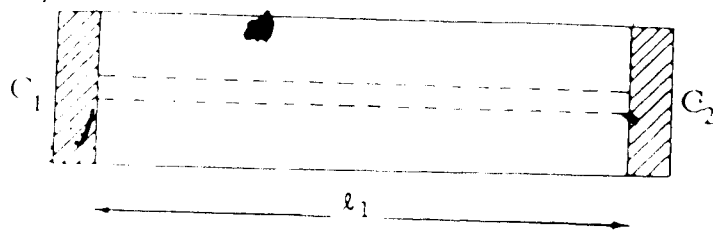
Figure 14. Schematic layout of a coaxial sample holder
and its transfer function

(a) windowed data

$f_2(t)$

0   T   t
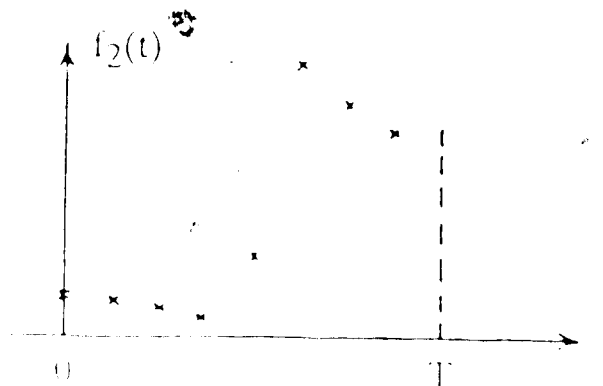
(b) periodic version

0   T   t

(c) TDR version

$f(t)$

$f_2(t)$

0   T   t
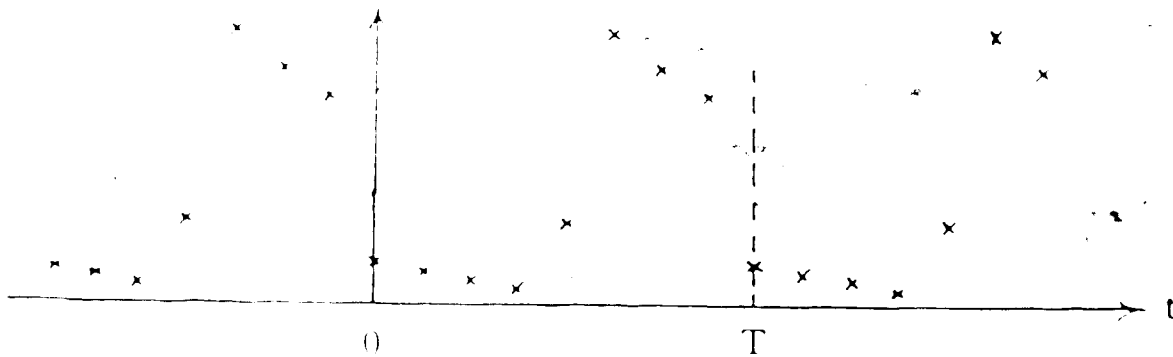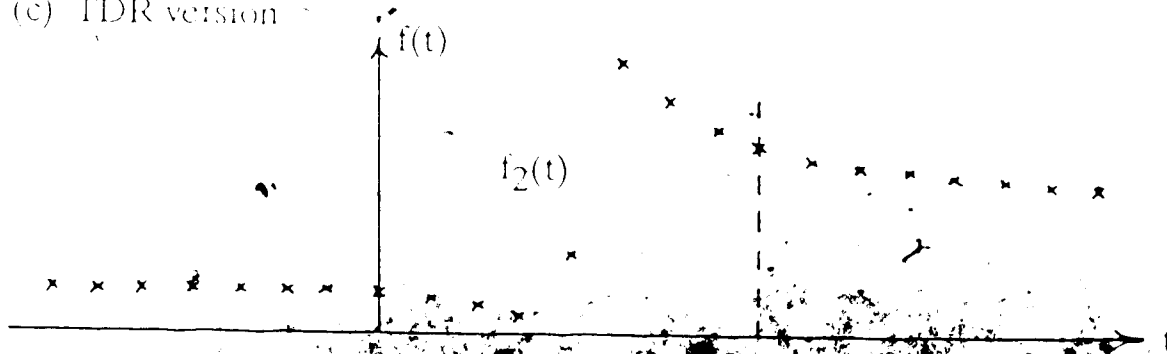
Figure 15. Problem in the transformation of TDR data from the time domain to frequency domain.

Sampling Oscilloscope
(TEK 7854)

Sampling
Head
(S-4)

Pulse
Generator
(S-52)

PC

Sample Holder
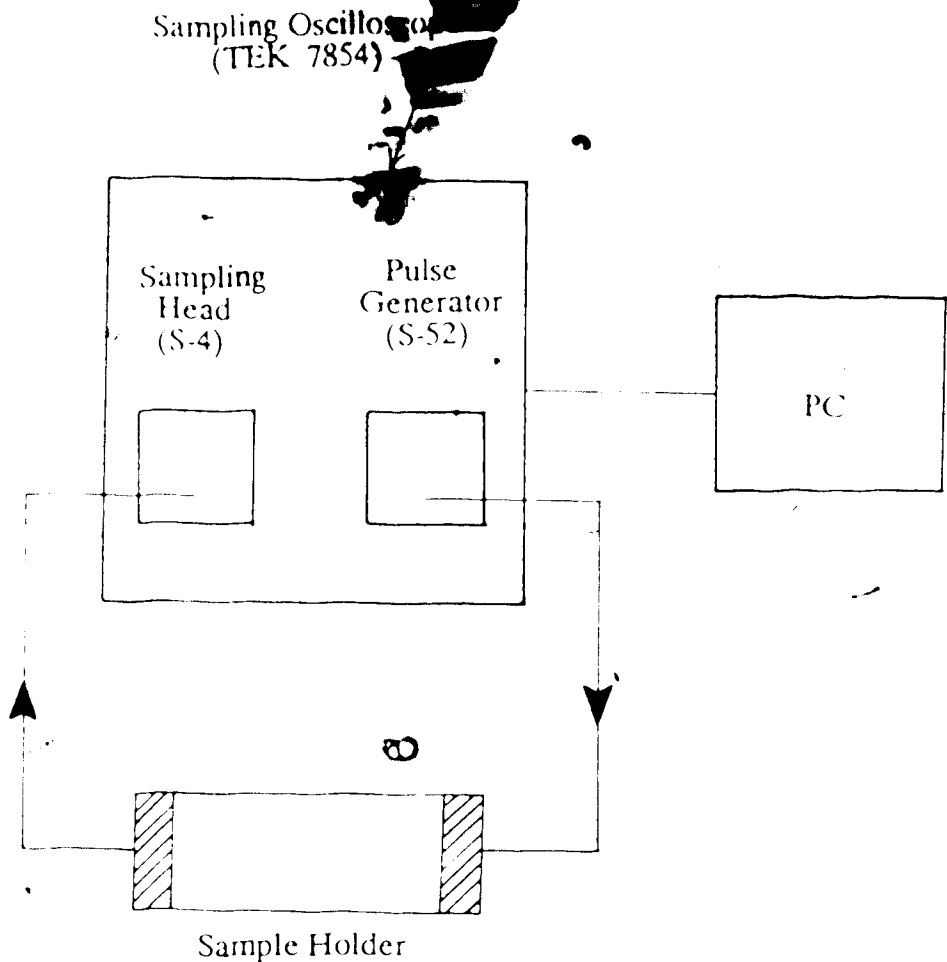
Figure 16. Schematic representation of the experimental setup
for time domain transmission measurements

was used thus improving the S/N ratio by about 30 dB. The factors influencing the sampling requirements for a TDR WFM and thus governing the choice of the time window are given in Section 3.4.

The stored waveforms in the oscilloscope were transferred to a personal computer (PC) with the help of an interactive signal processing program. The PC with suitable software, developed in-house, then computes the Fourier transform of the stored waveforms and the transfer functions given by Equations 3.3, 3.5 or 3.10. (j_ω) is then computed from the transcendental Equation 3.4, 3.6, or 3.9 depending upon whether the STM, MTM or the ratio method was used.

3.3 Sampling Requirements for TDR Waveforms

(i) <u>Desired Spectral Components</u>: The total duration of the time window, T, determines the frequency interval, f, between successive spectral components. Thus

$$T = t.n, \quad \text{and} \quad T = 1/\ f \qquad (3.11)$$

where t is the sample interval and n is the number of samples, chosen as 1024. Therefore, to obtain results at 0 MHz, 10 MHz, etc., T should equal (1.0/1.0E+07) or 100 ns. However, the following factors must also be considered.

(ii) <u>Aliasing</u>: Aliasing occurs when the sampling rate is less than the Nyquist rate. Therefore, the minimum sampling rate for a 35-ps rise-time pulse is about 20 Gsamples/s which implies $t=50$ ps. To be sure of avoiding aliasing, Ramirez [139] suggested a more stringent requirement for sampling at a rate of at least

3 samples per Hz, which gives a sampling interval of (1.0/30.0E+09) sec or, $t=33.3$ ps. Thus the required window should be (33.3*1024)ps, or $T=34.13$ ns to avoid aliasing.

(iii)<u>Experimental Experience</u>: The experience acquired from this work dictates that the greatest accuracy in $\varepsilon^*(j\omega)$ is obtained when 5 to 10 samples are taken in the rising portion of the step WFM. If 7 samples are taken during the 35 ps rise time of the pulse, $t=5$ ps and T equals (5*1024), or 5.12 ns.

In conclusion, the record length should be 5.12 ns or less. Although, most measurements in the present work were made with 5 or 10 ns time windows, some were made with 20 and 50 ns time windows which yielded less accurate values for $\varepsilon^*(j\omega)$.

In the following Section various sources of error in the measurements from the oscilloscope and other components, such as connectors and adapters, are discussed.

3.4 Sources of Error

There are five sources of error in the experimental results:

(i)   Mismatch error due to the connectors and the adapters between the S-52, pulse generator, and the dielectric sample, also between the dielectric sample and the S-4, sampling head;

(ii)   Error due to a shift in the time origin occurring between the measurements of input and output signals;

(iii)   Error in the signal amplitude caused by the nonlinearity in the vertical amplifiers of the oscilloscope;

(iv)   Error in the signal amplitude from the aperture jitter of the sampler; and

(v)   Other errors.

The effect of each of these errors is discussed below.

3.4.1   Mismatch error due to the connectors and adapters

3.4.1.1   Single Transmission Method

In this section the error, for a singly transmitted wave through the liquid , due to spurious reflections caused by non-ideal adapters and connectors at the ends of the sample holder is discussed. The schematic representation, along with VSWR's of various components between the S-52 pulse generator head and S-4 sampling head, are shown in Fig. 17(a). It is assumed that the cable between the S-52 and the SMA/7mm adapter is matched to the output of the pulse generator; the same is assumed true for the cable between the S-4 and the other adapter. The signal travelling from the pulse generator toward the sampling head is defined as the "forward signal" and that in the opposite direction the "reflected signal".

The maximum voltage standing wave ratio of a 7mm precision coaxial connector, VSWR1, and that of a SMA/7mm adapter, VSWR2, if terminated in their characteristic impedances are [140]

$$VSWR1 = 1.003 + 0.002f \qquad\qquad (3.12)$$

$$VSWR2 = 1.025 + 0.002f \qquad\qquad (3.13)$$

where f is the frequency in GHz. The mismatch error is considered only up to 10 GHz as that is the highest frequency in the measurements. At 10 GHz, from Equations 3.12 and 3.13, VSWR1 = 1.023 and VSWR2 = 1.045. Thus, at a frequency less than or equal to 10 GHz the maximum possible VSWR due to a connector and an adapter on the transmission line in Fig. 17(a), is VSWR3 = VSWR1 x VSWR2, or 1.069. The effects of both these

discontinuities can be lumped together and replaced with imaginary discontinuities at the interfaces A and D. As shown in Figure 17(b). Thus the VSWR's of the sections of transmission line from A to B and C to D is 1.069 and a corresponding value of reflection coefficient, ρ_1, for a wave incident on the interface A in Fig. 17(c) is 0.0333. The length of each of these sections, ℓ_1 is taken as the effective length of a connector, C_1, and an adapter, A_1, as shown in Figure 17(a). γ_1 is the propagation constant per unit length in sections AB and CD and is given by

$$\gamma_1 = \sqrt{j\omega\mu_0 \cdot j\omega\varepsilon_1} \qquad (3.14)$$

Where ε_1 is the equivalent dielectric constant of these lines which is related to the reflection coefficient ρ_1 by

$$\varepsilon_1 = \frac{(1+\rho_1)^2}{(1-\rho_1)^2} \qquad (3.15)$$

The length of the liquid in the sample holder is ℓ and is the same as the length of the transmission line BC in Fig. 17(c). γ is the propagation constant per unit length in the transmission line section BC and is given by,

$$\gamma = \sqrt{j\omega\mu_0 j\omega\varepsilon^*} \qquad (3.16)$$

The reflection coefficient, ρ_L, of the interface B for the forward wave is related to ε^* and ε_1 by

$$\rho_L = \frac{\sqrt{\epsilon_1} - \sqrt{\epsilon^*}}{\sqrt{\epsilon_1} + \sqrt{\epsilon^*}} \qquad\qquad (3.17)$$

For ease of description, the sides of the interfaces A,B,C and D in Fig. 17(c) are numbered 1,2,......8. The amplitudes of signals on these interfaces are given below.

If a wave of unit amplitude is incident on side 1 of interface A of Fig. 17(c), the part reflected, with amplitude ρ_1, is absorbed by the pulse generator. The amplitude of the signal on side 2 of the interface A is the algebraic sum of the incident and the reflected signals at interface 1. This is denoted by S_2 and is equal to $(1-\rho_1)$. A part of this transmitted signal, $(1-\rho_1)$, upon reaching interface B is transmitted into section BC. Its amplitude on side 4 is $(1-\rho_1)(1+\rho_L)e^{-\gamma_1 \ell_1}$ as shown in Fig. 17(c). The signal reflected at interface 3, $(1-\rho_1)\rho_L e^{-\gamma_1 \ell_1}$, is multiply-reflected in section AB. Physically $\ell_1 < \ell$. With any of the calibrating liquids of Table 3 in section BC, ℓ is at least an order of magnitude larger than ℓ_1. Thus, the multiply reflected waves in section AB closely follow the first-transmitted wave and the first few of these multiply-reflected waves can not be excluded from the first-transmitted wave in a transmission measurement described in Section 3.2. As the magnitude of ρ_1 is on the order of 0.01, only the first few multiply-reflected waves are significant; others have negligible amplitudes: their inclusion in the following analysis will negligibly affect the final result. Therefore, for the sake of the mathematical convenience, all the infinite number of multiple reflections in section AB are summed up and added to the first transmitted wave through section BC. The above is repeated for

the multiple reflections in section CD for similar reasons. The amplitudes of the first-transmitted waves with a liquid and air in the sample holder are given below:

(i) Output signal with a liquid in the sample holder.

When the incident signal on side 1 of interface A is real and has unity amplitude, the signal on side 2 of interface A is denoted as S_2 and is given by Equation 3.18.

$$S_2 = (1+\rho_1) \tag{3.18}$$

The total signal on side 3, S_3, due to multiple reflections in section AB is thus

$$S_3 = (1-\rho_1)e^{-\gamma_1 \ell_1} + (1-\rho_1)e^{-\gamma_1 \ell_1}\rho_L\rho_1 \; e^{-2\gamma_1 \ell_1}$$

$$+ (1-\rho_1)e^{-\gamma_1 \ell_1}(\rho_L\rho_1 e^{-2\gamma_1 \ell_1})^2 + \ldots$$

or

$$S_3 = \frac{(1-\rho_1)e^{-\gamma_1 \ell_1}}{(1-\rho_1\rho_L e^{-2\gamma_1 \ell_1})} \tag{3.19}$$

The signal on side 4, i.e., transmitted through interface B is, $S_4 = S_3$ $S_4 = S_3(1+\rho_L)$. The signal on side 5 of interface C is $S_5 = S_3(1+\rho_L)\; e^{-\gamma \ell}$. Similarly, the signal on side 6 of interface C is

$$S_6 = S_3(1-\rho_L)\; e^{-\gamma \ell}(1+\rho_L) \tag{3.20}$$

and the signal on side 7 of interface D is

$$S_7 = \frac{S_6\; e^{-\gamma_1 \ell_1}}{1-\rho_1\rho_L e^{-2\gamma_1 \ell_1}} \tag{3.21}$$

The signal at interface 8, with liquid in the sample holder, SOPL is

$$SOPL = S_7 (1 + \rho_1)$$

or

$$SOPL = \frac{\{(1-\rho_1^2)(1-\rho_L^2)e^{-2\gamma_1^\ell 1}\ e^{-\gamma\ell}}{(1-\rho_1\rho_L e^{-2\gamma_1^\ell 1})^2} \qquad (3.22)$$

(ii) Output signal with air in the sample holder.

In this case $\rho_L = \rho_1$. On making this substitution, Equation 3.22 gives the output signal with air in the sample holder, SOPA, as

$$SOPA = \frac{(1-\rho_1^2)^2 e^{-2\gamma_1^\ell 1} e^{-\gamma_a^\ell}}{(1-\rho_1^2 e^{-2\gamma_1^\ell 1})^2} \qquad (3.23)$$

where γ_a is the propagation constant per unit length in the sample holder filled with air and is given as $\gamma_a = j\omega\sqrt{u_0\varepsilon_0}$. Therefore, the transfer function of the liquid, $T_1'(j\omega)$, for a singly-transmitted wave with non-ideal connectors and adapters is,

$$T_1'(j\omega) = \frac{SOPL}{SOPA}$$

or

$$T_1'(j\omega) = \frac{(1-\rho_L^2)(1-\rho_1^2 e^{-2\gamma_1\ell_1})^2 e^{-\gamma\ell}}{(1-\rho_1^2)(1-\rho_1\rho_L e^{-2\gamma_1\ell_1})^2 \cdot e^{-\gamma_a\ell}} \qquad (3.24)$$

When the connectors and adapters are ideal, $\rho_1 = 0$ and the above equation reduces to Equation 3.4. The range of ϵ^* defined by the range of ρ_1 can be obtained from Equation 3.24. For the connectors and adapters used in this work $0.0106 \leq \rho_1 \leq 0.0333$.[#] This gives the range of uncertainty in the calculated values of ϵ^*.

3.4.1.2 Multiple transmission method.

For MTM, the approach of wave tracing, successfully used in STM, becomes unwieldy and difficult to follow. Therefore, ABCD parameter representation [141] is used for each section of the transmission line AD of Fig. 17(c). The schematic representation, of the transmission line AD, as a cascaded network is shown in Fig. 18, where [AC] is the ABCD matrix representation for the transmission line AB of Fig. 17(c), and [A*] that for BC. The propagation constant, γ_1, in AC is the same as in AB (of Fig. 17(c)) and is given by Equation 3.14; the characteristic impedance, Z_1, is defined by:

[#] The VSWR on lines AB and CD, VSWR3, can vary from VSWR2/VSWR1

to VSWR2.VSWR1, corresponding to $\rho_1 = 0.0106$ and 0.0333, respectively.

$$Z_1 = \sqrt{\frac{\mu_0}{\varepsilon_0 \varepsilon_1}} \qquad\qquad (3.25)$$

where ε_1 is defined by Equation 3.15. The propagation constant, γ, in A^* is defined by Equation 3.16, and the characteristic impedance, Z^*, in this section of line is defined as

$$Z^* = \sqrt{\frac{\mu_0}{\varepsilon_0 \varepsilon^*}} \qquad\qquad (3.26)$$

where ε^* is the complex dielectric constant of the liquid in the sample holder. The ABCD matrices for the cascaded sections AC and A^* of Fig. 18 are given as,

$$AC = \begin{bmatrix} \cosh\gamma_1 \ell_1 & Z_1 \sinh\gamma_1 \ell_1 \\ \frac{1}{Z_1}\sinh\gamma_1 \ell_1 & \cosh\gamma_1 \ell_1 \end{bmatrix} \qquad (3.27)$$

and

$$A^* = \begin{bmatrix} \cosh\gamma\ell & Z^*\sinh\gamma\ell \\ \frac{1}{Z^*}\sinh\gamma\ell & \cosh\gamma\ell \end{bmatrix} \qquad (3.28)$$

Each element of matrices AC and A^* is a function of frequency, ω, through γ_1, Z_1, γ and Z. The relationship between V_g and V_0 of Fig. 18

is, therefore, given as

$$\left| \begin{array}{c} V_g - Z_g I_i \\[2mm] I_i \end{array} \right| = AC \quad A^* \quad AC \quad \left| \begin{array}{c} V_0 \\[2mm] V_0/Z_L \end{array} \right| \qquad (3.29)$$

It may be noted that, in general, V_g, I_i, and V_0 are functions of frequency and more specifically could be written as $V_g(\cdot)$, $I_i(\omega)$ and $V_0(\omega)$. Let

$$A_L = AC \quad A^* \quad AC = \left[\begin{array}{cc} a_{11} & a_{12} \\[2mm] a_{21} & a_{22} \end{array} \right] \qquad (3.30)$$

Therefore, from Equations 3.29 and 3.30,

$$V_g - Z_g I_i = a_{11} V_0 + a_{12} V_0/Z_L \qquad (3.31)$$

and,

$$I_i = a_{21} V_0 + a_{22} V_0 Z_L \qquad (3.32)$$

From Equations 3.31 and 3.32, it can be shown that

$$\frac{V_0(\omega)}{V_g(\omega)} = \frac{1}{[a_{11}+a_{12}/Z_L+Z_g a_{21}+Z_g a_{22}/Z_L]} \qquad (3.33)$$

Equation 3.29 can be similarly solved, when the sample holder is filled with air. The propagation constant, γ_a, of the section BC of Fig. 17(c) and its characteristics impedance Z_a are given by

$$\gamma_a = j\omega\sqrt{\mu_0\epsilon_0} \qquad (3.34)$$

and

$$Z_a = \sqrt{\mu_0/\epsilon_0} \qquad (3.35)$$

The ABCD matrix A^* becomes,

$$A^* = A_a^* = \begin{bmatrix} \cosh\gamma_a l & Z_a\sinh\gamma_a l \\ \frac{1}{Z_a}\sinh\gamma_a l & \cosh\gamma_a l \end{bmatrix} \qquad (3.36)$$

Let,

$$A^a = AC \quad A_a^* \quad AC$$

$$\begin{bmatrix} a'_{11} & a'_{12} \\ a'_{21} & a'_{22} \end{bmatrix} \tag{3.37}$$

If V_{oa} is the output signal with air in the sample holder, V_{oa}/V_g can be obtained as

$$\frac{V_{oa}(\omega)}{V_g(\omega)} = \frac{1}{[a'_{11}+a'_{12} Z_g + Z_g a'_{21} + Z_g a'_{22} Z_g]} \tag{3.38}$$

Therefore, the transfer function of the liquid, $\Gamma_t'(j\omega)$, is given by

$$\Gamma_t'(j\omega) = \frac{[V_0(\omega) V_g(\omega)]}{[V_{oa}(\omega) V_g(\omega)]} \tag{3.39}$$

or,

$$\Gamma_t'(j\omega) = \frac{[a'_{11}+a'_{12} Z_g + Z_g a'_{21} + Z_g a'_{22} Z_g]}{[a_{11}+a_{12} Z_g + Z_g a_{21} + Z_g a_{22} Z_g]} \tag{3.40}$$

where a_{11}, a_{12}, a_{21} and a_{22} are given by Equation 3.30 and a'_{11}, a'_{12}, a'_{21} and a'_{22} by Equation 3.37. Equation 3.40 is solved numerically, because a_{11}, a_{12}, etc., are complicated functions of ω, ρ_1, η_1, and β_1. For example, a_{11} is given by the expression

Adapters

Connectors

Pulse Generator
(S-52)

Sampling Head
(S-4)

A₁   C₁   Liquid   C₁   A₁

VSWR1   VSWR1   VSWR1   VSWR1

(a)

(b)

A   B   C   D

ρ_1 ρ ρ

1 2 (ϵ_1, γ_1) 3 4 (ϵ, γ) 5 6 (ϵ_1, γ_1) 7 8

(c)
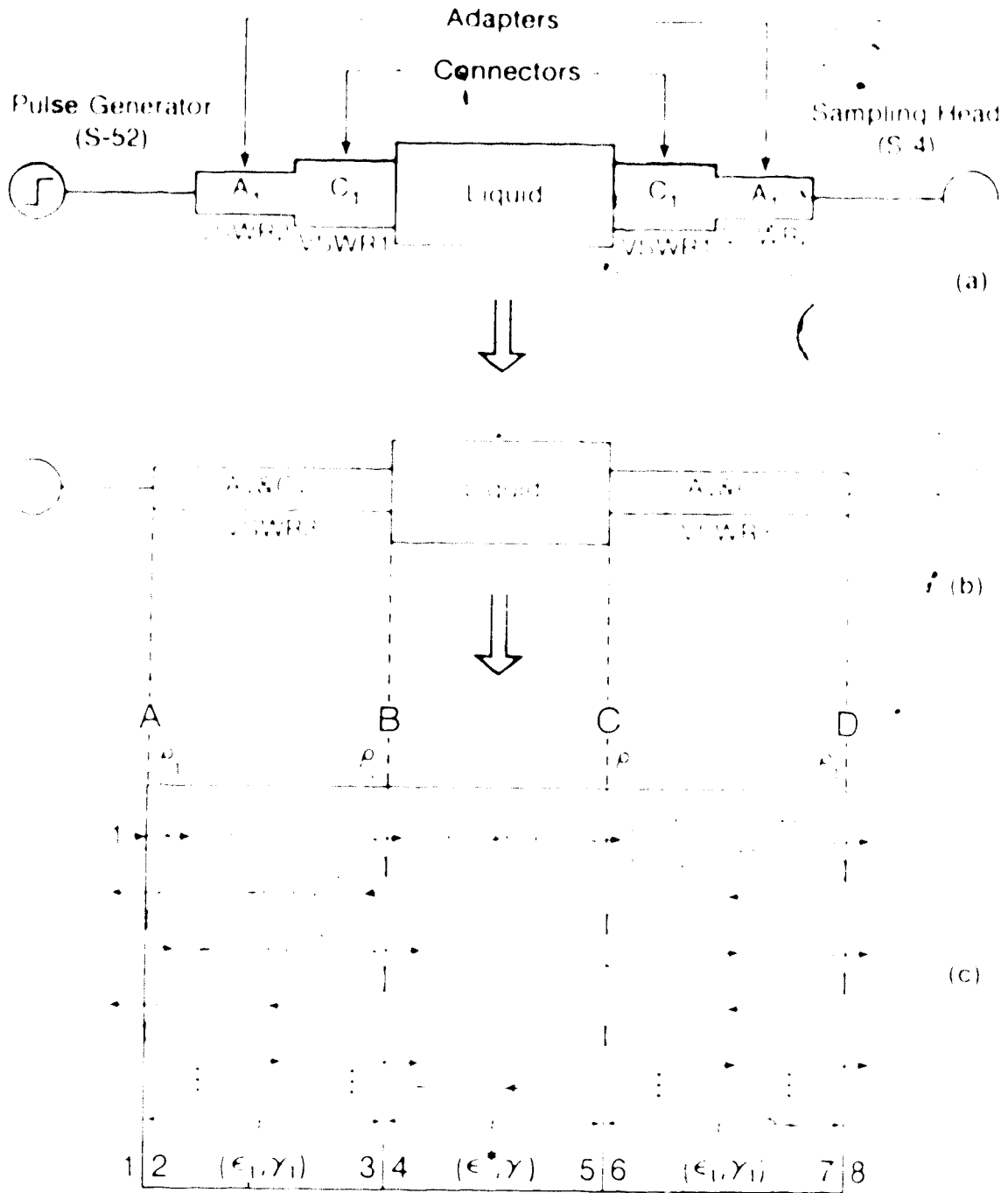
Figure 17 Transmission line representation of the measurement setup
(a) Sample holder with non-ideal connectors and adapters,
(b) Equivalent representation, (c) Bounce diagrams for reflections
and transmissions at the interfaces of the sample holder

$$a_{11} = \text{Cos}(\gamma_1 \ell_1)[\{\text{Cosh}(\gamma_1 \ell_1)\text{Cosh}(\gamma 1)\} + \{\frac{\varepsilon^*}{\varepsilon_1} \text{Sinh}(\gamma_1 \ell_1)\text{Sinh}(\gamma \ell)\}$$

$$+ \{\text{Sinh}(\gamma \ell)\}^2$$

$$+ \{\cdot \frac{\varepsilon^*}{\varepsilon_1} \frac{\text{Sinh}(\gamma_1 \ell_1)\text{Sinh}(\gamma \ell)\text{Cosh}(\gamma \ell)}{\text{Cosh}(\gamma_1 \ell_1)} \}]$$

Equation 3.40, like Equation 3.24, gives a range of values for ε^*, depending upon the range of ρ_1. In the special case when the pulse generator, sample holder and load are perfectly matched,

$$Z_g = Z_L = Z_a,$$

$$A_L = \begin{bmatrix} A^* \end{bmatrix} = \begin{bmatrix} \text{cosh}\gamma\ell & Z^*\text{sinh}\gamma\ell \\ \frac{1}{Z^*}\text{sinh}\gamma\ell & \text{cosh}\gamma\ell \end{bmatrix} \qquad (3.41)$$

$$A^a = A_a^* = \begin{bmatrix} \text{cosh}\gamma_a\ell & Z_a\text{sinh}\alpha_a\ell \\ \frac{1}{Z_a}\text{Sinh}\gamma_a\ell & \text{cosh}\gamma_a\ell \end{bmatrix} \qquad (3.42)$$

Thus, Equation 3.40 reduces to the familiar form of Equation 3.6, i.e., $T_t'(j\omega) = T_t(j\omega)$.

3.4.2   Error due to time shift between input and output waveforms

This error arises from the small and undesirable time shift that can occur between the input (IN WFM) and output waveforms (OUT

WFM). The time shift can occur due to a jitter in the time base of the oscilloscope. For example, with the Tektronix S-52 pulse generator head and S-6 sampling head plug-ins in the 7S12 TDR/sampler unit, the specified time jitter of the time base of the sampler, without signal averaging, is less than 10 ps. For the S-4 sampling head, without signal averaging, the jitter is more than 10 ps. As the jitter arises from a random noise in the time base of the oscilloscope, its effect reduces as $1/\sqrt{n}$, where n is the number of signal averages. Every waveform, therefore, was averaged 1000 times, before being stored. If the maximum jitter is taken as 20 ps (equal to that with the S-5 unit), it is expected that in the worst case the jitter in the origin of time is $20/\sqrt{10000}$ ps, or 0.63 ps. Although, this seems small, the sensitivities of ε' and ε'' to a time shift of this magnitude can be substantial as will now be shown.

A timing error, Δt, in the time domain introduces a phase error, $\Delta\theta = \omega\Delta t$, in the transfer function for the liquid being measured. This phase error produces an error in both the real and imaginary components of the computed complex dielectric constant. The sensitivity of the dielectric constant, $S_{\varepsilon'}$, and loss factor, $S_{\varepsilon''}$, to this phase error for all three types of transmission method and for two lengths of the sample holder have been computed and the plots of these sensitivities are given in Figures 19-24. Before discussing the results, the approach followed for the calculations of the sensitivities of ε' and ε'' with respect to the phase, θ, of the transfer function, $T(j\omega)$, of Equations 3.4 and 3.6 is given below.

3.4.2.1 Sensitivity of ε' and ε''

Equations 3.4 and 3.6 can also be written as

$$T(j\omega) = |T| \exp(-j\theta) \tag{3.43}$$

Also, $T(j\omega) = f(\varepsilon^*)$

or, $T(j\omega) = f_1(\varepsilon', \varepsilon'') + j\, f_2(\varepsilon', \varepsilon'') \tag{3.44}$

where $j = \sqrt{-1}$. From Equations 3.43 and 3.44

$$|T| = \sqrt{[f_1(\varepsilon', \varepsilon'')]^2 + [f_2(\varepsilon', \varepsilon'')]^2} \tag{3.45}$$

and

$$\theta = -\tan^{-1}\left[\frac{f_2(\varepsilon', \varepsilon'')}{f_1(\varepsilon', \varepsilon'')}\right] \tag{3.46}$$

Therefore, the total differentials of $|T|$ and θ are

$$d|T| = \left.\frac{\partial|T|}{\partial\varepsilon'}\right|_{\varepsilon''=Const.} \cdot d\varepsilon' + \left.\frac{\partial|T|}{\partial\varepsilon''}\right|_{\varepsilon'=Const.} \cdot d\varepsilon'' \tag{3.47}$$

$$d\theta = \left.\frac{\partial\theta}{\partial\varepsilon'}\right|_{\varepsilon''=Const.} \cdot d\varepsilon' + \left.\frac{\partial\theta}{\partial\varepsilon''}\right|_{\varepsilon'=Const.} \cdot d\varepsilon'' \tag{3.48}$$

It is known that $|T|$ is not affected by a change in θ. Therefore, in this case $d|T| = 0$. Therefore, from Equation 3.47, $d\varepsilon''$ is equal to

$$d\epsilon'' = - \frac{[\partial|T|/\partial\epsilon']d\epsilon'}{[\partial|T|/\partial\epsilon'']} \qquad (3.49)$$

From Equations 3.48 and 3.49

$$\frac{d\theta}{d\epsilon'} = \frac{\partial\theta}{\partial\epsilon'} - \left[\frac{\partial|T|/\partial\epsilon'}{\partial|T|/\partial\epsilon''}\right] \cdot \frac{\partial\theta}{\partial\epsilon''} \qquad (3.50)$$

Similarly for $\frac{d\theta}{d\epsilon''}$

$$\frac{d\theta}{d\epsilon''} = \frac{\partial\theta}{\partial\epsilon''} - \left[\frac{(\partial|T|/\partial\epsilon'')}{(\partial|T|/\partial\epsilon')}\right] \cdot \frac{\partial\theta}{\partial\epsilon'} \qquad (3.51)$$

The per cent sensitivities of ϵ' and ϵ'' for a change in θ can be defined by

$$S_{\epsilon'} = \left(\frac{1}{\epsilon'} \frac{d\epsilon'}{d\theta}\right) \cdot 100 \qquad (3.52)$$

and

$$S_{\epsilon''} = \left(\frac{1}{\epsilon''} \frac{d\epsilon''}{d\theta}\right) \cdot 100 \qquad (3.53)$$

The numerical value of $S_{\epsilon''}$, computed from Equation 3.53, gives the per cent change in the value of ϵ'' for a shift of 1 radian in the phase of the transfer function, $T(j\omega)$. At 3 GHz, a phase shift of one radian corresponds to a time shift (ΔT) of 53 ps. To elaborate further, if $S_{\epsilon''} = 5$ from Equation 3.53, for a phase shift of one radian, the value

of ε'' will change by 5% for a 53 ps shift in the time origin. The same is true for ε'.

These sensitivites were computed with the help of the MathCAD^{TM} package [142] over the following ranges of ε' and ε'': $\varepsilon' = 2,4,... 82$ and $\varepsilon'' = 0.5,1,...18$. These ranges for ε' and ε'' cover all the materials given in Table 2 except those having $\varepsilon''<0.5$. When $\varepsilon''<0.5$, $S_{\varepsilon''}$ becomes a very large negative number for both $\ell = 3.5$ and $\ell = 17$ cm for STM, as well as for MTM.

3.4.2.2 Results

The validity of Equations 3.52 and 3.53 was checked by comparing the predictions of these equations with a finite difference calculation. In the latter, a specific OUT WFM was shifted with respect to its corresponding IN WFM by a time increment of 5 ps, which approximately equals the time interval between two samples for a record length of 5 ns. These two waveforms were then analyzed using the procedure described in Section 3.3 to yield values of ε' and ε''. For 5 ps time shift (or, $5 \times 10^{-12} \omega$ phase shift), the ε' and ε'' values for the time shifted case and ε' and ε'' values from the unshifted OUT WFM and IN WFM were used to determine finite difference approximations to $d\varepsilon'/d\theta$ and $d\varepsilon''/d\theta$. The values obtained matched very well with those computed from Equations 3.52 and 3.53. This verification was repeated for time shifts of 10 ps and 15 ps; the results agreed for these time shifts also. After this verification of correctness, these two equations were used to compute values of $S_{\varepsilon'}$ and $S_{\varepsilon''}$ for all three transmission methods. The results covered the following ranges of parameters:

(i) Single Transmission Method

(a) Results given in Figure 19(a), (b) for:

$$\ell = 17 \text{ cm}, \ f = 3 \text{ GHz};$$

$$\epsilon' = 2,4,\ldots 82, \ \epsilon'' = 0.5,1,\ldots 18$$

(b) Results are given in Figures 20(a), (b) and 21 (a), (b) for:

$$\ell = 3.5 \text{ cm}, \ f = 3 \text{ GHz};$$

$$\epsilon' = 2,4,\ldots .40; \ 40, \ 42,\ldots 82,$$

$$\epsilon'' = 1,1.2,\ldots 5; \ 5, \ 5.65,\ldots 18.$$

(ii) Multiple Transmission Method

(a) Results are in Figures 22(a), (b) for:

$$\ell = 17 \text{ cm}, \ f = 3 \text{ GHz};$$

$$\epsilon' = 2,4,\ldots 82, \ \epsilon'' = 0.5,1,\ldots 18.$$

(b) Results in Figure 23(a), (b) for:

$$\ell = 3.5 \text{ cm}, \ f = 3 \text{ GHz};$$

$$\epsilon' = 2,4,\ldots 82, \ \epsilon'' = 0.5, \ 1,\ldots 18$$

(iii) Ratio method: Results in Figures 24(a), (b) are for:

$$\ell_1 = 17 \text{ cm}, \quad \ell_2 = 3.5 \text{ cm},$$

$$f = 3 \text{ GHz};$$

$$\epsilon' = 2,4,\ldots82, \quad \epsilon'' = 0.5,1,\ldots18.$$

From Figs. 19-24, it can be concluded that if there is an uncertainty regarding the time origin, the method along with the sample length should be chosen to obtain small values for $S_{\epsilon'}$ and $S_{\epsilon''}$. The best results, in this respect, are obtainable for those values of ϵ' and ϵ'' for which the sensitivity - surfaces intersect, or are close to, the $\epsilon'\epsilon''$ planes of Figs. 19-24. It is also concluded that the MTM will not give accurate results when the sensitivity functions have large magnitudes, for example close to the peaks of Figs. 22(b) and 23(b).

Figs. 25-27 provide the prospective user with guidance as to the ranges of ϵ' and ϵ'' that yield low values for $S_{\epsilon'}$ and $S_{\epsilon''}$ for each of the transmission methods. For example, the range of ϵ' and ϵ'' for which $-1\% < S_{\epsilon'}, < 1\%$ for the single transmission method at 3 GHz, $\ell=17$ and 3.5 cm are given in Fig. 25. In Fig. 25(a) in the region enclosed by the solid lines, $S_{\epsilon'}$, will change by $\pm$ 1% and $S_{\epsilon''}$ from 5.0 to 2.08% for a $\Delta T = 53$ ps. As discussed earlier it is expected that in the worst case $\Delta T \leq 5$ ps. Therefore, at 3GHz for the STM with $\ell=17$ cm and for the range of materials of Fig 25(a), the results are expected to be within $\pm$ 0.1% for ϵ' and 0.5% for ϵ'' due to the time shift error. The region

of low sensitivity shown in Fig. 25(b) is considerably smaller than that of Fig. 25(a).

The phase shift suffered by a wave in its transmission through a sample holder depends upon the ϵ^* of the material and the length of the sample holder. Therefore, for a longer sample holder, the per cent phase shift due to a given timing error, Δt, is smaller. Thus, with a longer sample holder, materials having a wider range of ϵ^* can be measured within a specified limit of timing sensitivity. This argument also applies to the MTM as shown in Fig. 26; the range of ϵ^* is more for a longer sample holder. However, in this case as shown in Figs. 22(b) and 23(b), the sensitivity in ϵ'', $S_{\epsilon''}$, changes wildly. These fluctuations limit the range of the materials which can be measured with MTM within a specified limit of sensitivity (e.g., $-1\% < S_{\epsilon''} < 1\%$). For the ratio method it is seen that $S_{\epsilon''}$ is always more than 1%. The area shown in this case is for $S_{\epsilon''} < 2\%$. $S_{\epsilon'}$ varies from 4.04% at $\epsilon^* = (34-j0.5)$ to 2.6% at $\epsilon^* = (83-j18)$. For the ratio method, the overall error in $S_{\epsilon''}$ due to the shift of time origin is larger than other methods discussed for the same range of ϵ^*.

The above discussion would suggest that one should choose a long sample holder to reduce the error due to the shift of the time origin. However, for a long sample holder the attenuation is large and the desired signal to noise ratio at the output end places an upper limit on the length of the sample holder. At 3 GHz, it was found that the 17 cm sample holder was unsuitable for measuring methanol, a methanol and water mixture (see Table 3), and distilled water, due to the large attenuation of these liquids. At frequencies above 3 GHz this problem will be worse as the amplitudes of the spectral components of an ideal

step pulse drop as ω^{-1}.

3.4.3   Error from the nonlinearity in the vertical amplifier of the oscilloscope.

According to the manufacturer of the Tektronix 7854 oscilloscope, the accuracy of the veritical amplifier is $\pm 3\%$ of the scale. That is, the maximum possible error in the ratio of OUT WFM and IN WFM could be up to 6%, at a particular point in time. Since the Fourier transform is a linear operation on the time domain signal, this will result in a corresponding maximum error of 6% in the magnitude of the ratio of the Fourier coefficients, i.e., $T(j\omega)$.

3.4.4   Error from the aperture jitter of the sampler

This amplitude error is proportional to the rate of change of the signal and the magnitude of the time jitter. According to the manufacturer, the jitter (without signal averaging) in the 7S12 unit is less than 20 ps; with signal averaging this jitter is substantially reduced. If a normal distribution is assumed for time jitter, taking 1000 averages reduces this random error by a factor of $1/\sqrt{1000}$ [143]. Thus, the average estimated time jitter is 20/1000 ps, or 0.64 ps. For a 200 mv step pulse with a rise time of 35 ps, the amplitude error could be up to $160/35 \times 0.64 = 2.92$ mV, or 1.46%, if the average slew rate of the input is taken equal to the slew rate of the signal at the time of sampling. This error is non-deterministic in nature and manifests itself as a noise in the Fourier coefficients.

3.4.5   Other errors

(1)   Low frequency errors

Although the EF-FFT algorithm substantially reduces this

error, the magnitudes of the few lowest frequency components are
slightly in error due to the EF-FFT modelling equations. These
spectral components at the extreme lower end of the spectrum have not
been used.

(ii)   High frequency errors

In the above set up the output data obtained with the FFT
procedure contains noise components larger than the signal components
for all frequencies above about 8 GHz. Thus, the transfer function
above this frequency is the ratio of two small, noise-dominated
components. These noisy high frequency components have not been used
in the computation of the dielectric constant.

3.4.6 Summary

In this section (3.4) the effects of the possible sources of error
in the transmission measurements were analysed and discussed. Five
sources of error were identified and the first three were considered
significant.

Equations 3.24 and 3.40, for the STM and MTM respectively, account
for the multiple reflections at the connector and adapter interfaces.
These equations thus give the results which would be obtained with non-
ideal connectors and adapters. The quantitative analysis for this
connection mismatch error was given in Section 3.4.1.

The effect of the shift of the time origin between IN and OUT WFM
was analysed in Section 3.4.2. From this analysis the per cent error
in the results can be computed, if the error, ξ, due to the time shift
is known. For example, if $\Delta t = 1 ps$, at 3GHz phase error, Δ, from this
time shift is $= 2\pi(3.10^9)(1x10^{-12})$, or 0.018 radians. And, the total

per cent error Δ_{ϵ}' due to this $\Delta\theta$ equals $(S_{\epsilon}'x0.018)$ and that in ϵ'' as $(S_{\epsilon}''x0.018)$. At 3 GHz and for the given sample lengths, the curves given in Figs. 19-24 can also be used to estimate this error.

The effect of error from nonlinearity in the amplifiers of the oscilloscope is discussed in Section 3.4.3. It is found that this error could be up to 6% of the magnitude of the transfer function, expressed by Equations 3.4 and 3.6. The estimation of the effect of this error on ϵ' and ϵ'' can be done simplistically by scaling these Fourier coefficients up or down by 6%.

3.5 RESULTS AND DISCUSSION

To determine the accuracy of the transmission methods (STM and MTM), the complex permittivities of six liquids of Table 3, were measured. Different time windows were taken to check the effect of the variation of the sampling interval (t), and sample holders of different lengths were used to determine the effect of the length of sample holder on the results.

The results obtained with various transmission methods and the percent deviations compared to the reference values for the six liquids are given in Table 10. As previously mentioned, at 3 GHz the complex permittivities of these liquids are known to acceptable accuracies. The accuracy of the transmission methods is taken as the percent deviations given in Table 10: it is assumed that the reference values are free of error. Although the results have been checked for quantitative accuracy at only 3 GHz, the variation of the dielectric constant with frequency had an acceptable trend.

From the above measurements it is found that:

(i)   The single transmission method, in most cases, gives the most accurate results. This seems reasonable for the following two reasons: (a) Spurious reflections from the pulse generator do not affect the recorded waveforms; and (b) For STM, generally $S^{\prime\prime}$ is smaller.

(ii) For medium loss materials in Table 3, for example for a mixture of methanol (6%) and benzene (94%) and for ethyl acetate, use of longer sample holder (≈ 17cm) gives more accurate results. For the errors in the STM results of Table 10, it is found that the contribution of the spurious reflections from the connectors and adapters, to the total error, is not very large. For water, this error from spurious reflections is up to 1% for $\cdot^{\prime}$ and 4% for $\cdot^{\prime\prime}$; for other liquids of Table 2, the error is still lower. It is also found that for materials with their $\cdot^{\prime\prime} < 0.5$, the magnitude of $S^{\prime}$ and $S^{\prime\prime}$ are very large. It is, therefore, concluded that for these materials the time shift and nonlinearity of the amplifiers of the oscilloscope are the bigger sources of errors. In general, the relative phase error from a fixed time shift between IN and OUT FMs would be less for a longer sample holder, because the wave suffers larger phase shift in its passage through it. This explains the more accurate results, for medium loss materials, obtained from a longer sample holder.

On the contrary, for high loss materials smaller sample holders (1, 3.5 or 6 cm) should be used. Otherwise the amplitudes of the spectral components at higher frequencies, for example at 3GHz, are very low and the system noise affects the results adversely.

(iii) As can be seen from Table 10, the results obtained from the ratio method are not always more accurate than those obtained from the single

transmission method and multiple transmission method. This indicates that, similar to the STM and MTM, for the ratio method the mismatch error is not the source of the largest error.

As discussed above, the magnitude of error due to the mismatch between the connectors and adapters is not very large. If desired the effect of these errors can be removed by using Equation 3.24 for the single transmission method and Equation 3.40 for the multiple transmission method. For the estimation of the error from a shift in the time origin, an experimental method based on a technique described by Peyrelasse et al. [144] is suggested below. Peyrelasse's technique is suitable for a time domain reflection measurement. For the transmission method a number of input waveforms with an empty sample holder (IN WFM) should be recorded at some intervals of time, t_1, t_2,...t_n. These are denoted as $v_1(t)$, $v_2(t+t_1)$ $v_3(t+t_2)...v_n(t+t_n)$. The Fourier transforms of all these waveforms, with respect to the reference waveform, $v_1(t)$, which are given as $V_2(\omega)/V_1(.)$, $V_3(.)/V_1(.)$, etc., are then computed. Ideally all the spectral components of these transforms should be $1\underline{/0}$; however, this is not always true. From the relative phases of $V_2(.)/V_1(.)$, $V_3(.)/V_1(.)$, etc., the time jitters, $t_1,t_2...t_{n-1}$, (at a given frequency) can be determined. If t_{av} is the average time jitter, all the OUT WF's may then be shifted by a time, t_{av}, with respect their IN WF's, to correct for the above error.

Table 10

Dielectric Measurements from Time Domain Transmission Methods

S No	Material	Freq (GHz)	Time Window (ns)	Length of Sample Holder (cm)	Method	% Deviation ε'	% Deviation ε''	Remarks
1	Methanol (6%) & benzene (94%)	3 0	10	17	SIM	1%	59%	Low loss material, large deviations due to ringing in the system
		3 0	5	17	SIM		40%	
		3 0	10	17	SIM		30%	
2	Ethyl Acetate	3 0						
		3 0						sample holder length for this material
		3 0						
		3 0						
		3 0						
		3 0						
		3 0						
		3 0						
		3 0						
		3 0						c) Improper choice of l and l
		3 0						
		3 0	10					
3	Acetone (10%) & Methanol (20%) & Benzene (70%)	3 0					14%	
		3 0						
		3 0						
		3 0						
		3 0						l₁ 17 cm, l₂ 5 cm
4	Methanol	3 0						
		2 0						
		1 0						
		0 3						d) Results checked against data from [149]
		0 1						
		0 1						
		1 0						
5	Methanol (60%) & Distilled Water (40%)	3 0	5		SIM			
		3 0	10	3 5	SIM			
		3 0	20		SIM			
		3 0	20		SIM		35%	
6	Distilled Water	3 0	5	3 5	SIM	12%	9%	
		3 0	10	3 5	SIM	3%	4 2%	
		0 3	10	17	SIM	3%	36%	
		0 3	20	17	SIM	4%	30%	e) Results Checked against data from [93]
		0 5	10	17	SIM	3%	13%	
		0 5	20	17	SIM	4%	76%	

+ Checked against data from [110]. Magnitude of the spectral components very small beyond 1 GHz

With a 17cm sample holder, the magnitude of the spectral components very small beyond 1 GHz

19(a)

$S_{\varepsilon'}$

(-, 18, 29.87)

ε''

(2, 0.5, 13.39)→

(82, 18, 2.08)

(82, 0.5, 2.06)

ε'
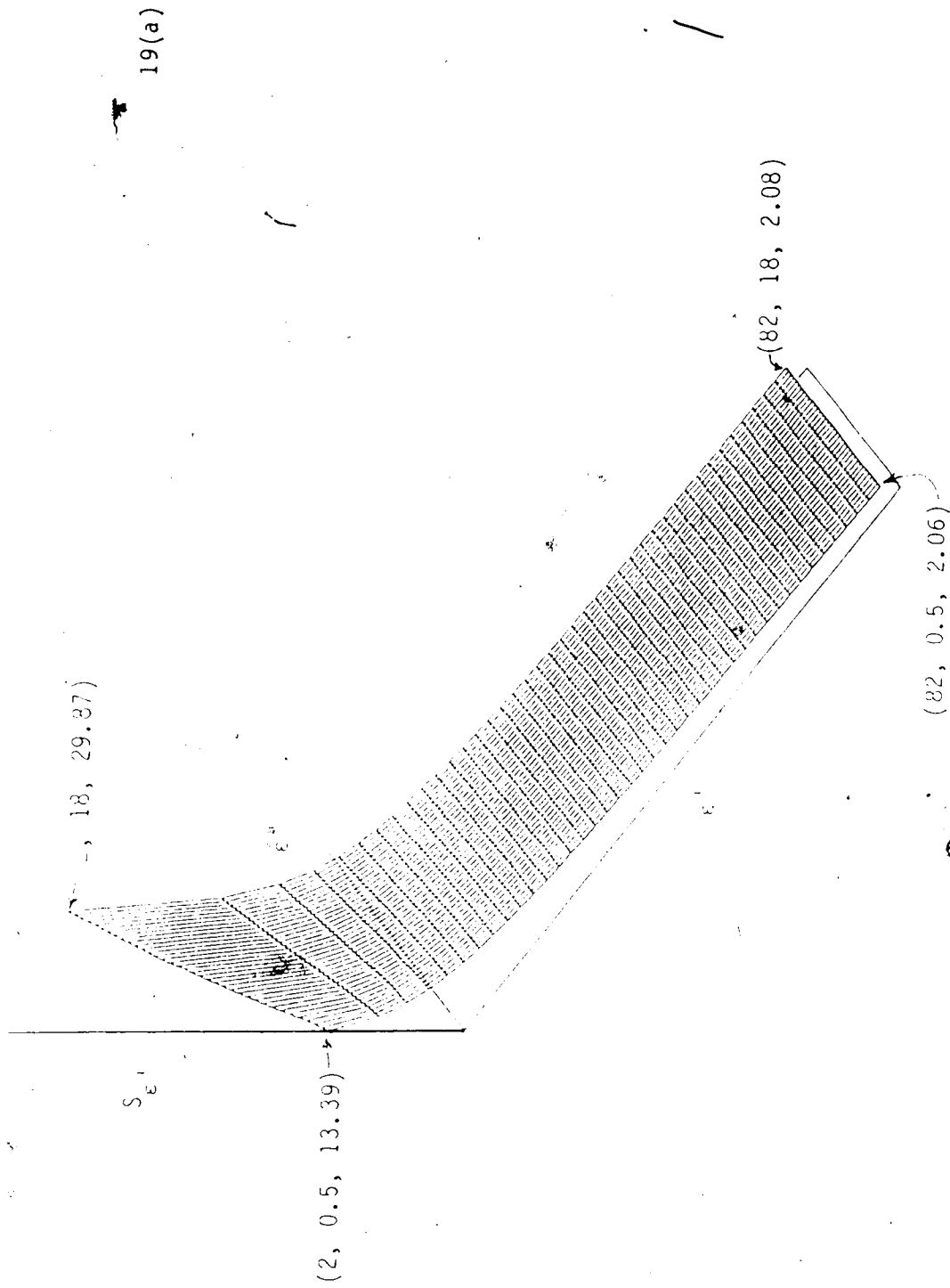
Figure 19(a).   Sensitivity of ε' ($S_{\varepsilon'}$) per radian relative shift; single transmission method, f = 3 GHz, λ = 17 cm. The points are shown in {ε', ε'', $S_{\varepsilon'}$(%)} format.

Figure 19(b). Sensitivity of $\varepsilon''(S_{\varepsilon''})$ per radian relative shift; single transmission method, f = 3 GHz, ℓ = 17 cm. The points are shown in $\{\varepsilon', \varepsilon'', S_{\varepsilon''}(\%)\}$ format.
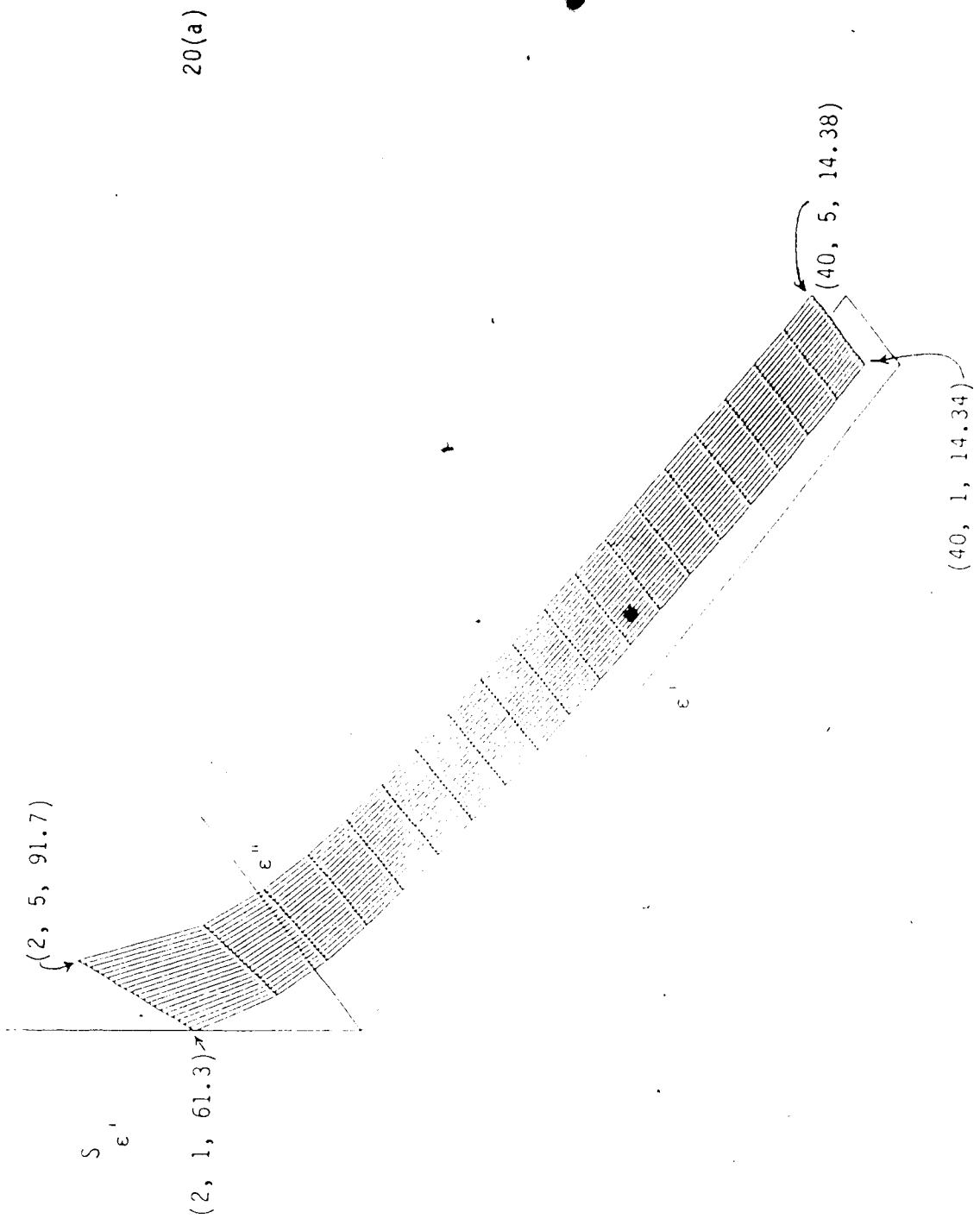
Figure 20(a). Sensitivity of ε' ($S_{\varepsilon'}$) per radian relative shift; single transmission method, $f = 3$ GHz, $\lambda = 3.5$ cm. The points are shown in $\{\varepsilon', \varepsilon'', S_{\varepsilon'}(\%)\}$ format.

20(b)

$S_{\epsilon''}$ (2, 5, 19.9)

(2, 1, 22.5)

(6, 1, 0.93)
(8, 1, -3.7)

(40, 5, 1.17)

(40, 1, -22.8)
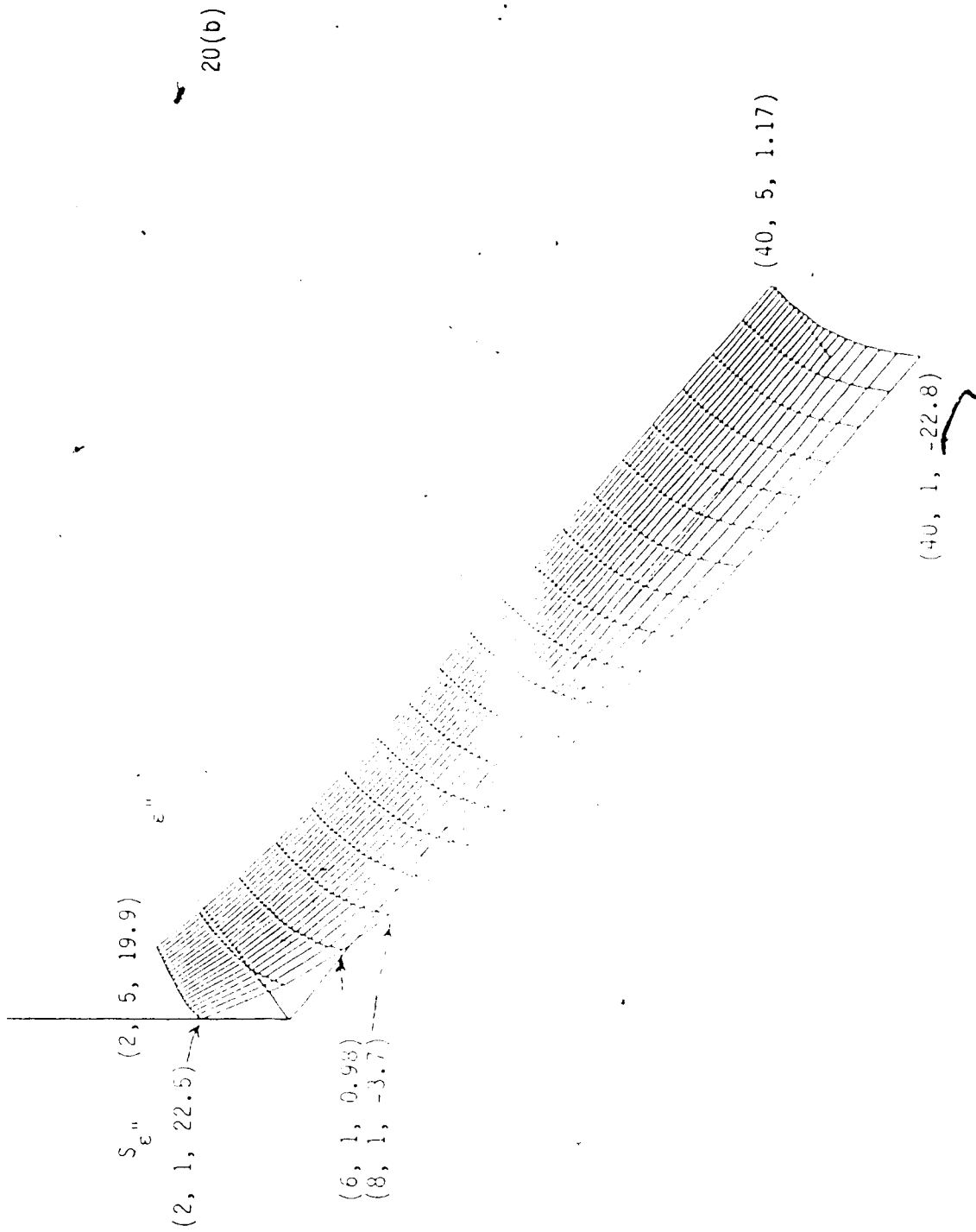
Figure 20(b). Sensitivity of $\epsilon''(S_{\epsilon''})$ per radian relative shift; single transmission method, f = 3 GHz, α = 3.5 cm. The points are shown in $\{\epsilon', \epsilon'', S_{\epsilon''}(\%)\}$ format.

21(a)

$S_{\epsilon'}$

$(40, 5, 14.38)$

$(82, 18, 10.1)$

$(82, 5, 10)$

ϵ'

ω'
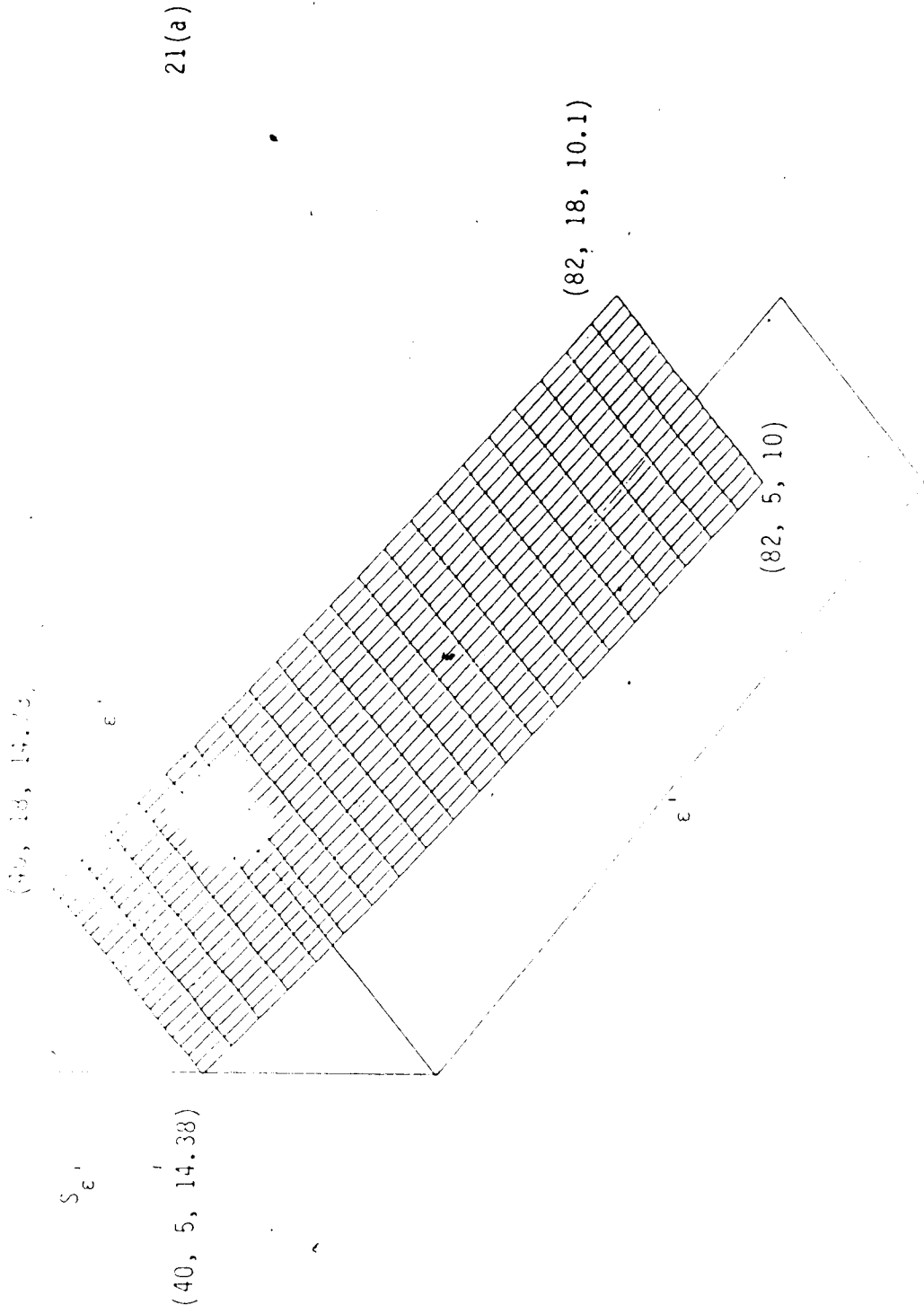
Figure 21(a). Sensitivity of ϵ' ($S_{\epsilon'}$) per radian relative shift; single transmission method, $f = 3$ GHz, $\lambda = 3.5$ cm. The points are shown in $(\epsilon', \epsilon'', S_t(\epsilon'))$ format..
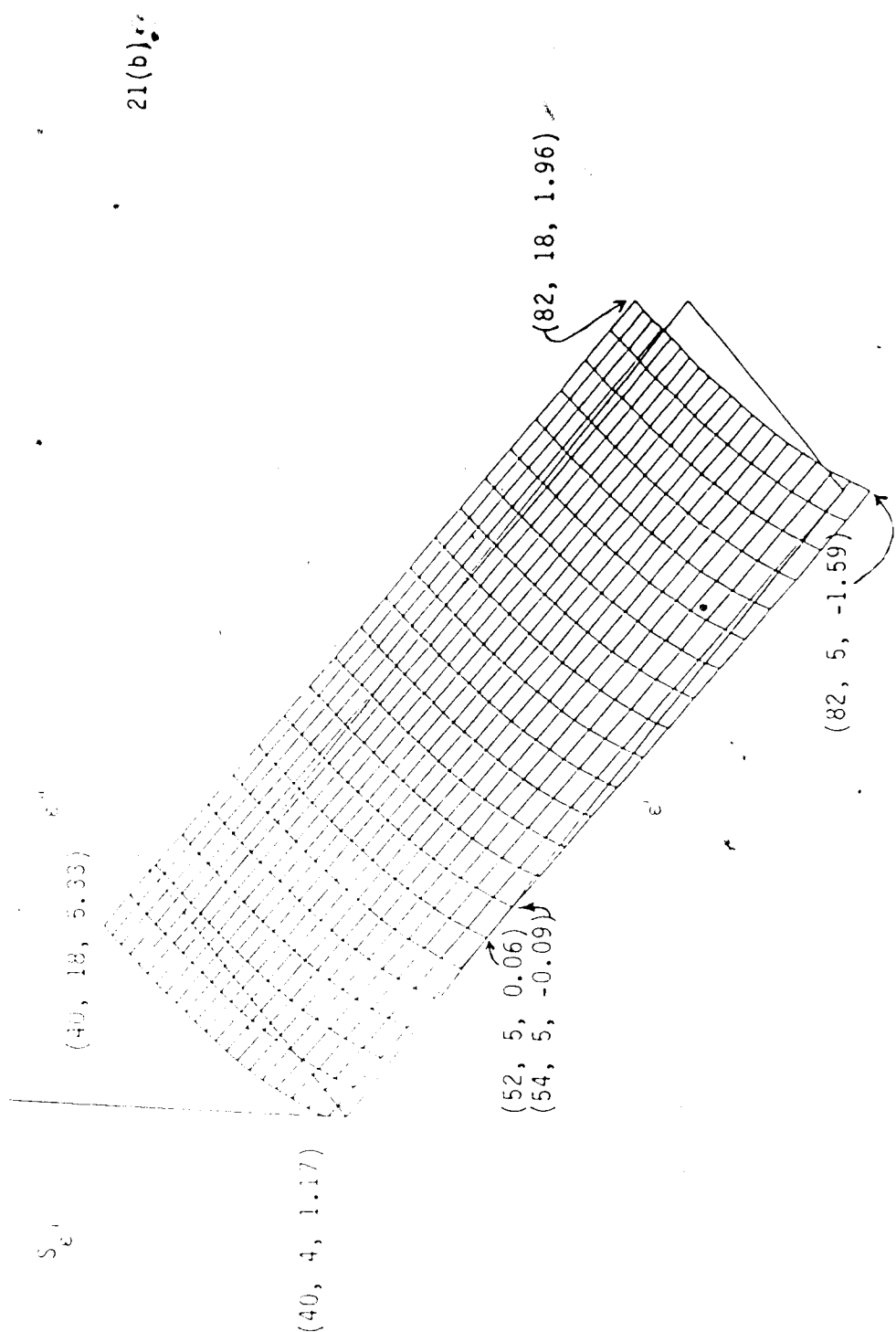
Figure 21(b). Sensitivity of $\varepsilon''(S_{\varepsilon''})$ per radian relative shift; single transmission method, f = 3 GHz, ℓ = **3.5 cm**. The points are shown in $\{\varepsilon', \varepsilon'', S_{\varepsilon''}(\%)\}$ format.

22(a)

(82, 18, 2.1)

(2, 18, 29.9)

ϵ'

(82, 0.5, 1.4)

(2, 0.5, 13.4)

$S_{\epsilon'}$
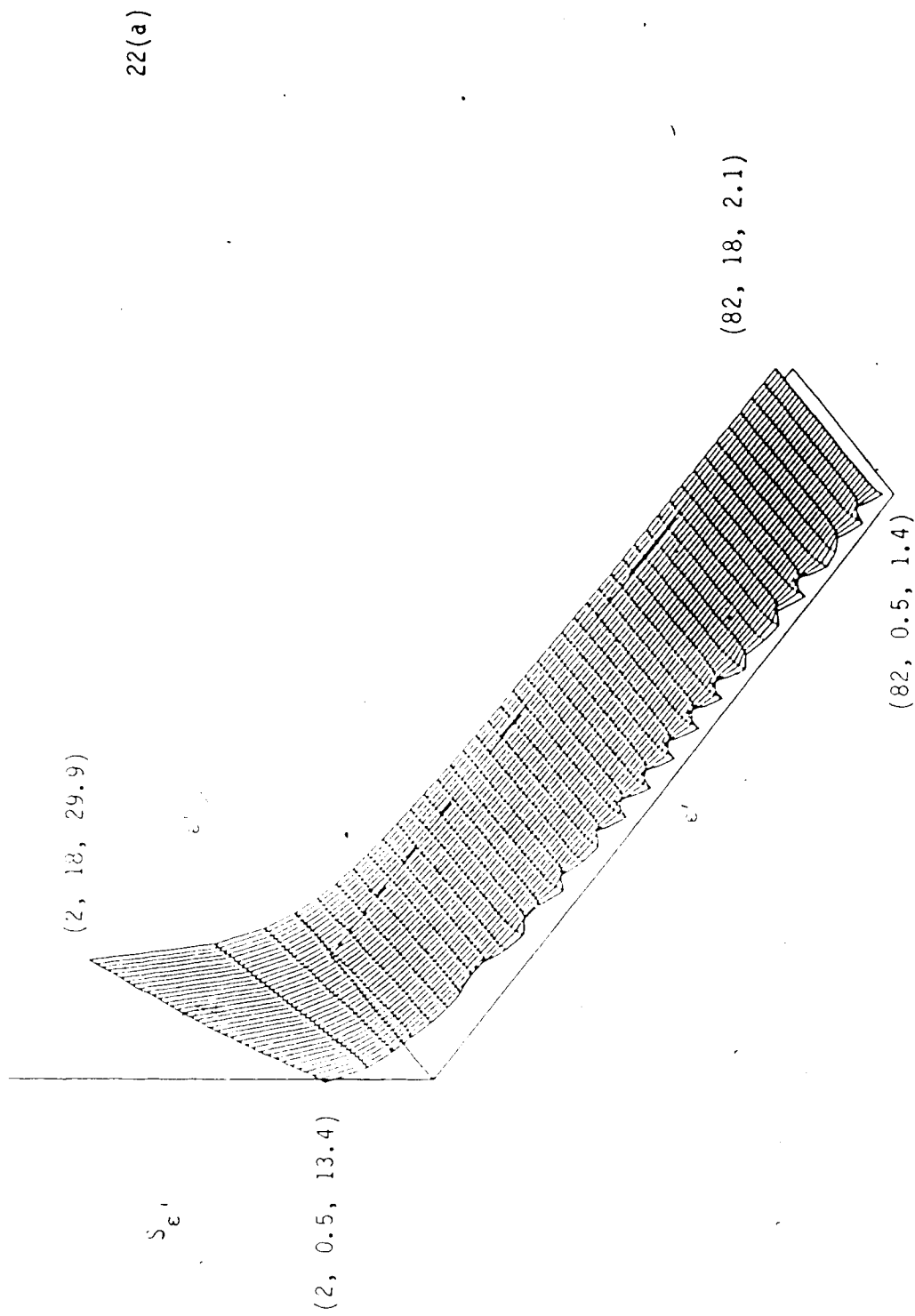
Figure 22(a). Sensitivity of $\epsilon'(S_{\epsilon'})$ per radian relative shift; multiple transmission method, $f = 3$ GHz, $\ell = 17$ cm. The points are shown in $\{\epsilon', \epsilon'', S_{\epsilon'}(\%)\}$ format.

$S_{\varepsilon''}$

$(2, 18, 2.88)$

ε'

$(32, 18, 0.94)$

22(b)

Figure 22(b). Sensitivity of $\varepsilon''(S_{\varepsilon''})$ per radian relative shift; multiple transmission method, $f = 3$ GHz, $\ell = 17$ cm. The points are shown in $\{\varepsilon', \varepsilon'', S_{\varepsilon''}(\%)\}$ format.

23(a)

(2, 18, 147.7)

(82, 18, 10.2)

(82, 0.5, 8.4)

$S_{\varepsilon'}$

(2, 0.5, 63.8)
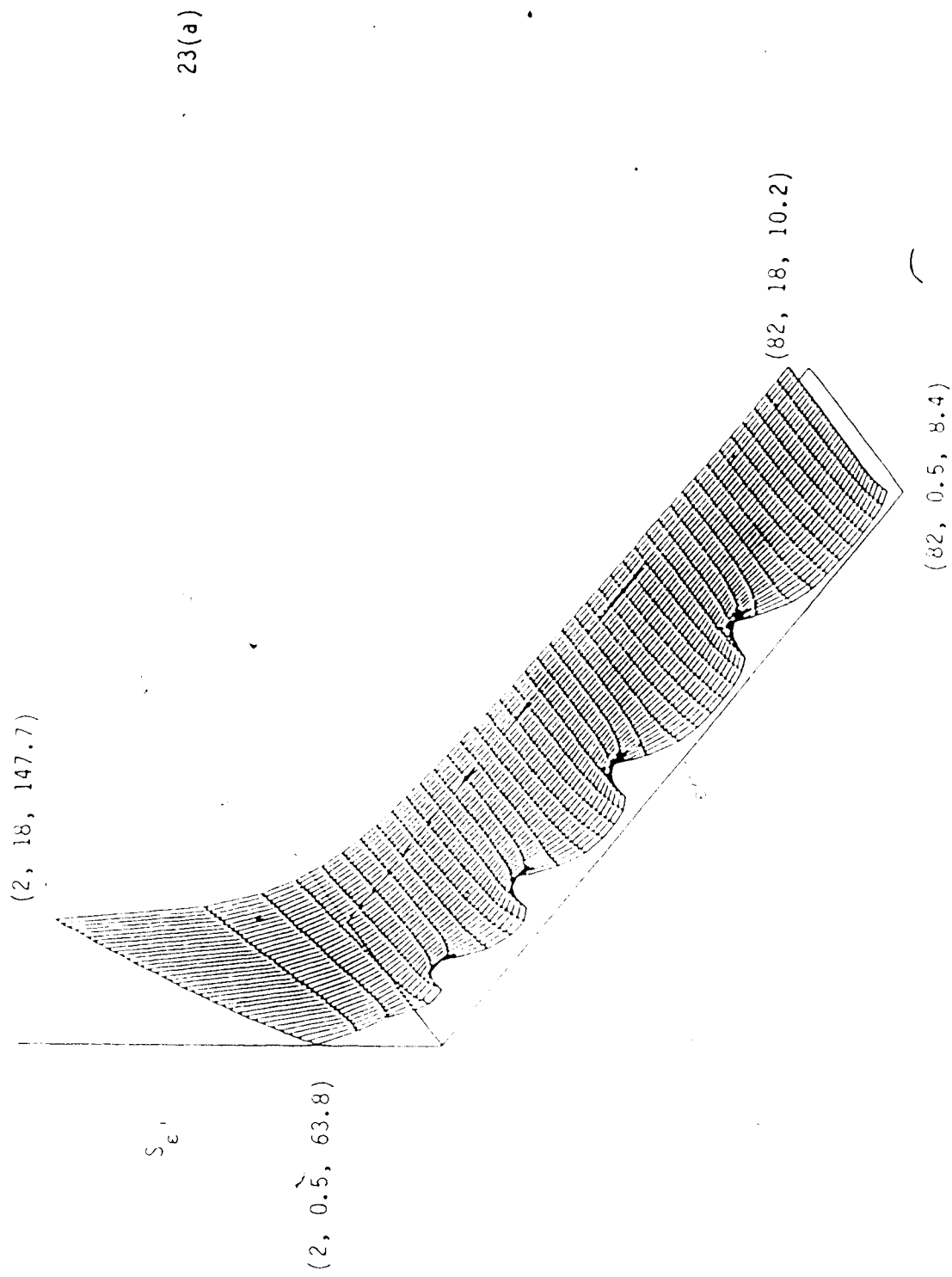
Figure 23(a). Sensitivity of $\varepsilon'(S_{\varepsilon'})$ per radian relative shift; multiple transmission method, $f = 3$ GHz, $\ell = 3.5$ cm. The points are shown in $\{\varepsilon', \varepsilon'', S_{\varepsilon'}(\varepsilon')\}$ format.
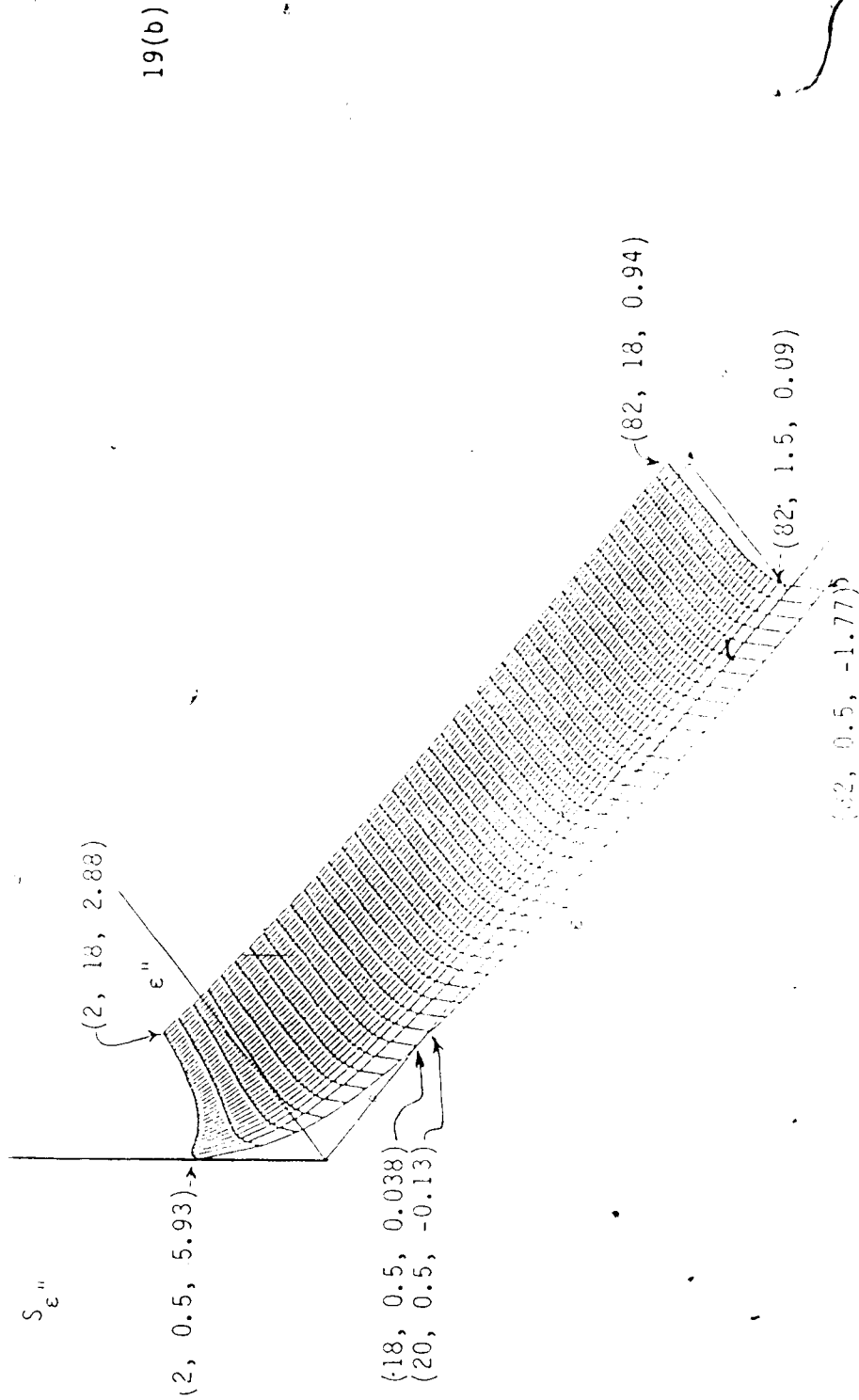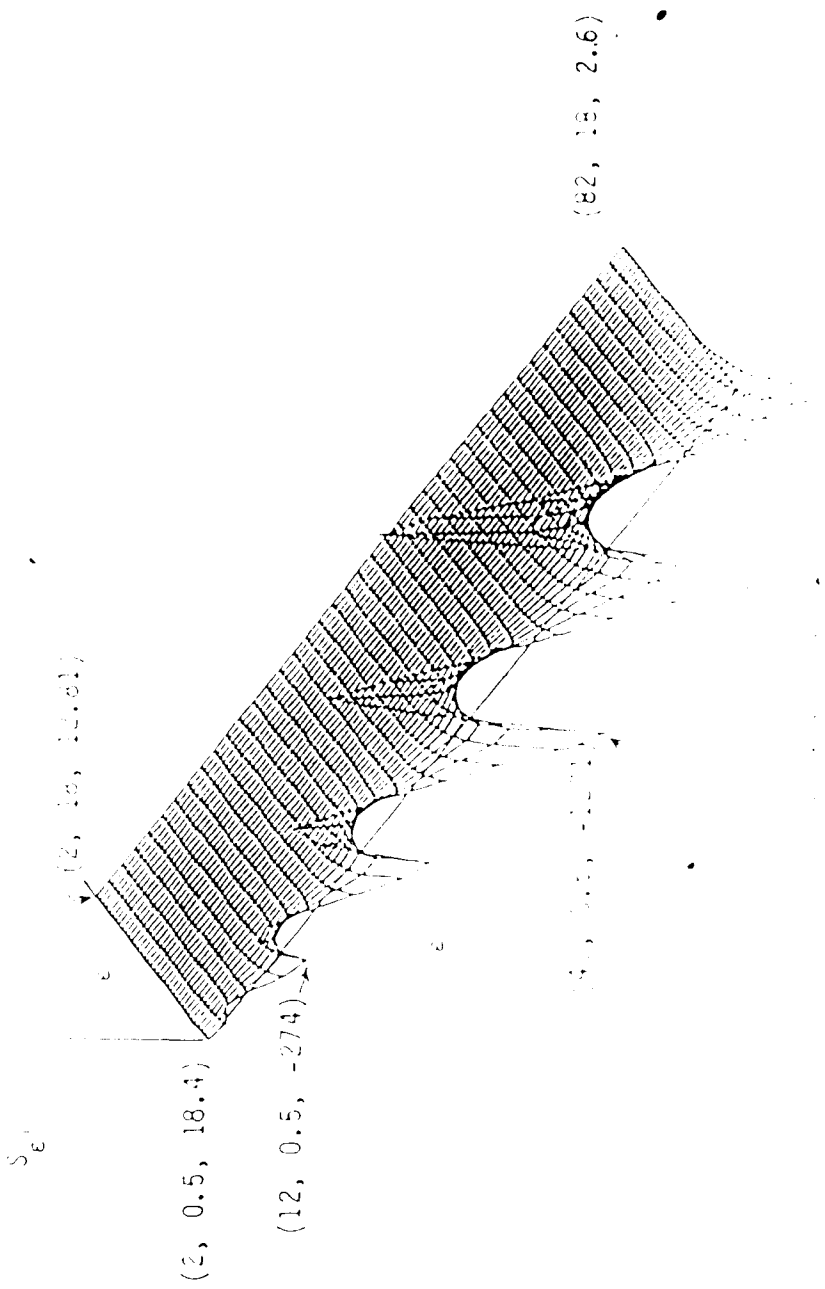
Figure 23(b). Sensitivity of $\varepsilon''(S_{\varepsilon''})$ per radian relative shift; multiple transmission method, $f = 3$ GHz, $\ell = 3.5$ cm. The points are shown in $\{\varepsilon', \varepsilon'', S_{\varepsilon''}(\varepsilon)\}$ format.

24(a)

$S_{\epsilon'}$

(82, 18, 2.61)

(20, 0.5, 17.83)
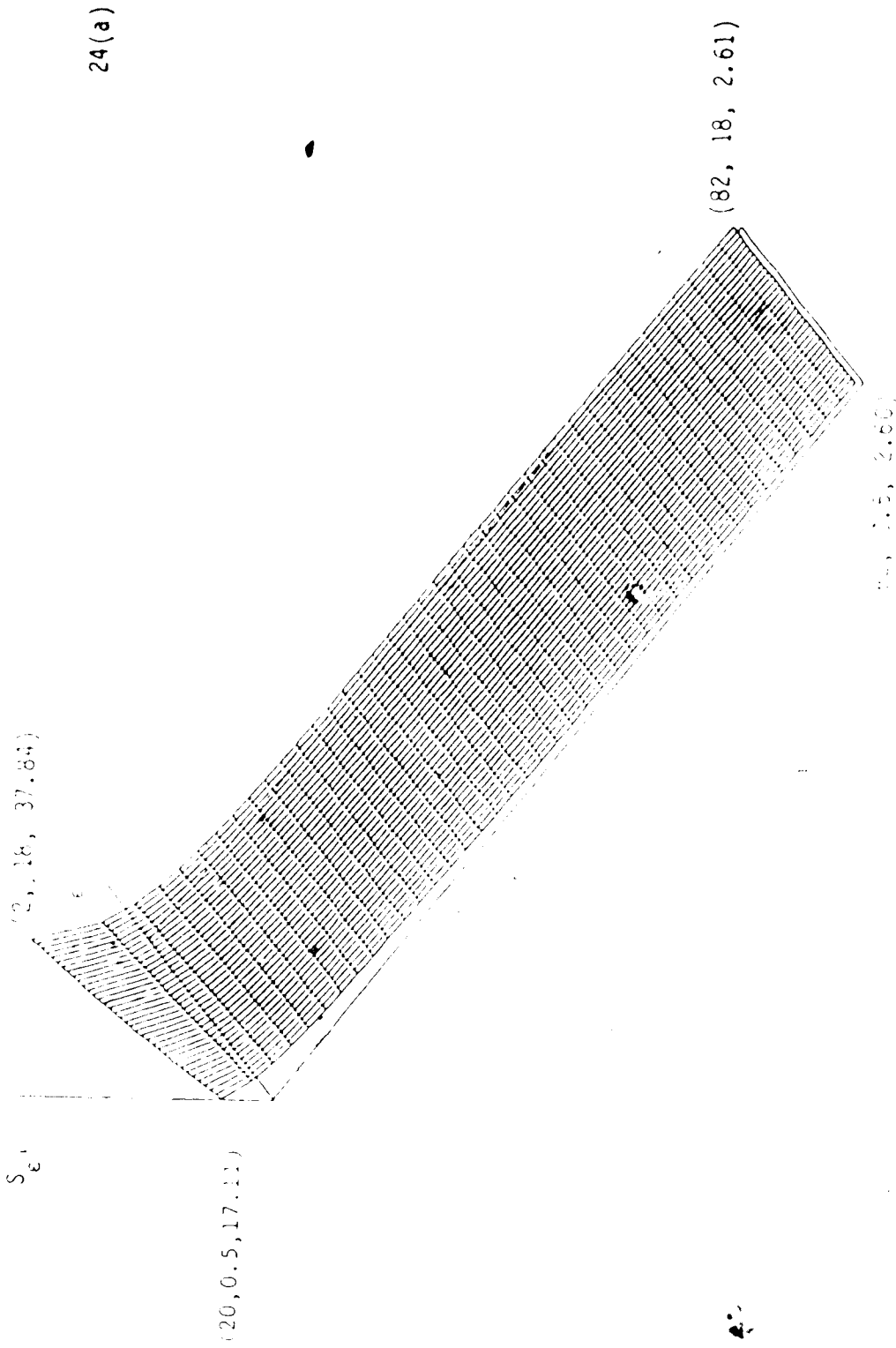
Figure 24(a). Sensitivity $S_{\epsilon'}$ per radian relative shift; ratio method, ℓ_1 = 17 cm, ℓ_2 = 3.5cm, f = 3 GHz. The points are shown in $\{\epsilon', \sigma, S_{\epsilon'}(\sigma)\}$ format.

24(b)

S_ε ...

(2, 0.5, ...)

(82, 18, 1.29)
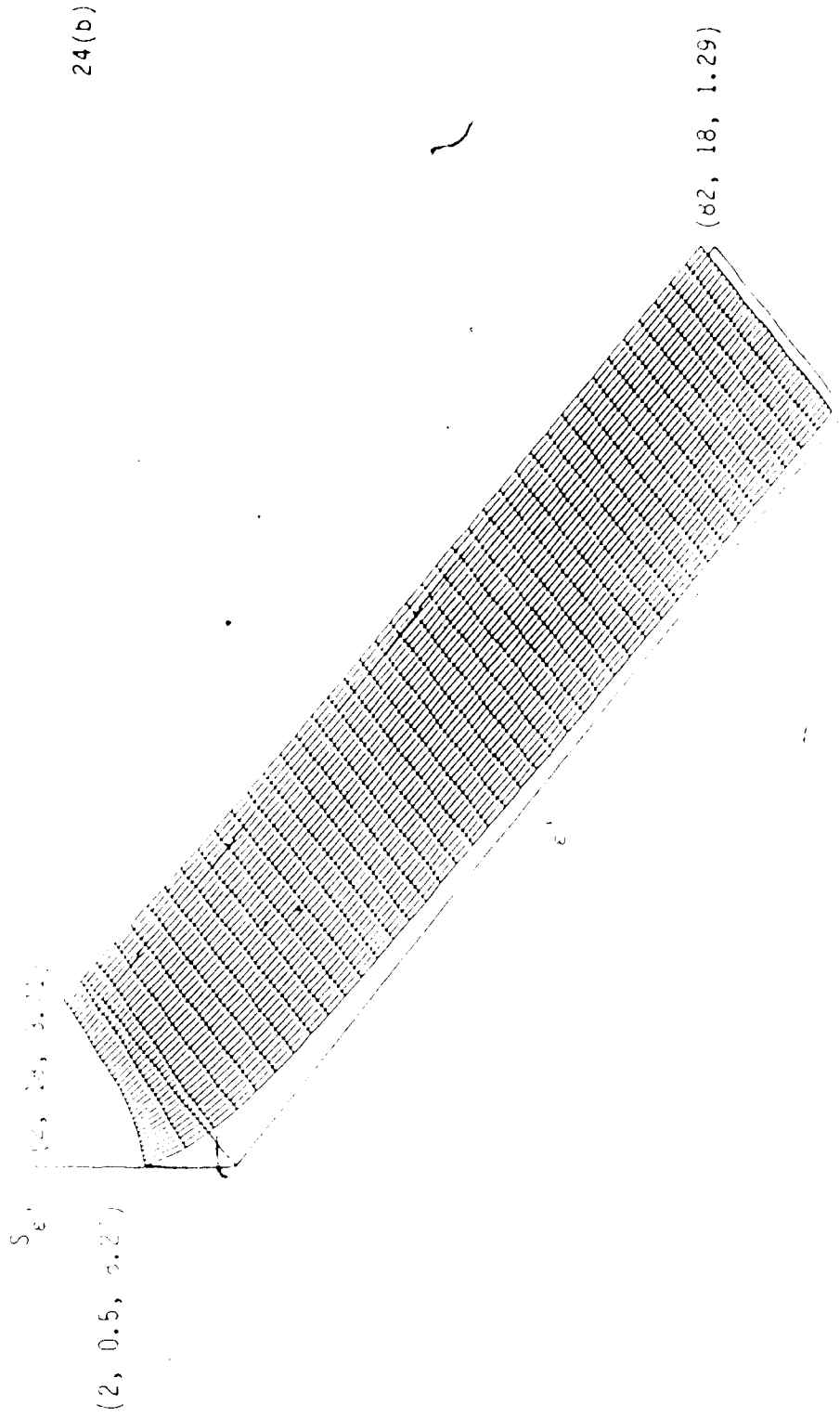
Figure 24(b). Sensitivity in ... per radian relative shift, ratio method, ... ℓ = 3.5cm, f = 3 GHz. The points are shown in ... format.
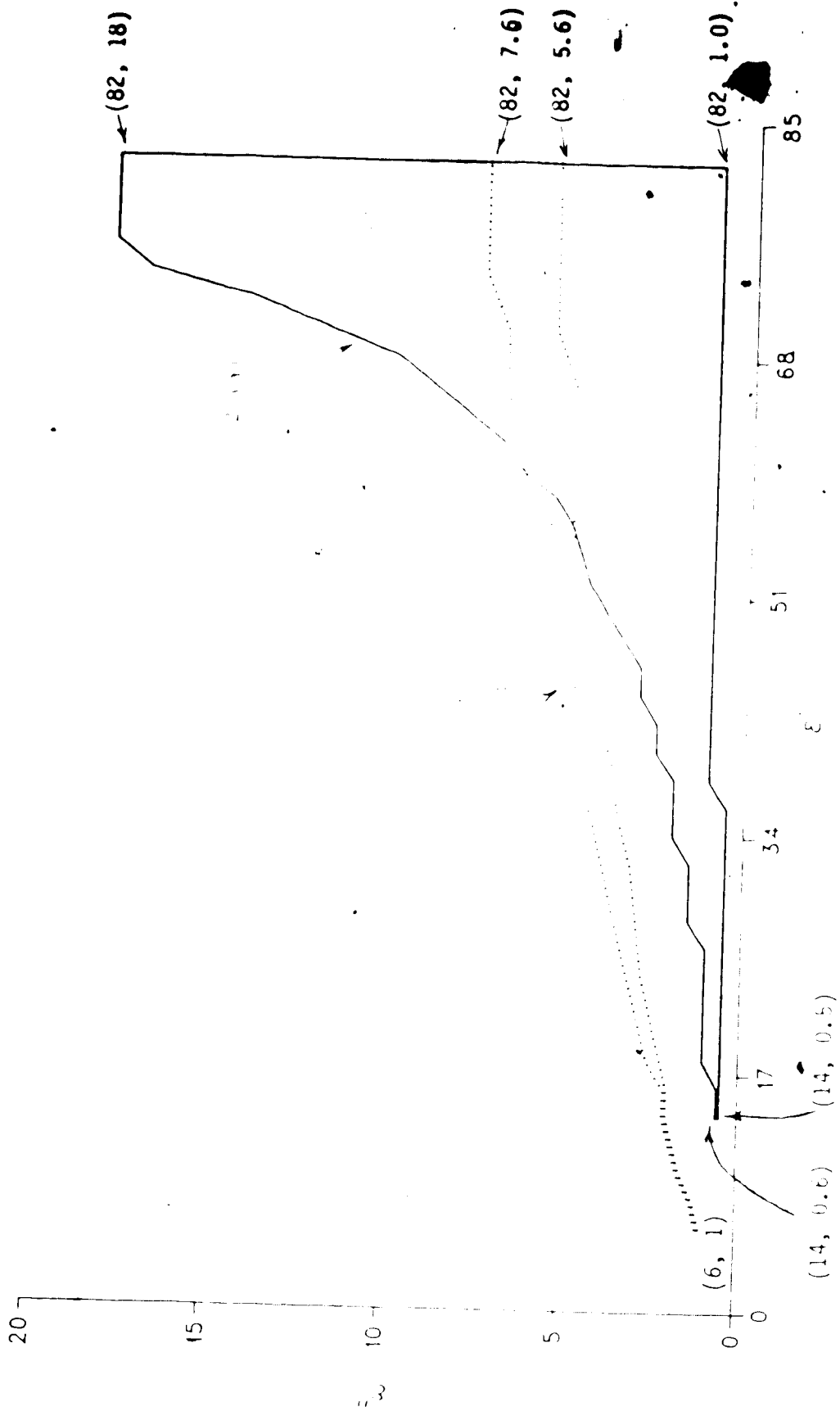
Figure 25. Regions for acceptable timing sensitivity for single transmission method.

(a) Length of the sample holder = 17 cm, f = 3 GHz. $S_{\tau\varepsilon}$ varies from 1 at (14, 0.5) and (14.06) to 2.06 at (82, 0.5) and 2.08 at (82, 15) for $-1 < S_{\tau\varepsilon} < 1$, (solid line).

(b) Length of the sample holder = 3.5 cm, f = 3 GHz. $S_{\tau\varepsilon}$ varies from 0.26 at (6, 1) to 10.03 at (82, 5.6) and (82, 7.6) for $-1 < S_{\tau\varepsilon} < 1$, (dotted line).

Figure 26. Regions for oscillating in log behavior... of multiple transmission method.

(a) Length of the sample holder = 17 cm, t = 3 GHz. S_1 varies from 1.10 at (18, 1) and (18, 1.1) to 2.0 at (82, 4) and 2.1 at (82, 18) for $-1.2 < S_2 < 1.2$ (solid line).

(b) Length of the sample holder = 3.5 cm, t = 3 GHz. S_1 varies from 10.1 at 4, 1 to 20.03 at (24, 5); 14.58 at (34, 6.5) to 15.73 at (40, 7); 11.51 at 65, ... to 10.24 at ..., 11.5) and ... at 1, 11.5) to -10.69 at (82, 14) for $-1.2 < S_2 < 1.2$ (dotted line).

(82, 18)
(82, 14)
(82, 12.5)
(82, 4.0)
(78, 2.5)
(73, 85)
85
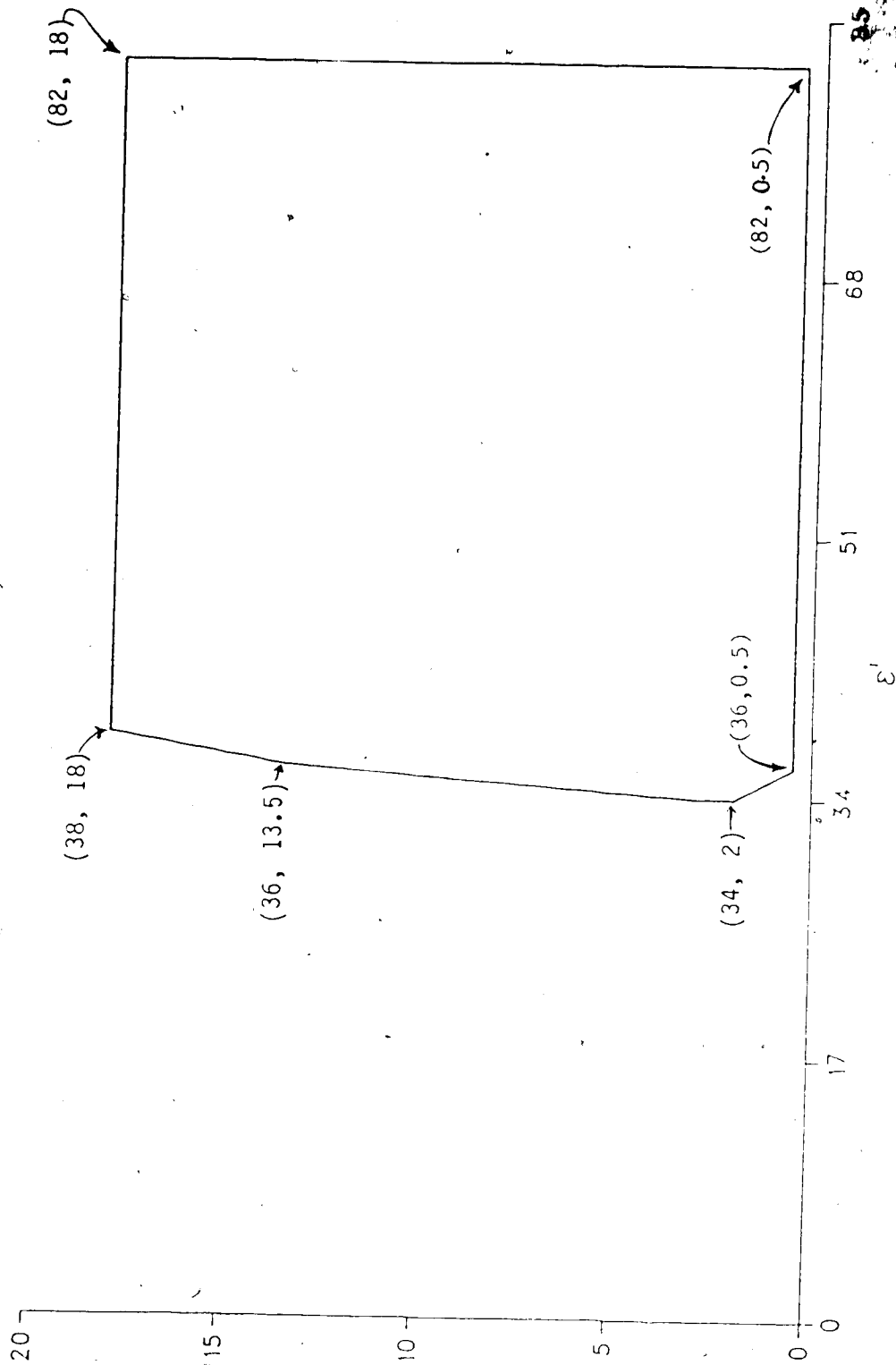
Figure 27. Regions for acceptable timing sensitivity for ratio method.

Length of the sample holder $\ell_1 = 17$ cm, $\ell_2 = 3.5$ cm, $f = 3$ GHz. $S_{\epsilon'} \leq 4$; 4.04 at $(34, 0.5)$ and 2.6 at $(82, 18)$ for $-2 < S_{\epsilon''} < 2$.

CHAPTER IV

A Model for Packaged Food Heating in Microwave Ovens

4.1 Absorption in a Layered Medium in a Microwave Oven

Most modern foods, when packaged for heating in a microwave oven, are layered media. Two schematic representations are given in Fig. 28. An individual layer for example, meat shown in Fig. 28(c), may further be a multilayered medium. With a constantly rising projected demand for microwave ovens and packaged foods [16,146], there is a need for a better understanding of the microwave heating of layered foods. In this chapter a model is given which can be used to estimate the energy absorption in various layers of a pre-packaged food. This model can also be used for browning calculations: e.g., the model predicts a spacing of 10-50 mm between pizza and a transparent conducting film for optimum results (incidentally, the spacing in a commercial package of Pillsbury, Ltd. is ∿28 mm).

Food heating in a microwave oven is a complex phenomenon involving heat and mass transfer. Water vapours from the lower layers rise upwards and make the dielectric properties of all food layers a function of time. This process makes exact calculations extremely difficult. The static model given in this chapter is only an approximation of the actual heating process; to fully account for the reality a dynamic model is required. The research in this area is new as discussed recently by Risman [5], and it is expected to take some time before a realistic model is fully developed. If this method were applicable, even in a very approximate sense, to heating of layered

foods in microwave ovens, it could provide useful initial design information for food packaging and susceptor materials. It is shown in Section 4.3 that the absorption in a thin water load in a microwave oven follows this model approximately. The model also demonstrates the significance of the temperature dependence of the complex dielectric constant of a material when heating layers in, for example, prepackaged foods. The theoretical basis for the model is given in the next section.

4.2 Theoretical Basis for the Model

The preliminary heating tests on thin water loads (3 mm - 10 mm), in a microwave oven, showed that the absorption is a function of thickness of the water load. Stratton's [19] solution for the reflection and transmission of a plane wave normally incident on a layer of water in air also shows a similar absorption response. It is, therefore, considered that simple plane wave solutions merit investigation for studying absorption in a layered material in a resonant (multimode) microwave oven. Accordingly, in Fig. 29 the normal incidence of a plane wave on two homogeneous layers backed by a perfect metal reflector is considered. The reflection coefficient, R, from the upper surface is given by [20]:

$$R = (Z_1 - \eta_0)/(Z_1 + \eta_0) \tag{4.1}$$

where $\eta_0 = (\mu_0/\varepsilon_0)^{1/2}$, the free space value (377 ohms), and

$$Z_1 = \eta_1 (Z_2 + \eta_1 \tanh(\gamma_1 d_1))/(\eta_1 + Z_2 \tanh(\gamma_1 d_1)) \qquad (4.2)$$

$$Z_2 = \eta_2 \tanh \gamma_2 d_2, \quad Z_3 = 0$$

In the above equations γ_1, γ_2; d_1, d_2; and η_1, η_2 are the propagation constants, the thickness of the layers and the intrinsic impedances of layers 1 and 2 respectively. η_1 and η_2 are, in general, complex quantities.

The transmission coefficient from layer 1 to layer 2, T_{12}, is given by [20]:

$$T_{12} = \left[\frac{2\eta_1}{\eta_1 + \eta_0}\right] \left[\frac{2 Z_2}{Z_2 + \eta_1}\right] \cdot \left\{ 1 - \left(\frac{\eta_0 - \eta_1}{\eta_0 + \eta_1}\right) \left(\frac{Z_2 - \eta_1}{Z_2 + \eta_1}\right) e^{-2\gamma_1 d_1} \right\}^{-1} e^{-\gamma_1 d_1}$$

$$(4.3)$$

and the absorption in layer 1 is given by:

$$|A_1|^2 = 1 - |R|^2 - |T_{12}|^2 [\eta_0 \; \text{Real} \; (Z_2^{-1})] \qquad (4.4)$$

In the special case where layer 2 is free space, Real (Z_2^{-1}) becomes η_0^{-1}. All these terms are temperature dependent through the complex relative dielectric constant $\epsilon^*(\theta) = \epsilon'(\theta) - j\epsilon''(\theta)$ where θ signifies temperature.

To check the results from the above model, Equation 4.4 was used to solve for two cases at 2,450 MHz: a film of water in free space (Fig. 29(b)) and a film of water backed by a perfect metal reflector (Fig. 29(c)). In doing this the dielectric data for water according to

Risman [123] at three temperatures, 20, 50 and 80°C, was used. These values are given in Table 11. In order to verify the computer solutions for the model, first an example given by Stratton [19] was solved. The results obtained were in agreement with Stratton [19]. However, the results, for a similar problem, obtained from this model did not agree with those given by Ruck [147]. Therefore, the reflection and transmission of a slab of lossy dielectric material were computed from two more models, one given by van Gemert [129] and another by Jones [148] and also by Fuoss [149], see Appendix II. The results obtained from both the above models also matched exactly with those from Equation 4.4 and Stratton's solution.

For a system with two layers the results have been checked by solving an example given by Ramo [150]. The solution obtained using Wait's model [20] and the Jones/Fuoss matrix model [148,149] agree with that of Ramo [150].

Solutions obtained for a system of three layers (water on a borosilicate glass plate backed by a metal sheet) from the above two models [20;148,149] also agree very well, as discussed below. It was felt necessary to investigate all the models and check the solutions, because one result obtained from this plane wave model (for a semi-transparent conducting film) may be important in practice.

The theoretical plots of absorption vs. water layer thickness, d, obtained from Equation 4.4 are shown in Figures 30 and 31. Two important points are apparent. First, a small change in layer thickness (i.e., one quarter wavelength in the water, $\lambda^w/4$) can alter the absorption by almost one order of magnitude (e.g., from p_1 to p_2 in

Fig. 31). This effect is more pronounced with the metal reflector. Secondly, maximum absorption at one temperature in a layer becomes a minimum for a change of only $30^{\circ}C$ (e.g., p_1 and p_2 on Figs. 30 and 31). Thus, if a film is regarded as analogous to a susceptor at temperature θ_1, it is an "anti-susceptor" at θ_2, where $\theta_2 - \theta_1$ is quite small with water. It may be emphasized that this is so far very theoretical: it illustrates only layer resonance phenomena — and its temperature dependence — in the case of water.

If the above is extended to more general cases (Fig. 29(a)), it is found that the resonance absorption is still pronounced. As an example (and one which is the logical next step for microwave oven considerations) a solution has been obtained when a low-loss borosilicate glass plate ($\varepsilon^* = 4.05 - j0.0043$) is included as a layer between the water film and the metal. This example is shown in Fig. 32. Both models [20;148,149] give identical results. A high peak-to-valley ratio for absorption with changing layer thickness still occurs and the temperature separations (between θ_1 and θ_2) are still pronounced.

It was also computed from this model that a transparent conducting film of thickness 20 Å, when placed at a distance of 10-50 mm over a

thick metal sheet would absorb about 50% of the energy in an incident plane wave, see Fig. 33. Therefore, with a 6.4 mm borosilicate glass tray ($\varepsilon^* = 4.05 - j0.0043$) in the bottom of the oven cavity the optimum distance of such a film, for near maximum absorption in it, is 0-37.5 mm (substract the effective thickness, $6.4\sqrt{4.05}$ mm, of the glass tray from 10-50 mm). This calculation possibly explains ~ 28 mm as the chosen height of a metallized plastic browning film above the oven base in a commercial pizza package (Pillsbury, Ltd.).

For the above calculations the model of Fig. 29(a) is used with the following parameters: $d_1 = 20\overset{o}{A}$, $\varepsilon'' = 4.84 \times 10^7$ (see ahead), and $\varepsilon' = 1.0$. The optically thin metallized plastic film is modelled as a dielectric sheet for the above calculations, because analogous to a dielectric sheet, this film also reflects and transmits an incident wave. The ε'' of the film was calculated from its surface resistance, which was calculated as 75.0 ohms per square from the reflection coefficient of the film at 2.45 GHz [151]. The numerical evaluation of ε'' is as follows: $R_s = 1/\sigma L$ or, $1/\sigma L = 75$ ohms per square, where σ is the alternating current bulk conductivity at 2.45 GHz and L is the thickness of the film. L was estimated to be 20 $\overset{o}{A}$. This gives $\sigma = 0.66 \times 10^7$ S/m, or $\omega\varepsilon''/\varepsilon_0 = 0.66 \times 10^7$ S/m, for which $\varepsilon'' = 4.84 \times 10^7$ at 2.45 GHz. Even if L were greater in reality - $40\overset{o}{A}$ or $60\overset{o}{A}$ - the distance, d of Fig. 33 for the optimum absorption remains almost unaltered; only the per cent absorption in the film decreases. Such a film would only require more time for producing the desired heating effect.

The choice of $\varepsilon' = 1.0$ seems justified by the fact that the number of bound charges, in the film, is negligible in comparison to the free

charges. However, it is found that even if ϵ' were in the range 1-100, the error in the computed values of A is negligible, because the magnitude of the ϵ^* of the film is determined by the large value of ϵ''.

4.3 Experimental Analysis

Experiments were designed to measure the energy absorbed in water layers in a microwave oven having a top power feed and a mode stirrer. The objective was to determine whether the power absorbed in a tray of water could be related to the plane wave model. In order to make depth measurements more easily, a trace of non-ionic surfactant (Wyandotte Pluronic F68) was used in the water to reduce the meniscus.

Two types of heating tests were done: constant-time heating test and constant-temperature-rise test. In a constant-time heating test the water layer is started from below ambient in an attempt to reduce the heat loss. In these tests, layers of different thicknesses were heated for the same time; thus, the incident energy was the same for all cases. This caused different temperature rises for different volumes and, therefore, some error in the results due to different radiation losses and ranges of $\epsilon^*(\eta)$. Total heat absorbed by water layers in the thickness range $3 < d < 25$ mm and different surface areas is shown in Fig. 34. The trend with these curves is to show the theoretical resonance effect; however, the magnitudes measured are $<$ 2.1 (peak-to-valley). It was difficult to make consistent measurements on water films having d <3 mm.

In an attempt to improve the accuracy by further reducing the heat loss, water layers were heated in a thermally insulated styrofoam

container (Fisher Scientific U3-531 serum biomailer; internal diameter 16.2 cm, wall thickness 3 cm) for different durations of time, such that the temperature rise was almost the same (to within $\pm$ 5°C) for all layer thicknesses. This reduced the error due to the variation of ϵ^* with temperature. This is called a constant-temperature-rise test. As the heating times were different for different d's, total power absorbed for a fixed time was then calculated from the measured total power. The results are shown in Fig. 35, inset lower curve. The upper curve (inset) results from applying an oven efficiency correction factor, according to Fig. 36 [152] for the different volumes of water involved in each layer heating test. Although this is a reasonable correction to apply, it is imprecise and merely indicates that the peak-to-valley ratio is greater in practice. With the same correction applied to the results in Fig. 34 together with a temperature correction factor using the data in Table 11, the largest estimated peak-to-valley ratio from all these experiments is about 5:1 (d < 10 mm, Fig. 34(d) and still typically of the order of 2:1 in all other cases.

The absorption in water layers in the styrofoam container at oblique incidence is also computed. It is found that the ratio of A_{max} to A_{min} decreases continuously with increasing angle of incidence. Near the Brewster angle for water ($\sim 83^o$) the maximum ratio is about 5:1, as shown in Fig. 37. Here total reflectance, $|R|^2$ is taken as $[|R_{||}|^2 + |R_\perp|^2]/2$, where $R_{||}$ is the reflection coefficient for the parallel polarized wave and $R_\perp$ is that for perpendicularly polarized wave. Equations A.2-4 and A.2-5 of Appendix II were modified to include the effect of the angle of incidence according to [147,148].

4.4 Discussion

Although the peak-to-valley ratio may be small in practice, enhanced heating can obviously occur in layers of selected thickness. If the oven cavity between the mode-stirrer and the load is taken as a waveguide with dimensions 39.4x34.8 cm (base dimensions of the oven in this case, Figs. 34 and 35), then λ_g=12.39 cm for the TE_{10} mode (λ_0=12.24 cm at 2,450 MHz). Higher order modes will have larger values of λ_g. From Fig. 34 it is seen that the peak-to-valley separations in water films correspond to an "equivalent average free space wavelength", $\overline{\lambda}$, in the range 12.0 $\pm$ 0.5 cm, an agreement which is not as close as one would expect to see. From the experimental results given in Fig. 35, $\overline{\lambda}$ is 12.20 cm, which is also less than the theoretical minimum value of 12.39 cm. Temperature effects of ε^* may again be responsible. This observation supports the belief that a TE cavity mode behaves like a TEM wave inside a high dielectric constant load [5].

The temperature dependence of a resonance response of the type studied may be significant in practice; certainly the magnitude of the effects illustrated in Figs. 29-31 and verified, albeit weakly, for water merit further investigation. In showing, by analogy, that a susceptor at one temperature can be the opposite, an anti-susceptor at another, it is being suggested that, in principle, there is a possibility of achieving either hot planes and/or controlled temperature gradients in layered foods with the correct material dimensions and packaging. For example, if the temperature function of the dielectric constant were known, it may be possible to choose a

critical thickness for a material such that it is susceptible to heating at $-10^{\circ}C$ but not at $20^{\circ}C$. If this is so, it might be possible to thaw small food portions rapidly and uniformly. Another application of this principle could be in enhanced dielectric heating of the surfaces of layered foods for browning: here a film would act as a "susceptor" up to a predetermined temperature (e.g., $200^{\circ}C$) and then only as an insulator.

In the next chapter, the heating tests done in a microwave oven on some browning agents, pastes and sugar-alcohol mixtures are described.

Table 11

Dielectric Data for Water at 2.45 GHz[a], 10 - 80°C

Temperature (°C)	ε'	ε''
10	80.5	13.2
20	77.4	9.7
30	74.9	7.4
50	69.4	4.5
80	61.8	2.8

[a] According to Risman's estimate [123]; these values, for 2.45 GHz, do not appear in the immediate literature. These have been estimated, by the use of Debye's first-order approximation of dielectric dispersion, from data measured at 2.8 GHz.
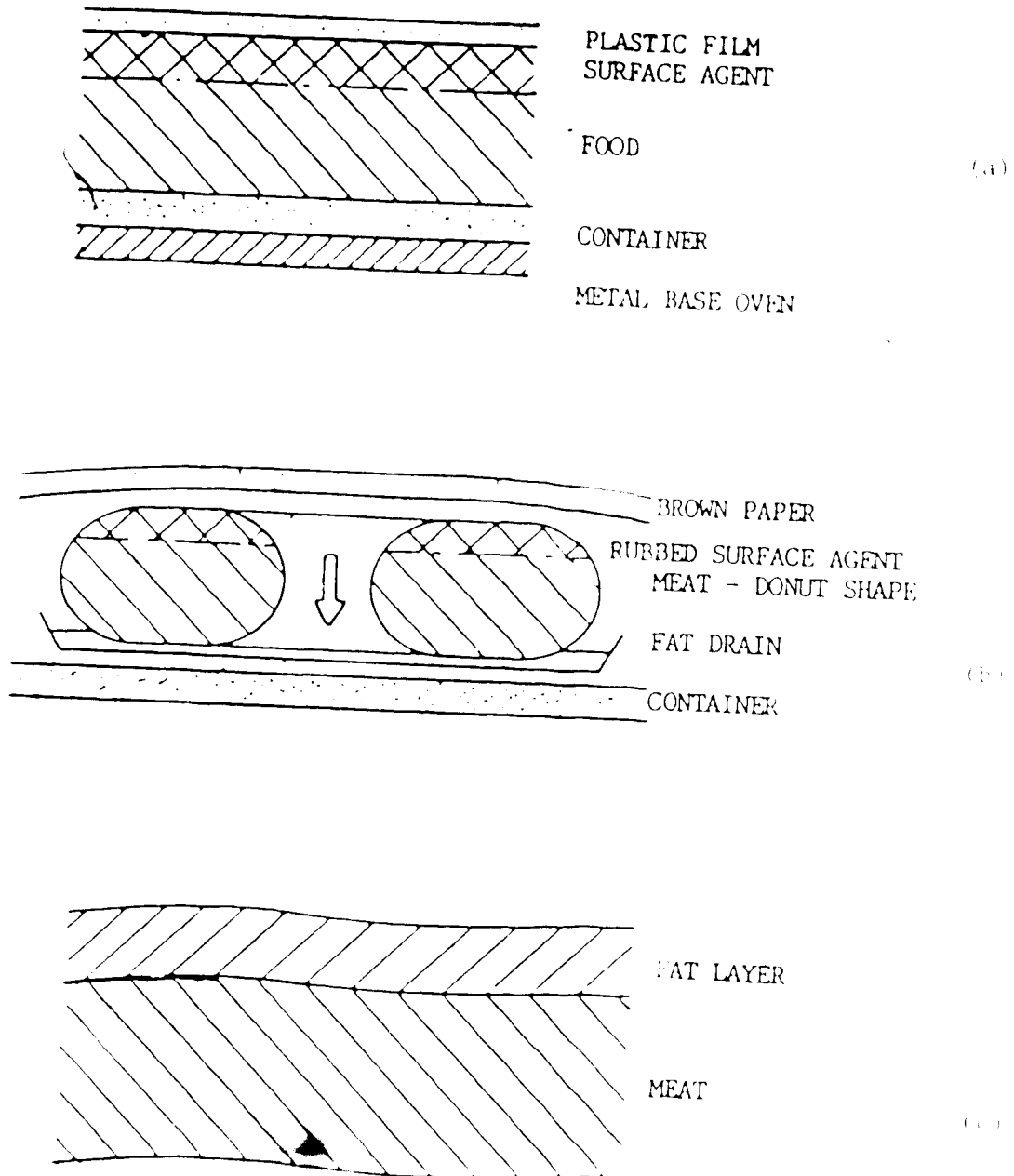
Fig. 28. Schematic representation of some actual or
packaged foods as a layered medium

Free Space

Plane wave
(Normal incidence)

η_0, γ_0

Layer 1

η_1, γ_1

d_1

Infinite Width
Assumed

x

Layer 2

η_2, γ_2

d_2

Layer 3
(Metal Reflector, $\eta_3 = 0$)

(a)

d_1

η_1, γ_1

$d_2 = 0$,
$\eta_2 = \eta_3 = \eta_0$

x

(b)

η_1, γ_1

d_1

$d_2 = 0$,
$\eta_2, \eta_3 = 0$

(c)
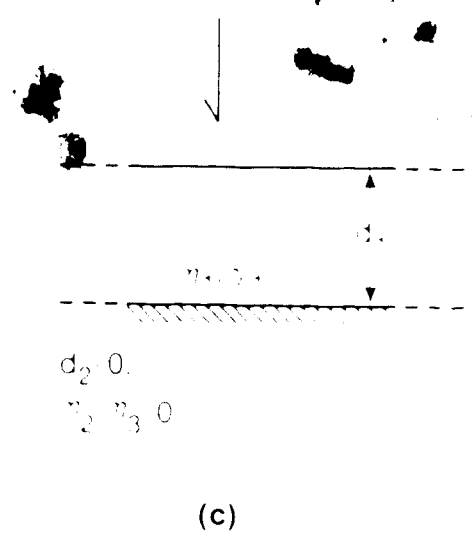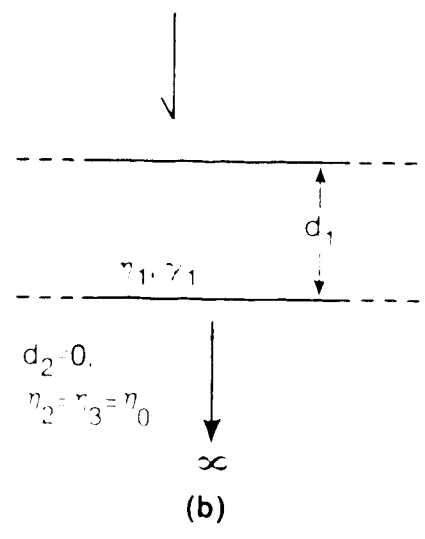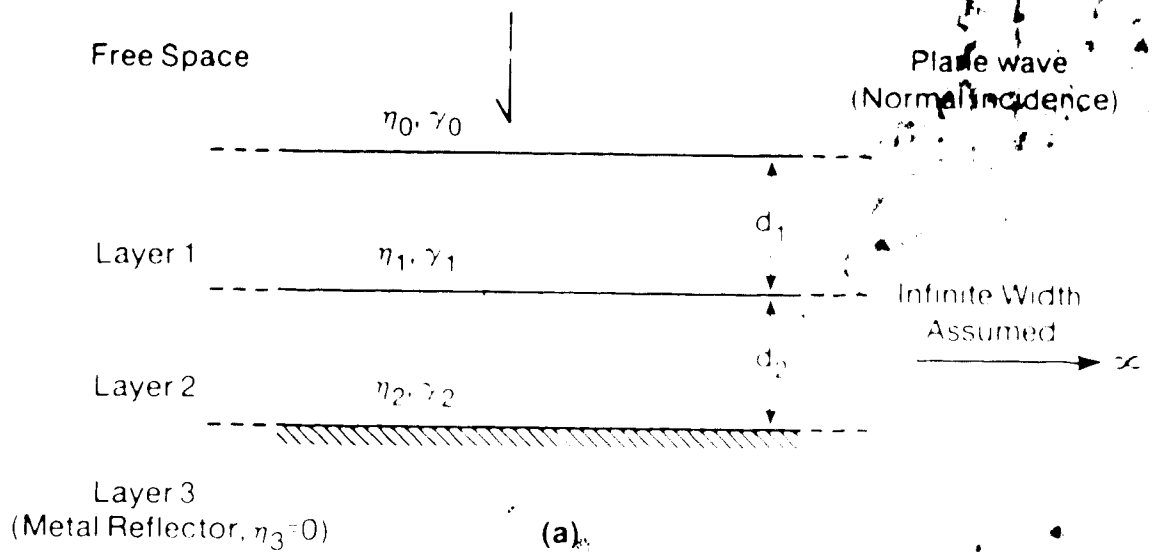
Figure 29. Plane wave (normal incidence) on a medium
(a) general case, two layers with a metal reflector
(b) single layer in free space (no metal reflector).
(c) single layer on a metal reflector
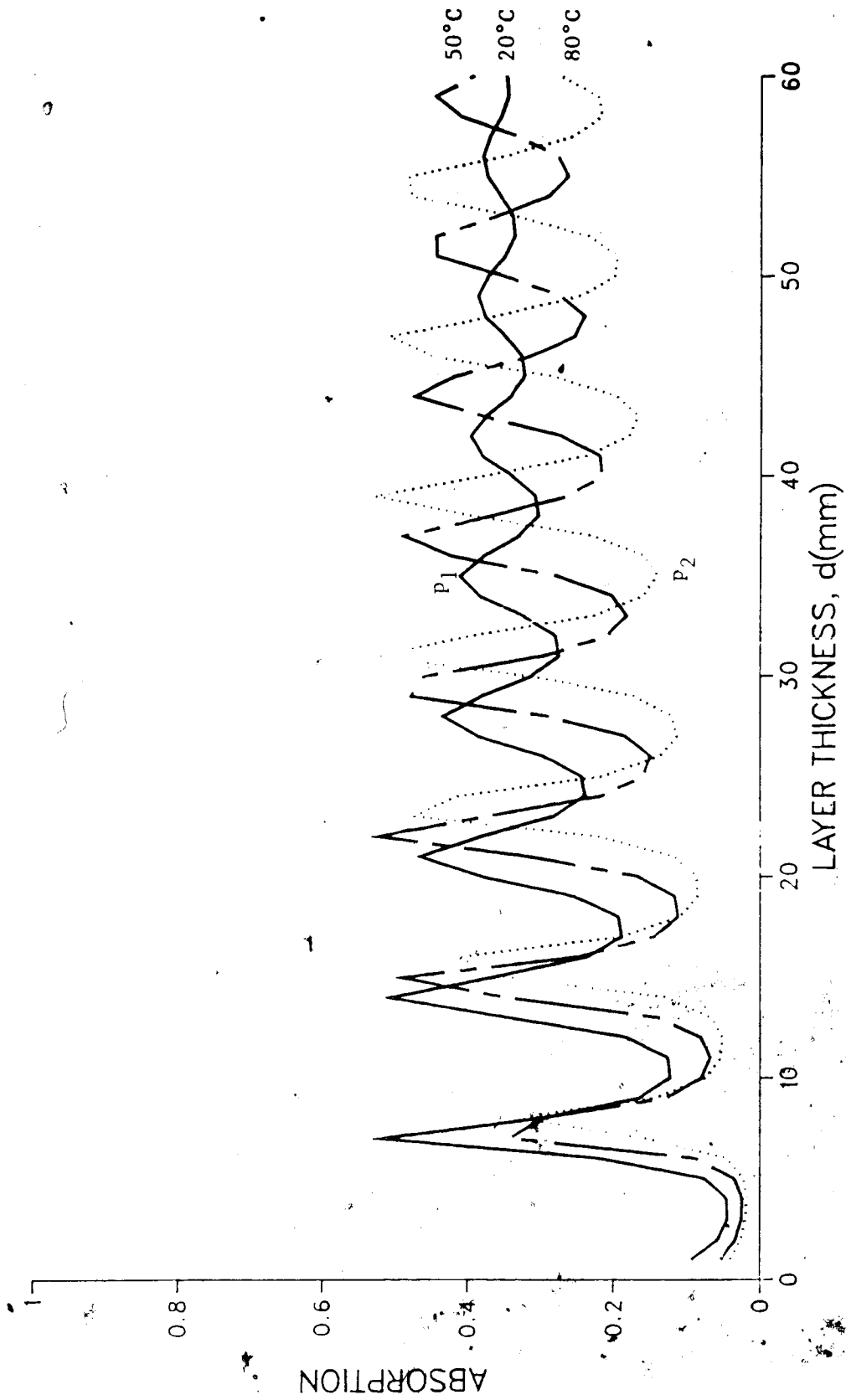
Figure 30. Variation of normally incident plane wave absorption with thickness for a water layer in free space at temperatures 20, 50, 80°C and a frequency of 2,450MHz.
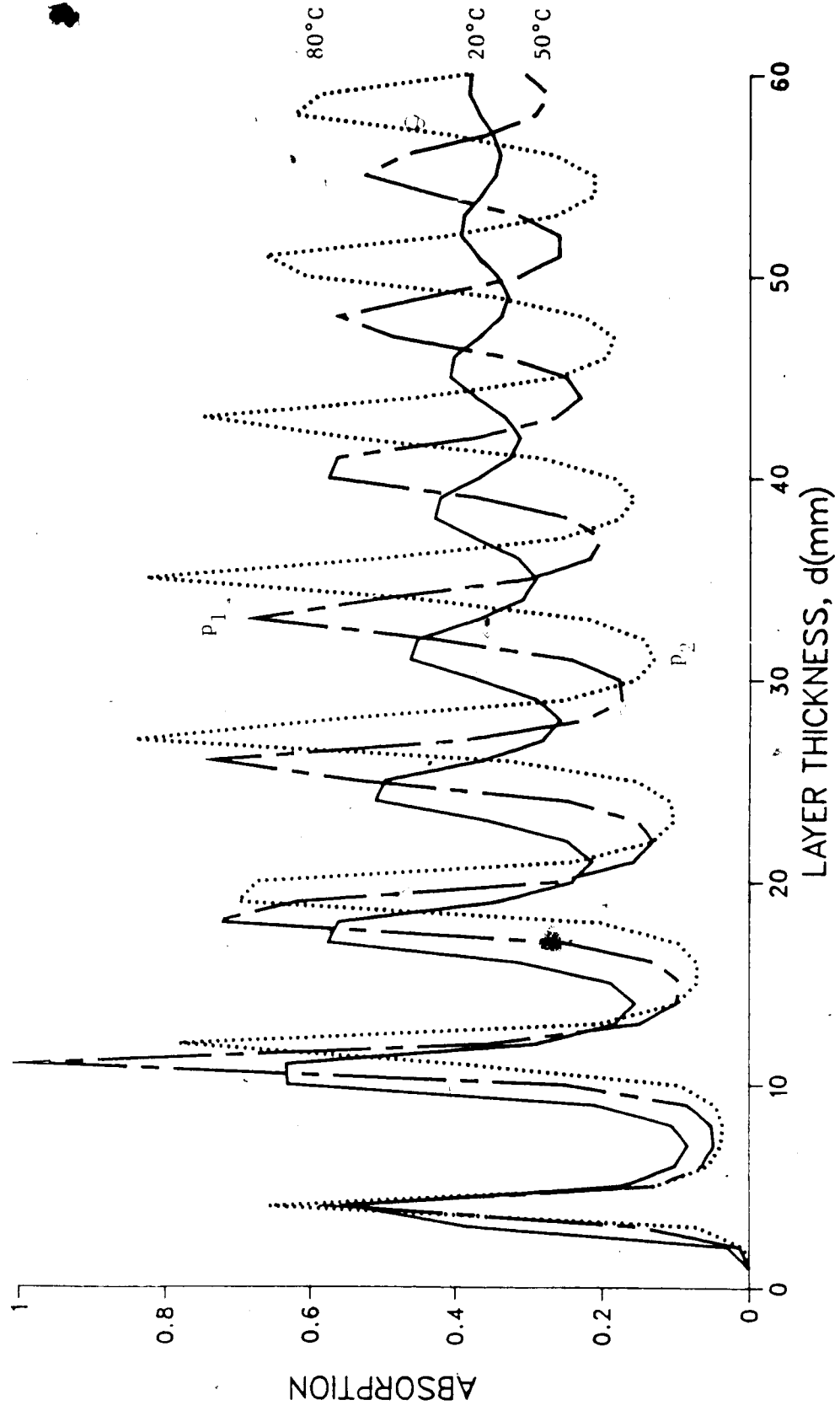
Figure 31. Variation of normally incident plane wave absorption with thickness for a water layer backed by a metal reflector at temperatures 20, 50, 80°C. (2,450MHz).
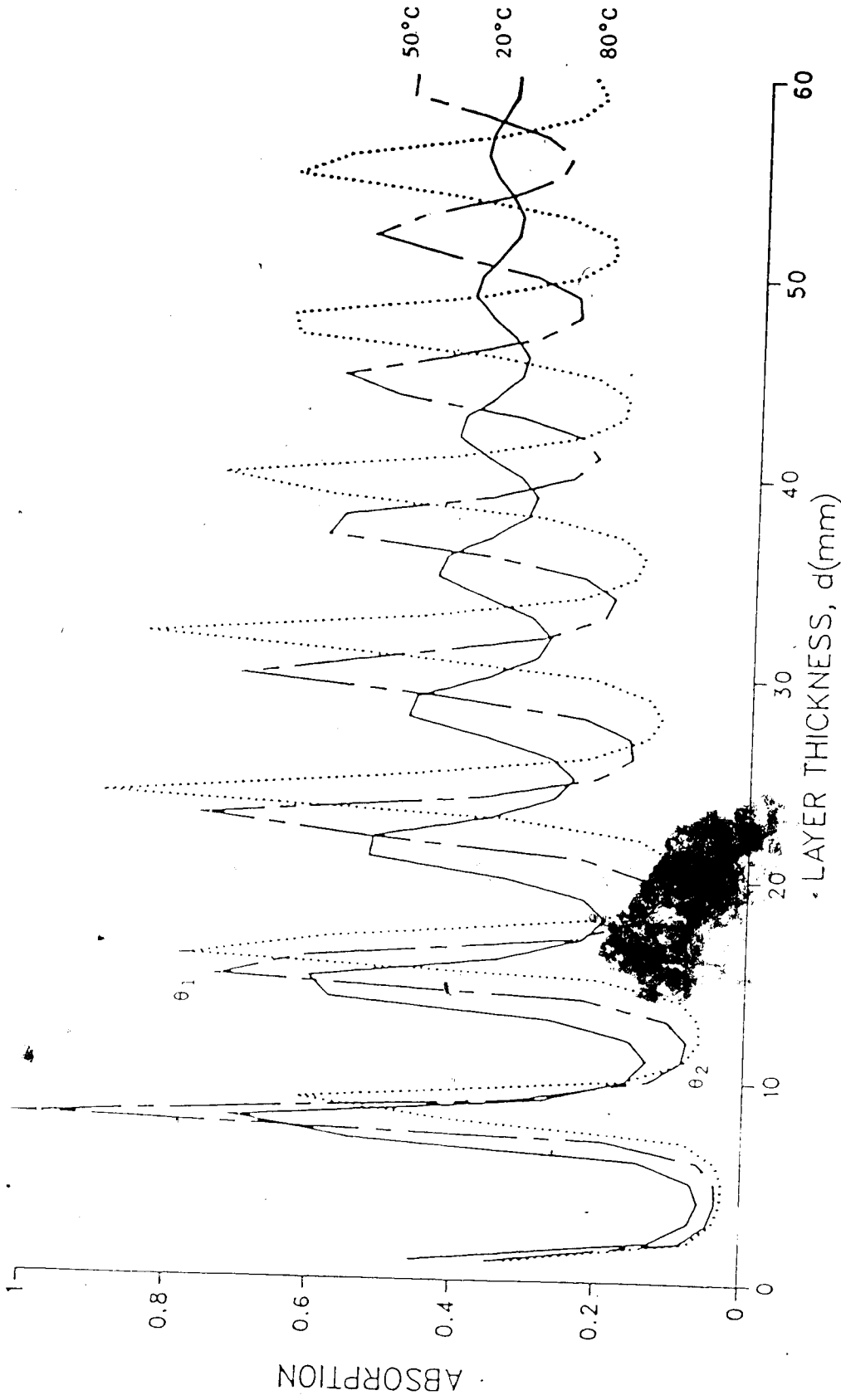
Figure 32.—Variation of normally incident plane wave absorption with thickness for a water layer above a borosilicate glass plate (thickness 0.64cm) on a metal reflector at temperatures 20, 50, 80°C (2,450MHz). Both models [20] and [148,149]give the same response.
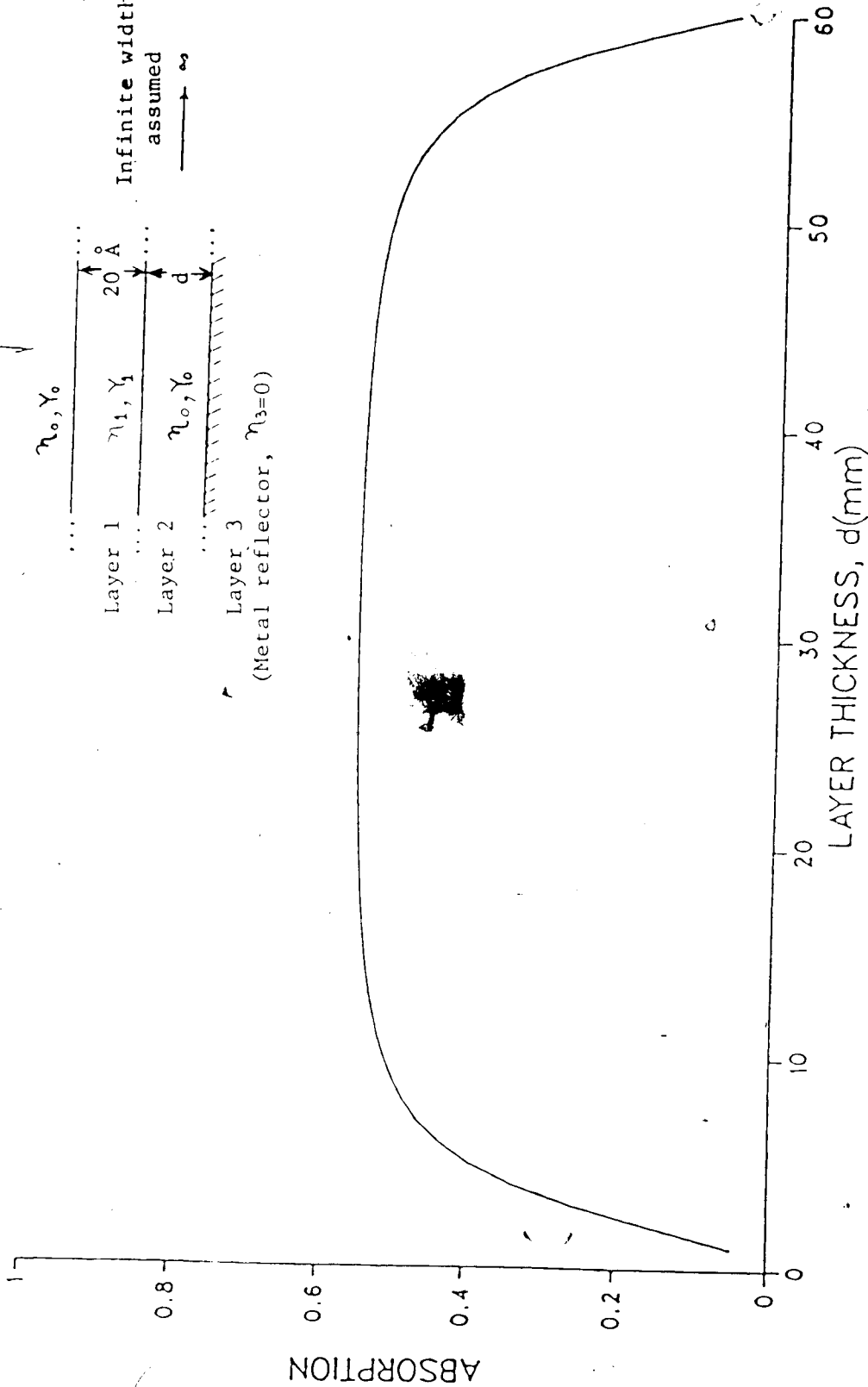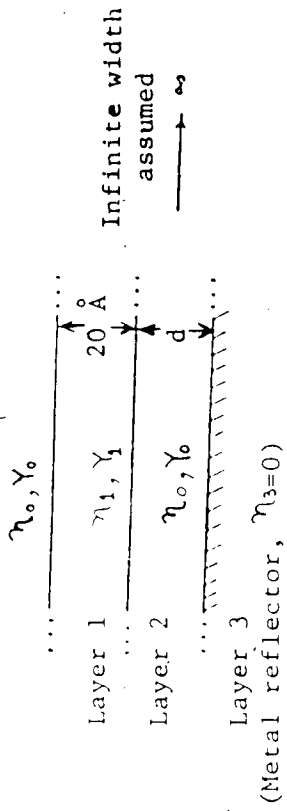
Fig. 33. Variation of absorption in a microwave semi-transparent conducting film, thickness 20 Å, at a distance d over a thick metal sheet as shown in inset.
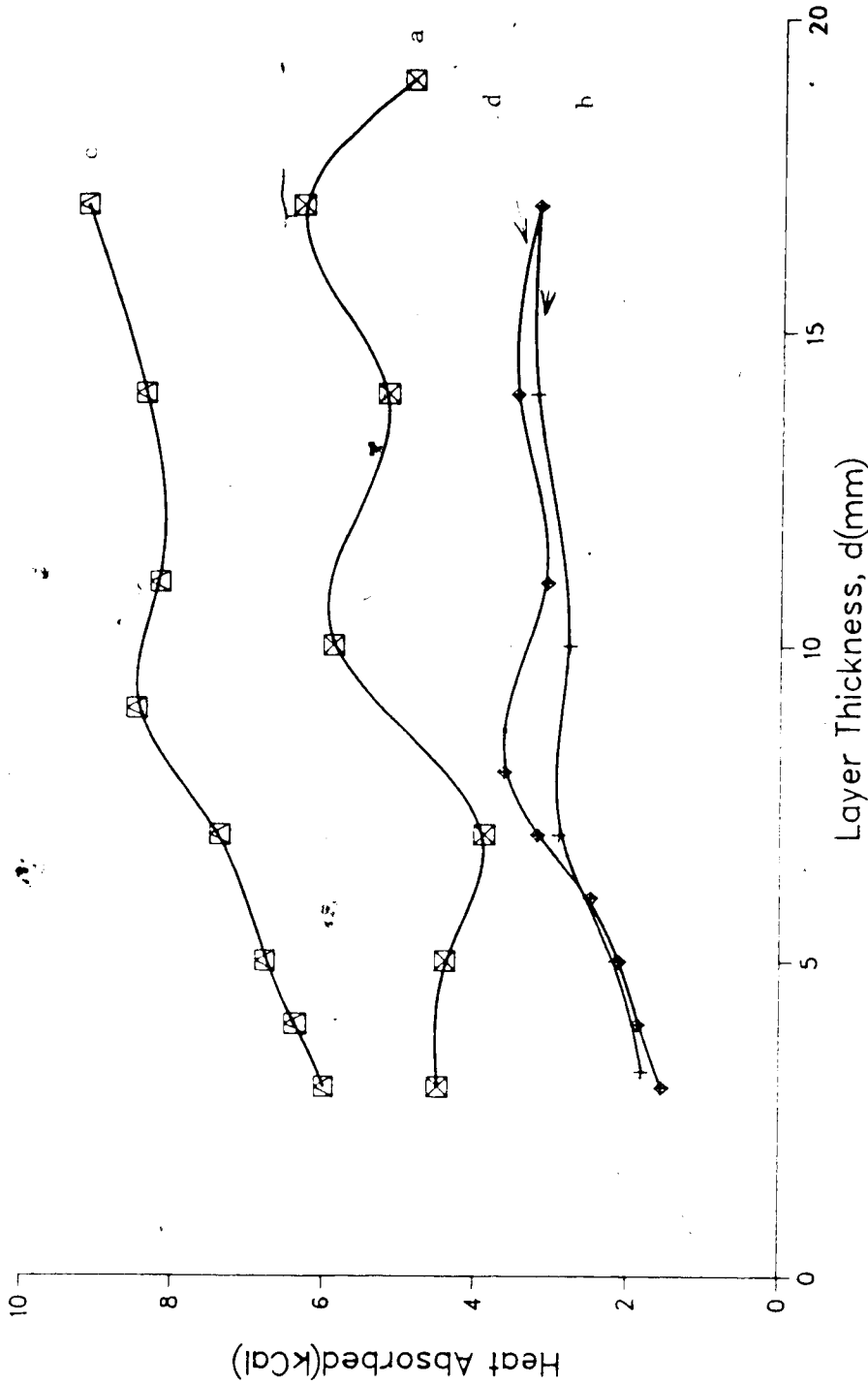
Figure 34. Heat absorbed in water layers in a 700W microwave oven. Water starting temperature typically 18°C, typical temperature rise 3-15°C, with the oven ambient temperature 23-26°C:

(a) Metal tray (31.25x28.5xdepth 5.15cm) on oven floor (65% of the oven floor area); heating time, 40 seconds.

(b) Borosilicate glass tray (25x16xdepth 4 cm, thickness 0.51cm) on oven floor (30% of floor area); heating time, 20 seconds.

(c) Plastic (TupperwareTM tray (28.5x28.5xdepth 5.25cm. thickness 0.2cm), on oven floor (60% of floor area); heating time, 50 seconds.

(d) Borosilicate glass tray (34x22x4cm, thickness 0.64cm), on oven floor (51% of floor area); heating time, 30 seconds.

138
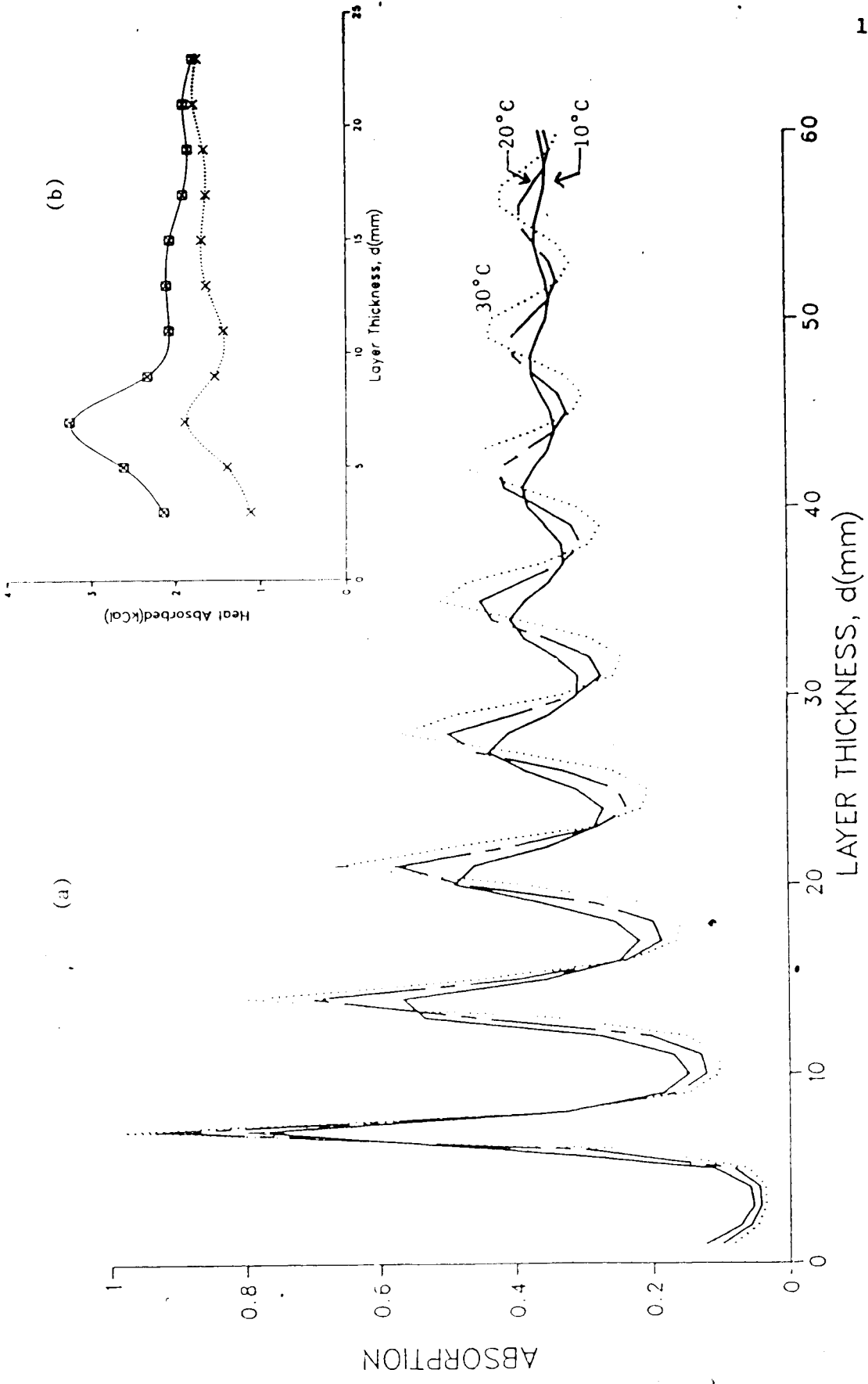
Figure 35. (a) Theoretical solution for water film in a styrofoam container on oven floor at temperature 10, 20, 30°C (2,450MHz). (b) Measured values of heat absorbed per unit volume, constant temperature rise method, equivalent to (a) above at 20°C.

EFFECT OF LOAD SIZE ON MICROWAVE OVEN POWER OUTPUT

OVEN #2 PANASONIC NE-7800CA
RATED POWER = 700 WATTS
OVEN COLD

LOAD (ml):	50	100	125	250	500	750	1000	2000
POWER (W):	299	401	452	473	625	723	740	760

OVEN WARM

LOAD (ml):	250	500	750	1000
POWER (W):	416	549	635	650
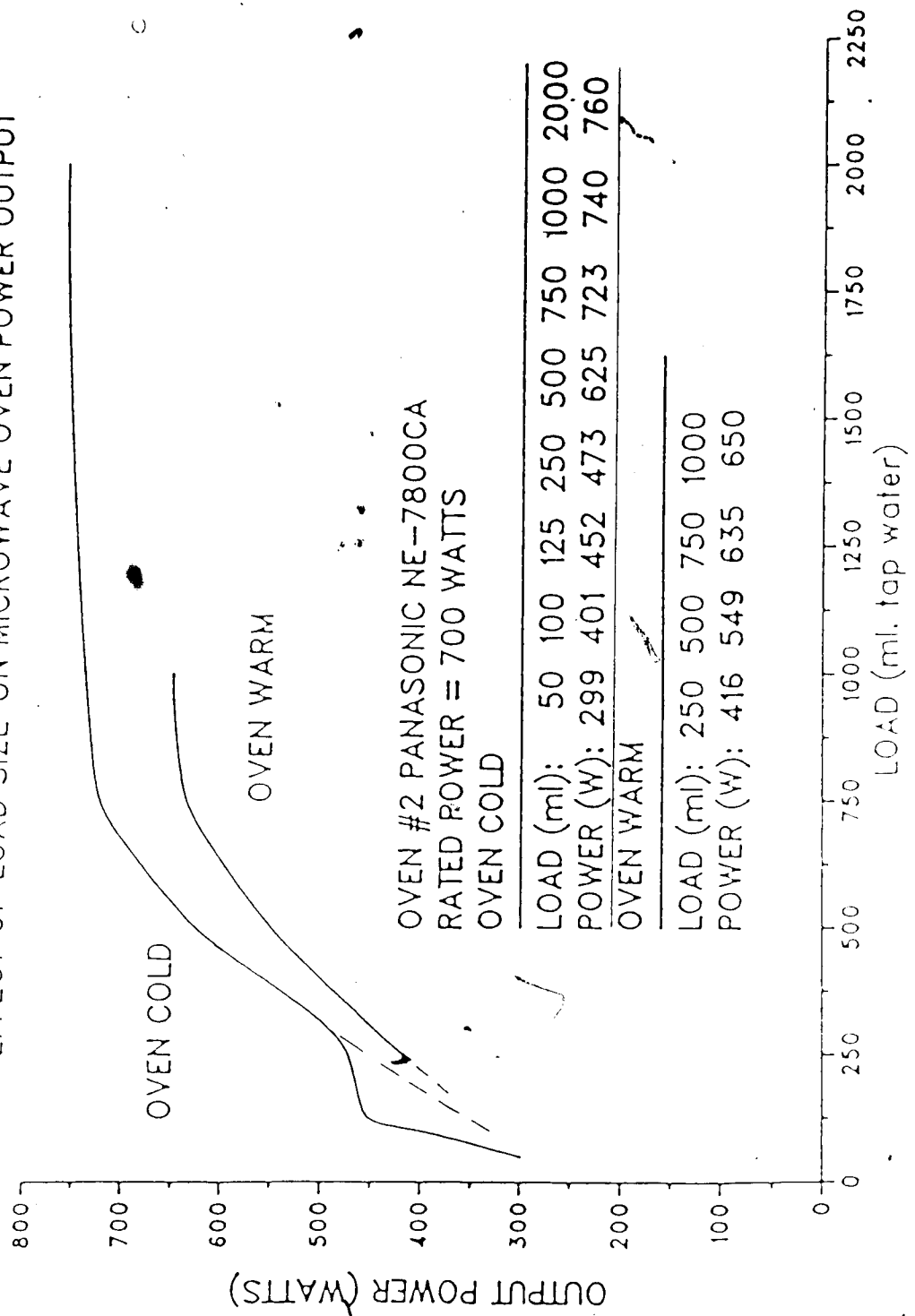
Figure 36. Effect of load size on microwave oven power output. The correction is based on the extrapolation of the oven (magnetron) power output. The correction taken from these results (for the water layer volumes used here) is based on the average slope of the curves as indicated by the lower dashed lines.
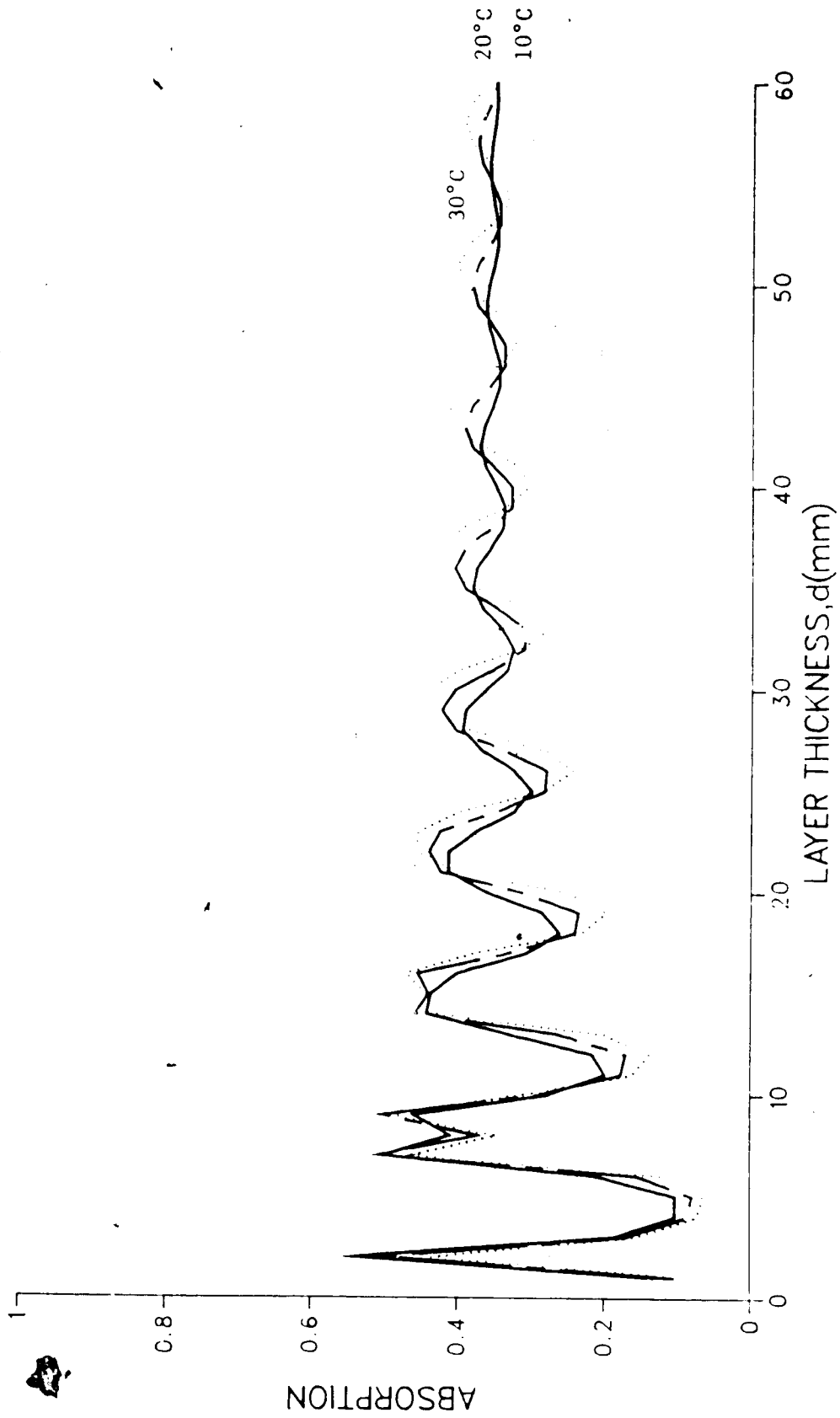
Figure 37. Theoretical solution at 2,450MHz for a water film in a styrofoam container on the oven floor (see text) at an angle of incidence of 83° at temperatures of 10, 20 and 30°C.

CHAPTER V

Microwave Browning

The need to brown certain cooked food surfaces needs no emphasis. Foods such as pizza, meat, crispy snack foods, and french fries, etc., on heating in a microwave oven, are either dried due to uniform heating or the moisture is driven towards the outer surface resulting in undesirable sogginess. Browning, thus, remains a problem in microwave heating.

The browning in foods can be of two types: enzymic and nonenzymic. Whereas the enzymic browning of certain foods, e.g., fruits and vegetables, is undesirable [153], the nonenzymic browning of some foods is highly desirable. The nonenzymic browning reactions are either due to carbonization or caramelization and require a temperature around $200^{o}C$ [154]. Three different approaches have been used for achieving the browning in microwave cooking. These are:

(i) Using susceptor materials;

    (a) Ferrite trays [155],

    (b) Chemical susceptors [2,3], and

    (c) Film type susceptors (resistive or semiconducting films) [17];

(ii) Using field intensification [156]; and

(iii)From browning agents

The results of the browning tests done on different foods with the mixtures and pastes of Chapter II and some other mixtures are given in the following section.

5.1 Browning Tests in a Microwave Oven

Simple evaluations were made of some of the pastes and mixtures discussed in Chapter II. A few other mixtures containing equal volumes of honey and glycerin with salt (NaCl) from 0-12.5%, by weight, were also tested to find the optimum NaCl concentration for heating performance; the dielectric constants of some of these mixtures are given in Table 12. Taste was also considered. These tests are intended to show the behavioural trend of a few materials. The tests performed can be classified into three categories:

(a) Browning with inert substrates and dry foods

To evaluate the individual performance of the pastes and mixtures, a thin layer ($\sim$ 2 mm thick) of these was spread on either an inert substrate, such as a piece of cardboard ($\sim$ 6x4x0.15 cm) or on a dry laminar food, e.g., a rice cracker. Cardboard pieces were chosen to simulate a dry food, because when heated these neither release water vapour nor absorb any to alter their dielectric properties substantially. A cardboard substrate thus represents an inert surface of the layer heating model of Chapter IV. The results are shown in Figs. 38, 39, 41 and 43.

(b) Browning with moist foods

A thin layer was applied on french fries, potato wedges, pizza and ham. The results are shown in Fig. 42.

(c) Effect of height on browning

. Rice crackers and cardboard pieces, each with a thin layer of a mixture or paste, were placed on styrofoam pedestals of heights from $< \bar{\lambda}/4$ to 5 $\bar{\lambda}/4$ from the metal bases of the oven cavity; $\bar{\lambda}$ is the

average estimated wavelength in oven cavity as discusssed in Chapter
IV. The results are shown in Fig. 40.

5.2 Discussion

(i) A sugar and glycerin mixture has potential as a browning agent on
dry laminar foods. While glycerin boils (bp ~230°C), this mixture
imparts a brown colour to the food surface partly due to searing and
partly due to caramelization of sugar. However, it is unsuitable for
non-laminar foods, e.g., potato wedges and chips with crumpled
surfaces, because the mixture, which is not a paste, flows and collects
at low spots on the food. This results in burning.

(ii) A sugar alcohol mixture does not seem suitable for meats (for
example, ham), mainly due to a strong influence on their taste.

(iii) The effect of food-height, from the metal base of the oven
cavity, on the rate of heating of the food could not be established.

Table 12

Dielectric Data for Some Mixtures and Their Constituents

2.9 GHz, 23°C

Material	ϵ'	ϵ''
1. (a) Egg yolk[a]	43	12.5[b]
(b) 1 egg yolk plus 1g glucose	25	11
(c) 1 g NaCl added to (b)	15	11
a) Egg yolk plus glycerin 33%(v/v)[c]	29	14.5
(b) 1 g NaCl added to (a)	29	15
(C) 1 g KCl added to 2(a)	29	18
3. (a) Honey[d]	7	2.3
(b) Honey/glycerin[e], equal volumes	7	2.1
(c) 1 g NaCl with 5ml each of honey and glycerin	8	4
(d) 5ml H_2O added to 3(c)	69	29
(e) 5ml egg yolk added to 3(d)	69	31

[a] From Section 2.6 where temperature data is given.

[b] When $\epsilon'' > 10$, value is rounded to nearest 0.5.

[c] 2/3 yolk, 1/3 glycerin.

[d] Clear commercial honey: BeeMaid[TM], Canada.

[e] Fisher Scientific Company, U.S.A.; Lot 732371.

Fig. 38. Surface browning tests in a 700W Panasonic oven on cardboard pieces (∿6x4x0.15 cm). A thin layer (∿2 mm) of mixture #3 (10 ml honey + 10 ml glycerin + 0.5 g NaCl) on the left, mixture #12 (paste of icing sugar and glycerin + 1 g NaCl) in the centre, and Marmite[TM] [95] on the right-all heated, for 45 s on full power, on a 2.5 cm (∿ 1/4) pedestal placed over the oven's borosilicate glass base-plate (thickness 0.64 cm).

Fig. 39. Surface browning tests with some mixtures in a 700 W Panasonic oven at full power:

(a) Observation #1, top right hand paper towel. Rice crackers (Taipan brand) heated for 60 s with thin layers of mixture #2 (10 ml honey + 10 ml glycerin + 1 g NaCl) on the left, mixture #3 (10 ml honey + 10 ml glycerin + 0.5 g NaCl) in the centre and mixture #13 (10 ml honey + 10 ml glycerin + 0.25 g NaCl) on the right.

(b) Observation #2, bottom right hand paper towel. Rice crackers (Taipan brand) heated for 60 s with thin layers of mixture #3 on the left, mixture #7 (10 ml honey + 10 ml glycerin) in the centre, and mixture #15 (10 ml glycerin + 5 g icing sugar + 0.5 g NaCl) on the right.

(c) Observation #3, top left hand paper towel. Taco tortilla chips (Old Dutch brand) heated for 60 s with thin layers of mixture #3 on the left, mixture #13 in the centre and mixture #15 on the right.

(d) Observation #4, bottom left hand paper towel. Taco tortilla chips (Old Dutch brand) heated for 40 s with thin layers of mixture #2 on the left, mixture #17 (15 ml glycerin + 5 ml Crosse and Blackwell Browning[TM][96]) in the centre and mixture #7 on the left.

National Library
of Canada

Bibliothèque nationale
du Canada

Canadian Theses Service

Service des thèses canadiennes

NOTICE

AVIS

THE QUALITY OF THIS MICROFICHE
IS HEAVILY DEPENDENT UPON THE
QUALITY OF THE THESIS SUBMITTED
FOR MICROFILMING.

UNFORTUNATELY THE COLOURED
ILLUSTRATIONS OF THIS THESIS
CAN ONLY YIELD DIFFERENT TONES
OF GREY.

LA QUALITE DE CETTE MICROFICHE
DEPEND GRANDEMENT DE LA QUALITE DE LA
THESE SOUMISE AU MICROFILMAGE.

MALHEUREUSEMENT, LES DIFFERENTES
ILLUSTRATIONS EN COULEURS DE CETTE
THESE NE PEUVENT DONNER QUE DES
TEINTES DE GRIS.
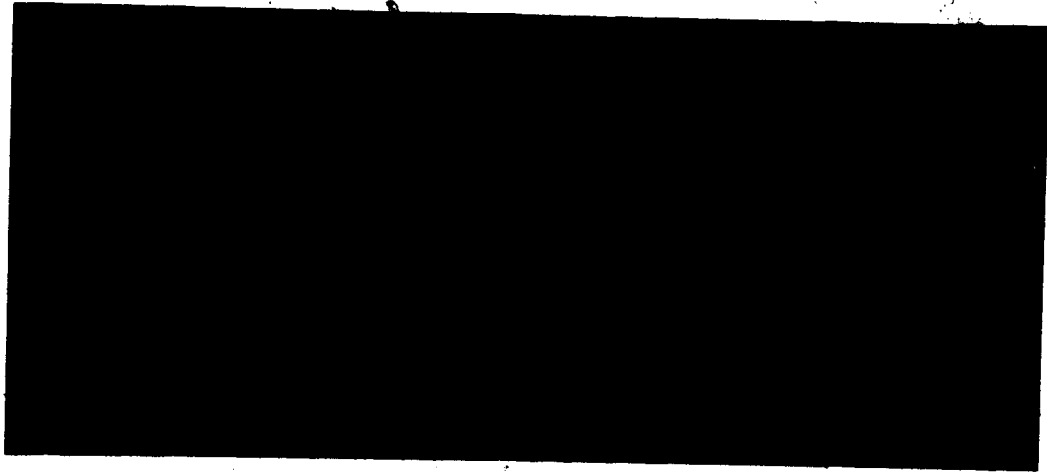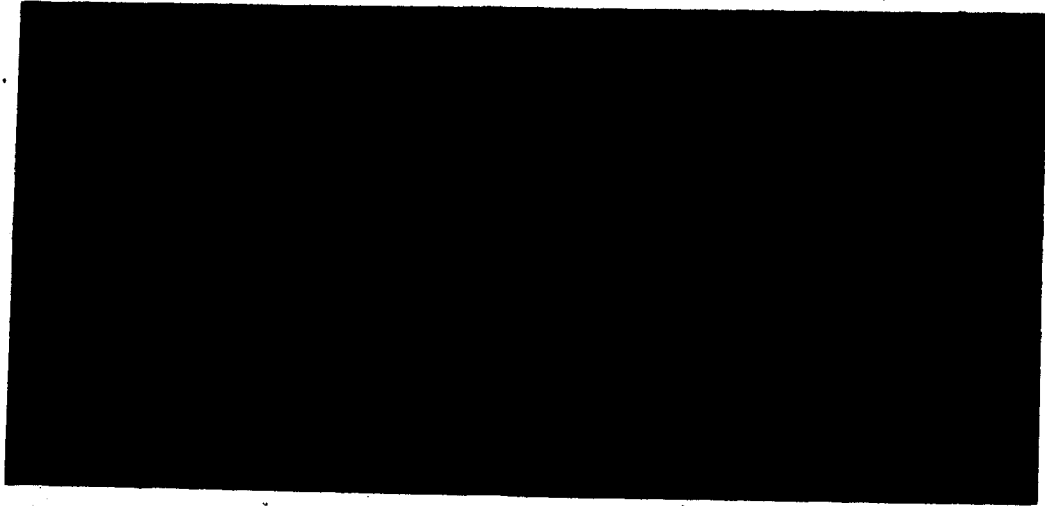
Fig. 38(top), Fig. 39(bottom),

Obs.#3	Obs.#1
Obs.#4	Obs.#2

. Figure titles on facing page.

Fig. 40. Surface browning tests when food at a variable height from $< \lambda/4$ to $3 \lambda/4$ from the 700 W Panasonic oven's base metal sheet. Rice crackers (Taipan brand) with thin layers (~ 2 mm) of mixture #3 heated for 60 s on full power on pedestals of heights shown; λ is the equivalent average free space wavelength in the oven, ~ 12 cm (see Chapter IV).

Fig. 41. Browning results of Fig. 40 (on the right hand paper towel) compared with those of Marmite[TM][95](on the left hand paper towel). Rice crackers (Taipan brand) with Marmite[TM] heated for 40 s in a 700 W Panasonic oven at full power on pedestals of variable heights as indicated in Fig. 40.

Fig. 42. Surface browning tests on ham. Two pieces preheated for 60 s on full power in the 700 W Panasonic oven. Mixture #18 (10 ml honey + 10 ml glycerin + 2.5 g NaCl) liberally applied and further heated for 150 s.
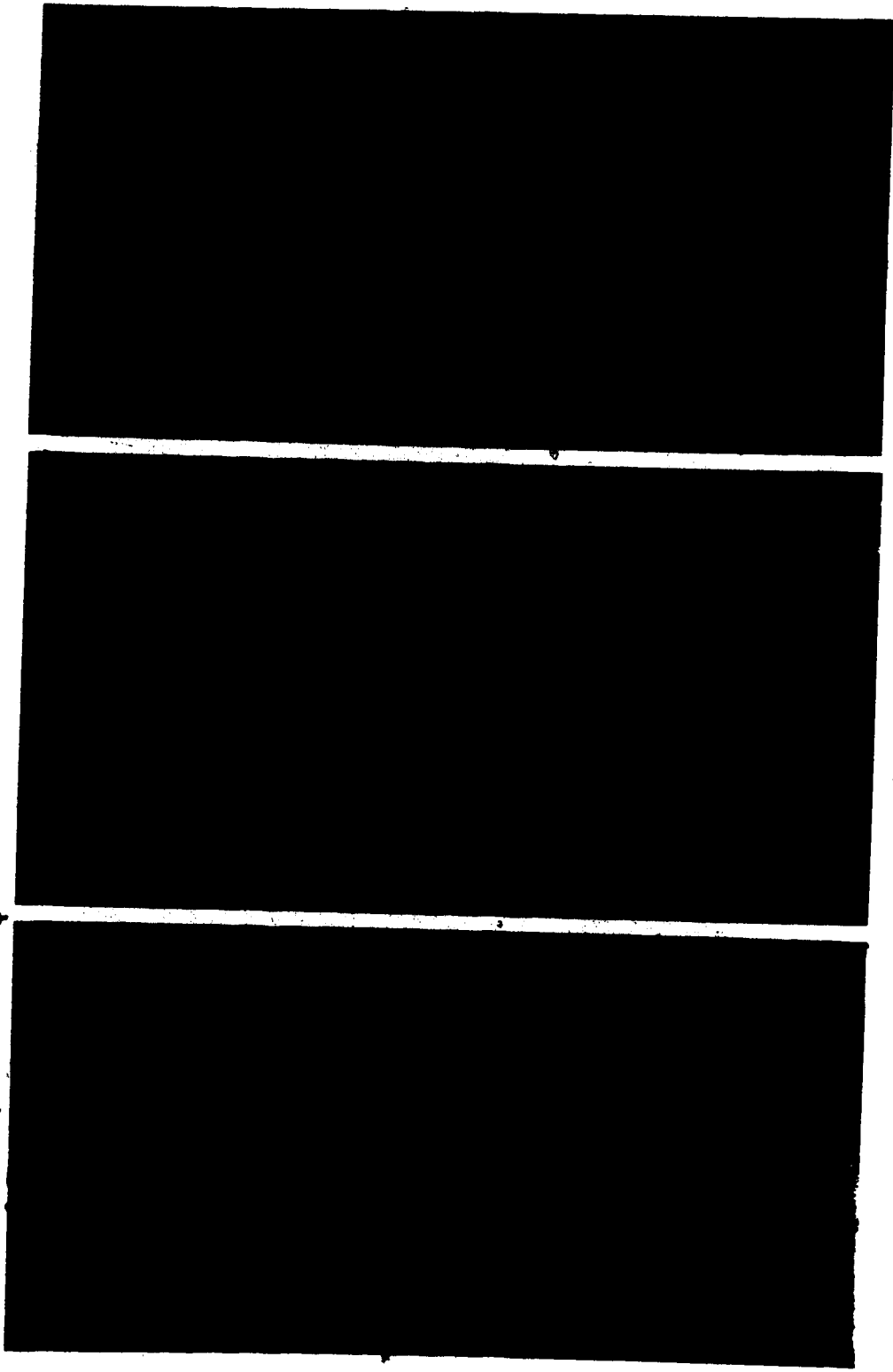
Figs. 40(top), 41(center), and 42(bottom). Figure titles on facing page.

Fig. 43. Surface browning tests on cardboard pieces ($\sim$ 6x4x0.15 cm) in a Panasonic microwave oven at its full rated power(700 W).

(a) A thin film ($\sim$ 2 mm) of Paste#1 (icing sugar [103] and ethanol paste of Fig.10) on the left and Paste#2 (same concentration as Paste#1, but ethanol replaced with glycerin) on the right for 2 min.,

(b) Paste#3 (Paste#1 + 1 g NaCl) on the left and Paste#4 (thick paste of icing sugar in 10 ml glycerin + 1 g.NaCl) on the right for 50 s,

(c) Mixture #2 on the left and Paste#9 (1 egg yolk + 2 g wheat flour + 2 g NaCl) on the right for 1 min.
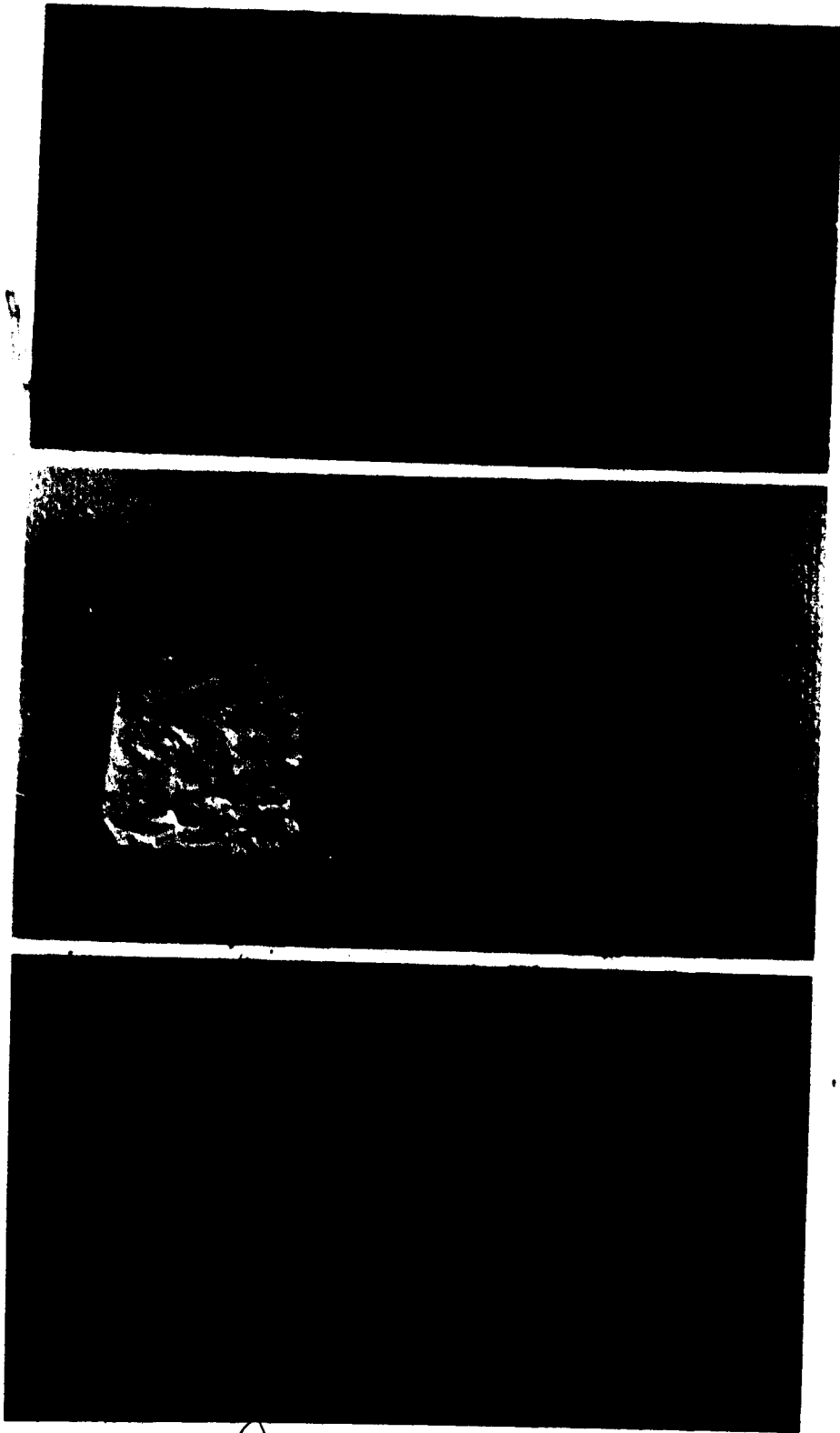
Figs. 43: a(top), b(center), c(bottom). Figure titles on facing page.

Figure 43 Surface browning tests on cardboard pieces ($\sim$ 6x4x0.15 cm) in the Panasonic microwave oven at its full rated power(700 W).

(d) Mixture #3 on the left, Paste#4 in the centre and Marmite[TM][95] on the right for 50 s,

(e) Mixture #2 on the right and Marmtie[TM] on the left for 1 min.,

(f) Mixture #1 (10 ml honey + 10 ml glycerin + 2 g NaCl) on the left, mixture #2 in the centre, and mixture #3 on the right for 40 s.

Figs. 43: d(top), e(center), f(bottom). Figure titles on facing page.

CHAPTER VI

Conclusions and Suggestions for Further Work

6.1 Conclusions

On the basis of the work reported in this thesis, the following conclusions are drawn:

(i) For the TM_{012} cavity in the laboratory, the calibration method discussed in Sections 2.3 to 2.5 is more appropriate than using the perturbation equation (Appendix I). The difference between the actual dielectric constants (ε') of the calibrating liquids of Table 3 and those computed from the perturbation equation varies from 8% for distilled water to 63% for ethyl acetate as given in Table A.1 of Appendix I; the deviation for the loss factor (ε'') varies from 3% to 138%. large.

It seems that these deviations are due to the cavity's mechanical arrangement for holding the sample, three-piece construction, slots on the walls of the cavity and excessive perturbation allowed; for example, for water it is 7%. Due to the above, the actual relationship between ε' and Δf, and ε'' and $\delta(1/Q_L)$, are no longer linear.

(ii) The worst case accuracy of the measurement technique is estimated to be 11%; and, the precision 2%.

(iii) Similar to chloride pastes, some sugar-alcohol mixtures have a potential for use as a thermostatic susceptor material. By their virtue of being edible, sugar-alcohol mixtures have an advantage over chloride pastes: apart from their possible use in sealed pouches (similar to chloride pastes as discussed in the US Patent [2]), these mixtures can also possibly be used as "spray-on" browning agents on some foods.

153

(iv) As discussed in Chapter IV, a semi-transparent conducting film can be modelled as a lossy dielectric 'sheet. Thus, by using semi-transparent films with different surface resistances different heating rates can be achieved. This concept can be used in designing microwave dinner packages, in which different food-items require heating at different rates, to attain the desired degree of cooking at the same time.

(v) Time domain transmission methods can be used for dielectric measurements on the liquids listed in Table 3. The highest frequency of measurement is determined by the total rise-time of the pulse generator and sampling head. By using sample holders of different lengths, liquids with different loss factors can be measured up to this highest frequency. The lowest frequency of measurement is determined from the sampling requirements discussed in Section 3.3.

The single transmission method is considered more accurate than the multiple transmission method for the following reasons:

(a) spurious reflections in the system which are not included in the analysis presented in Section 3.4.1, e.g., at the pulse generator and the sampling head, can be avoided in single transmission method, and

(b) errors due to the shift in time origin, $S_{\epsilon'}$, and $S_{\epsilon''}$, are smaller. It is found that, in a single transmission method, these multiple reflections cause a larger error in the measured ϵ^* for materials like distilled water ($\epsilon^* = 78 - j11$, 3 GHz) than for a liquid mixture with ϵ^* close to 6+j1. However, in different single transmission measurements on distilled water, the maximum possible error from the above source is computed to be of the order of 1% for ϵ', and 4% for ϵ''. These results show that the mismatch between components located between the pulse

generator and the sampling head is not the largest source of error. In fact, the contribution to the total error can be larger either from the time shift between input and output waveforms or from the nonlinearity in the amplifiers of the oscilloscope. The error from the time shift between input and output waveforms can be substantial for a material, for a given length of sample holder and frequency (Section 3.4.2). For the ranges of $\overset{*}{\epsilon}$, given in Figures 25-27, the time jitter error has a relatively smaller effect on the results and these may be acceptable for applications such as microwave heating. A technique is also discussed in Section 3.5(iii) which may be helpful in estimating the error due to time jitter in a particular measurement setup.

It is concluded that if precautions are taken to minimize the time origin error, the non-linearity in the amplifiers of the oscilloscope is the single largest source of error in time domain transmission methods.

6.2 Suggested Further Work

6.2.1   Dielectric measurements in an untuned cavity

Microwave oven cavities have been used for dielectric measurements in the mm wave region, at 156 GHz [157] and 70 GHz [158].   At 70 GHz, the dimensions of a commercial oven cavity (e.g., Panasonic NE-7800CA) are about 100 times that of the wavelength; and thus, for samples larger than the wavelength, the field is essentially uniform.   It may be useful to find the lowest frequency at which an untuned cavity of a reasonable size (or internal structure, such as more than one mode stirrer) could be used for dielectric measurements. This method, if applicable at 2.45 GHz, will provide an opportunity for conducting

measurements in the real heating environment. Also, this seems to be the only possible method in which the dielectric measurements can be made on actual loads at their specified rate of heating.

It is suspected that the final ϵ^* (and μ^*) of a ceramic depends upon its rate of heating. An immediate application of the above technique could be in the confirmation of the above statement. If the above statement is found true, the ϵ^* and μ^* of ceramics can be tailored simply by adjusting the rates of their heating. This concept may be of use in the developing field of microwave sintering of ceramics.

6.2.2 Automation of the dielectric measurement

About five hours are required to obtain the simple curve shown in Figure 4. Of these five hours, about an hour is needed for sample preparation and the rest of the time goes into conducting the temperature run, computing $\epsilon^*(T)$ and then drawing the curve. If a substantial number of measurements have to be taken, automation of the entire sequence of operations may be worth the effort.

The equipment needed for the suggested automation is as follows:

(a) A microwave source with HP-IB interface (HP 8350B)

(b) Power meter with HP-IB interface (HP 436A)

(c) Plotter with HP-IB interface (HP 7470A)

(d) A microcomputer (HP 85)

(e) Temperature controlled oven with an HP-IB compatible interface (Despatch Lab oven)

The above hardware can be connected as shown in Fig. 44, and programmed to imitate the steps of measurements described in Section 2.5. Once the measurements are complete, the microcomputer can be

instructed to compute ε^* at different temperatures, according to the Equations given in Section 2.4. Finally, with the help of another program, a plot of ε^* vs. temperature can be obtained on the plotter.
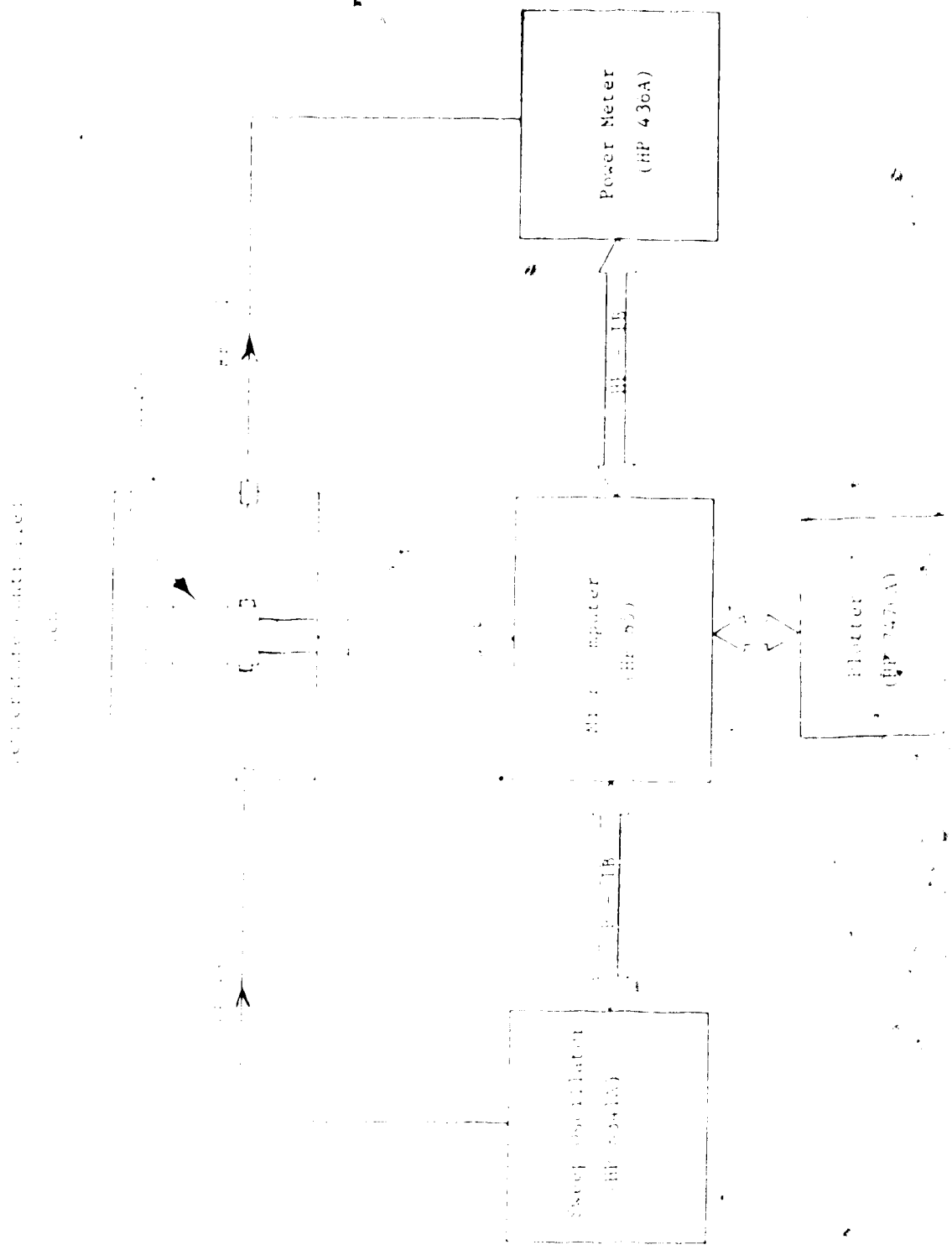
Fig. 47. Block diagram of a microcomputer controlled dielectric measurement system

References

[1] H.F. Huang, "New product concepts in microwavable food packaging",
Microwave World, vol. 8, pp. 5-7, 1987.

[2] U.S. Patent No. 4,283,427: Microwave Heating Package and
Susceptor Composition, April 11, 1981.

[3] U.S. Patent No. 4,190,757: Microwave Heating Package and Method,
Feb. 26, 1980.

[4] R.C. Jain and W.A.G. Voss, "Variation of absorption with material
thickness in a microwave oven".(Submitted to the IEEE Trans. MTT,
1988).

[5] P.O. Risman, T. Ohlsson and B. Wass, "Principles and models of
power density distribution in microwave oven loads", The Journal
of Microwave Power and Electromagnetic Energy, vol. 22, pp. 193-
198, 1987.

[6] R.F. Schiffman, "Microwave and dielectric drying", in Handb of
Industrial Drying. Ed., A.S. Mujumder, Marcel Dekker, Inc.,
New York, pp. 327-356, 1987.

[7] W.L. Griffin and W.A. Hendrix, "Microwave heating and drying in
textile processing - present and future", IEEE Trans. IA, vol. 22,
pp. 115-120, 1986.

[8] P.J. Hulls, "Development of the industrial use of dielectric
heating in the United Kingdom", The Journal of Microwave Power,
vol. 17, pp. 29-38, 1982.

[9] A.W. Guy, J.F. Lehmann, and J.B. Stonebridge, "Therapeutic
applications of electromagnetic power", Proc. IEEE, vol. 62, pp.
55-75, 1974.

[10] M. Meisels, "Industry warming to microwave power", Microwaves,
pp. 10-17, May, 1968.

[11] J. Martin, "On a wing and a microwave", Canadi⬤rch, pp. 24-25, February, 1988.

[12] Canadian Electrical Association Research and Development Report No. CEA. No. 411 U 481, "Microwave, Radio-frequency, and Infra-red Devices:Their Uses and Potential in Industry", prepared by the Ontario Hydro Research Division, pp. A-1-A-3, April 1986.

[13] N.E. Bengstsson and T. Ohlsson, "Microwave heating in the food industry", Proc. IEEE, vol. 62, pp. 44-45, 1974.

[14] J.M. Osepchuk, "A history of micrwoave heating applications", IEEE Trans. MTT, vol. 32, pp. 1200-1224, 1984.

[15] A.B. MacKay, Experimental Study on Microwave Oven Design, Ph.D. Thesis, University of Alberta, pp. 1-2, 1977.

[16] W.A.G. Voss, "The world microwave oven market", A report from Voss Associates Engineering, Victoria, Canada, July, 1987.

[17] T.M. Bohrer, "Packages incorporating microwave interactive heaters (summary)", J. Microwave Power EE, vol. 22, p. 167, 1987.

[18] M.N. Afsar, J.R. Birch, and R.N. Clark (Ed. G.W. Chantry), "The measurement of the properties of materials", Proc. IEEE, vol. 74, pp. 183-199, 1986.

[19] J.A. Stratton, Electromagnetic Theory. McGraw-Hill Book Company, New York, pp. 513-516, 1941.

[20] J.R. Wait, Electromagnetic Wave Theory. Harper & Row Publishers, New York, pp. 130-137, 1985.

[21] L.P. Ligthart, "A fast computational technique for accurate permittivity determination using transmission line methods", IEEE Trans. MTT, vol. 31, pp. 249-254, 1983.

[22] S. Etemad, A.J. Heeger, and A.G. MacDiarmid, "Polyacetylene, $(CH)_x$: The prototype conducting polymer", Annual Review on Physical Chemistry, vol. 33, pp. 443-469, 1982.

[23] M. Kryszeski, "Electrical conductivity of semicrystalline and amorphous polymers and related problems", Journal of Polymer Science: Symposium No. 50, pp. 359-404, 1975.

[24] H. Mark, "Electro-and photoresponsive polymers", Journal of Polymer Science: Polymer Symposium No. 62, pp. 1-12, 1978.

[25] K.F. Schoch, Jr., "Electrically conductive polymers and their applications", IEEE Electrical Insulation Magazine, vol. 2, no. 1, pp. 20-25, 1986.

[26] C.J.F. Böttcher, Theory of Electric Polarization. vol. 1, Elsevier Scientific Publishing Company, New York, pp. 1-3, 1973.

[27] W. Meyer, "Dielectric measurements on polymeric materials by using superconducting microwave resonators", IEEE Trans. MTT, vol. 25, pp. 1092-1099, 1977.

[28] A.R. von Hippel (Ed.), Dielectric Materials and Applications. John Wiley and Sons, New York, 1954.

[29] American Institute of Physics Handbook. Third Edition, McGraw Hill Book Company, section 5, p. 119, 1972.

[30] H. Kilp, "Precise · measurements of the complex permittivity of low-to-medium loss standard liquids at 285 GHz", Journal of Physics E: Scientific Instruments, vol. 10, pp. 985-989, 1977.

[31] A. van Loon and R. Finsey, "Measurement of Complex Dielectric Constants of Liquids at Frequencies from 60 to 150GHz", The Review of Scientific Instruments, vol. 45, pp. 523-525, 1974.

[32] L. Zanforlin, "Permittivity measurements of lossy liquids at mm-wave frequencies", IEEE Trans. MTT, vol. 31, pp. 417-419, 1983.

[33] G.A. Burdick, T.J. Lyon and J.E. Pippin, "Measurements of large dielectric constants and loss tangents at 35 GHz", IEEE Trans. on IM, vol. 13, pp. 318-323, 1964.

[34] G. Dakermandji, A New method for measuring the complex permittivity of highly conducting dielectric materials at microwave frequencies. Ph.D. Thesis, Duke University, 1976.

[35] R.J. Cook and R.J. Jones, "Measurement of electrical properties: relative permittivity and loss angle", Plastics and Rubber: Materials and Applications, pp. 216-224, September, 1976.

[36] M. Sucher and J. Fox (Ed.), "Handbook of Microwave Measurements", vol. II, Polytechnic Press of the Polytechnic Institute of Brooklyn, pp. 495-546, 1963.

[37] J. Chamberlain and G.W. Chantry (Ed.), "High frequency dielectric measurement", Proceedings of a Tutorial Conference held at NPL, England, 1974.

[38] M. Magid, "Precision determination of the dielectric properties of non-magnetic high loss microwave materials", IEEE Trans. IM, vol. 17, pp. 291-298, 1968.

[39] S.B. Cohn, and K.C. Kelly, "Microwave measurement of high-dielectric constant materials", IEEE Trans. MTT, vol. 14, pp. 406-410, 1966.

[40] H.E. Bussey, "Measurement of RF properties of materials : A survey", Proc. IEEE, vol. 55, pp. 1046-1053, 1967.

[41] A.C. Lynch, "Precise measurements on dielectric and magnetic materials", IEEE Trans. IM, vol. 23, pp. 425-431, 1974.

[42] J.R. Birch and R.N. Clarke, "Dielectric and optical measurements from 30 to 1000 GHz", The Radio and Electronic Engineer, vol. 52, no. 11/12, pp. 565-585, 1982.

[43] C.K. Campbell, "Free-space permittivity measurements on dielectric materials at millimeter wavelengths", IEEE Trans. IM, vol. 27, pp. 54-58, 1978.

[44] J. Musil and F. Zacek, "Microwave measurements of complex permittivity by free space methods and their applications", Elsevier Science Publishing Company, Inc., New York, 1986.

[45] S.O. Nelson, L.E. Stetson, and C.W. Schlaphoff, "A general computer program for precise calcualtion of dielectric properties from short circuited waveguide measurements", IEEE Trans. IM, vol. 23, pp. 455-460, 1974.

[46] M.C. Chau, Microprocessor-controlled ANA system for de-embedding FET parameters. M.Sc. Thesis, University of Alberta, pp. 38-67, 1984.

[47] A. Kraszewski, M.A. Stuchly, and S.S. Stuchly, "ANA calibration method for measurements of dielectric properties", IEEE Trans. IM, vol. 32, pp. 385-386, 1983.

[48] W. Barry, "A broad-band, automated, stripline technique for the simultaneous measurement of complex permittivity and permeability", IEEE Trans. MTT, vol. 34, pp. 80-84, 1986.

[49] W.B. Weir, "Automatic measurement of complex dielectric constant and permeability at microwave frequencies", Proc. IEEE, vol. 62, pp. 33-36, 1974.

[50] C. Akyel, R.C. Labelle, A. Jean Berteaud, and R.G. Bosisio, "Computer-aided permittivity measurements of moistened and

pyrolized materials in ▨▨▨ RF fields (Part 1)", IEEE Trans. IM, vol. 34, pp. 25-31, 1985.

[51] A. Kumar and D.G. Smith, "The measurement of the permittivity of sheet material at microwave frequencies using an evanescent waveguide technique", IEEE Trans. IM, vol. 25, pp. 190-193, 1976.

[52] Maria A. Rzepecka, "A cavity perturbation method for routine permittivity measurement", The Journal of Microwave Power, vol. 8, pp. 3-11, 1973.

[53] A.M. Nicolson and G.F. Ross, "Measurement of the intrinsic properties of materials by time-domain techniques", IEEE Trans. IM, vol. 19, pp. 377-382, 1970.

[54] R.E. Barker, Jr., and C. Huang, "Comparative studies on dielectric properties of liquids and solids by time-domain reflectometry", IEEE Trans. EI, vol. 20, pp. 927-930, 1985.

[55] D.U. Shimin, "A new method for measuring dielectric constant using the resonant frequency of a patch antenna," IEEE Trans. MTT, vol. 34, pp. 923-931, 1986.

[56] E. Tanabe and W.T. Joines, "A nondestructive method for measuring the complex permittivity of dielectric materials, at microwave frequencies using an open transmission line resonator", IEEE Trans. IM, vol. 25, pp. 222-226, 1976.

[57] P.O. Risman, and N.E. Bengtsson, "Dielectric properties of food at 3 GHz as determined by a cavity perturbation technique", The Journal of Microwave Power, vol. 6, pp. 101-124, 1971.

[58] P.O. Risman, and N.E. Bengtsson, Brief Communication: Dielectric constants for high loss materials, a comment on earlier measurements. The Journal of Microwave Power, vol. 8, pp. 185-

188, 1973.

[59] R.J. Sheppard, "An automated coaxial line system for determining the permittivity of a liquid," J. Phys. D:Appl. Phys. vol. 5, pp. 1576-1587, 1972.

[60] W.R. Scott, Jr., and G.S. Smith, "Dielectric spectroscopy using monopole antennas of general electrical length", IEEE Trans. AP, vol. 34, pp. 919-929, 1986.

[61] Gestblom and B. Jonsson, "A computer controlled dielectric time domain spectrometer", J. Phys. E:Sci. Instrum., vol. 13, pp. 1067-70, 1980.

[62] B. Gestblom, "The sampling oscilloscope in dielectric frequency domain spectroscopy", J. Phys. E:Sci. Instrum., vol. 15, pp. 87-90, 1982.

[63] R. Chahine and T.K. Bose, "Measurement of small dielectric loss by time-domain spectroscopy:application to water/oil emulsions", IEEE Trans. IM, vol. 32, pp. 360-363, 1983

[64] B. Agdur and B. Enander, "Resonances of a microwave cavity partially filled with a plasma", The Journal of Applied Physics, vol. 33, pp. 575-581, 1962.

[65] P. Hedvall, "Cavity method for measuring plasma properties", Ericsson Technics, vol. 1, pp. 97-107, 1963.

[66] T.W. Athey, M.A. Stuchly, and S.S. Stuchly, "Measurement of radio frequency permittivity of biological tissues with an open-ended coaxial line: Part 1", IEEE Trans. MTT, vol. 30, pp. 82-86, 1982, and M.A. Stuchly, T.W. Athey, G.M. Samaras and G.E. Taylor, "Measurement of radio frequency permittivity of biological tissues with an open-ended coaxial line: Part II -

Experimental results", IEEE Trans. MTT, vol. , pp. 87-92, 1982.

[67] B. Bianco, G.P. Drago, M. Marches, C. Martini, G.S. Mela, and S. Ridella, "Measurements of complex dielectric constant of human sera and erythrocytes", IEEE Trans. IM, vol. 28, pp. 290-295, 1979.

[68] T.K. Bose, A.M. Bottreau, and . Chahine, "Development of a dipole probe for the study of dielectric properties of biological substances in radiofrequency and microwave region with time-domain reflectrometry", IEEE Trans. IM, vol. 35, pp. 56-60, 1986.

[69] S.C. Olson and M.F. Iskander, "A new in-situ procedure for measuring the dielectric properties of low permittivity materials", IEEE Trans. IM, vol. 35, pp. 2-6, 1986.

[70] M.F. Iskander and J.B. Dubow, "Time-and frequency-domain techniques for measuring the dielectric properties of rocks:a review", The Journal of Microwave Power, vol. 18, pp. 55-74, 1983.

[71] E.C. To, "Dielectric properties of food materials", The Journal of Microwave Power, vol. 9, pp. 303-315, 1974.

[72] M.A. Rzepecka and R.R. Perceisa, "Permittivity of some dairy products at 2450MHz", The Journal of Microwave Power, vol. 9, pp. 277-288, 1974.

[73] A. Kumar and D.G. Smith, "Microwave properties of yarns and textiles using a resonant microwave cavity", IEEE Trans. IM, vol. 26, pp. 95-98, 1977.

[74] B. Terselius and B. Ranby, "Cavity perturbation measurements of the dielectric properties of vulcanizing rubber and polyethylene compounds", The Journal of Microwave Power, vol. 13, pp. 327-332,

1978.

[75] M. Kent, "Time domain measurements of the dielectric properties of frozen fish", The Journal of Microwave Power , vol. 10, pp. 37-40, 1975.

[76] B.P. Kwok, S.O. Nelson and E. Bahar, "Time-domain measurements for determination of dielectric properties of agricultural materials", IEEE Trans. IM, vol. 28, pp. 109-112, 1979.

[77] H.A. Bethe and J. Schwinger, N.R.D.C. Report D1-117. Cornell University, March, 1943.

[78] T. Kahan, "Methode de perturbation appliquee a l'etude des cavites electromagnetiques", C.r. Acad. Sci., Paris, 221, pp. 536-538, 1945, and E. Argence and T. Kahan, Theory of waveguides and cavity Resonators. Hart Publishing Company, Inc., New York, 1967.

[79] J.C. Slater, Microwave Electronics. D. Van Nostrand Company, Inc., New Jersey, pp. 80-81, 1950.

[80] H.B. G. Casimir, "On the theory of electromagnetic waves in resonant cavities", Philips Research Report, vol. 6, pp. 162-182, 1951.

[81] P. Hedvall and J. Hagglund, "Cavity method for measuring dielectric constants at microwave frequencies", Ericsson Technics, vol. 1, pp. 89-96, 1963.

[82] Gilbert Morin and Manfred Nachman, "A new method for measuring anisotropy at microwave frequencies", vol. 28, pp. 198-204, 1979.

[83] B. Lax and K.J. Button, Microwave Ferrites and Ferrimagnetics. McGraw Hill Book Company, Inc., New York, pp. 323-354, 1962.

[84] R.A. Waldron, The Theory of Waveguides and Cavities. Gordon and Breach Science Publishers, New York, 1967.

[85] A.J. Baden Fuller, Ferrites at microwave frequencies. Peter Peregrinus Ltd., London, pp. 235-254, 1987.

[86] M. Stockhausen and M. Kessler, "Concerning measurements of high complex permittivity by the resonator perturbation method", J. Phys. E: Scientific Instruments, vol. 13, pp. 732-736, 1980.

[87] S. Sen, P.K. Saha and B.R. Nag, "New cavity perturbation technique for microwave measurement of dielecrtric constant", The Review of Scientific Instruments, vol. 50, pp. 1594-1597, 1979.

[88] E.F. Labuda and R.C. LeCraw, "New technique for measurement of microwave dielectric constants", The Review of Scientific Instruments, vol. 32, pp. 391-392, 1961.

[89] C.M.B. Walker, Dielectric Constant of Water-DMSO Solutions and Numerical Modelling of Microwave Heating. Ph.D. Thesis, University of Alberta, pp. 13-41, 1977.

[90] (a) E. Medved, Food preparation and theory. Prentice Hall, N.J., Chapter 19:pp. 280-286, 1986. (b) A more detailed account of the physical chemistry of the egg is given in W.J. Stadelmann, and O.J. Cotterill, Egg Science and Technology. 3rd ed. Avi Westport Company, Chapter 6:pp. 97-122, 14:pp. 302-305, 1986.

[91] W.B. Westphal and A. Sils, Dielectric Constant and Loss Data. MIT Technical Reports AFML-TR-72-39 (April): p. 202, 1972.

[92] K.H. Norris, and A.W. Brant, "Radio frequency as a means of grading eggs", Food Technol. 6(6), pp. 204-208, 1952.

[93] T. Rosenkratz and P. Higgins, "The technology of microwave absorbing materials for microwave packaging - beyond vacuum metallizing to the next susceptor generation", Microwave World, vol. 8, No. 6, pp. 10-15, 1987.

[94] "Solving the problem of 'microwave browning'". Food Engineering, pp. 98-100, September 1981, see also M.J. Boreglund, J. Rum and S.J. Thoms, "Does meat really brown in the microwave?" Microwave World, vol. 1, No. 6, pp. 10-15, 1980.

[95] Bovril Canada Inc., Montreal. Ingredients: yeast extract, salt, dehydrated carrots, onions and spices.

[96] McNeill & Libby of Canada, Chatham, Ontario. Ingredients: caramel, water, salt and glucose solids.

[97] Nadixcorp Ltd. Markham, Ontario. Ingredients: caramel, water, dried vegetables (carrots, onions, celery, parsnips, turnips), salt, dried parsley and spices.

[98] R.E. Mudgett, "Electrical properties in foods" in Engineering Properties of Foods. Eds. M.A. Rao and S.S.H. Rizvi, Marcel Dekker, New York, pp. 349-357, 1986.

[99] An aqueous ionic solution at $40^{\circ}C$ and 3 GHz has the highest (negative) value of $d\varepsilon'$, ε'/df which could be found for materials of this type; the difference (2.45 - 2.85 GHz) is -10%. See Figure 7.13 of [98] or, in more detail, R.E. Mudgett, A Physical Basis for Prediction of Dielectric Properties in Liquids and Solid Foods at UHF. Ph.D. Thesis, M.I.T., Boston, 1974.

[100] R.E. Mudgett, "Electrical properties of foods", in Engineering Properties of Foods, Ed. M.R. Rao and S.S.H. Rizvi, Marcell Dekker, Inc., p. 358, 1986.

[101] B.D. Roebuck, and S.A. Goldblith, "Dielectric properties of carbohydrate-water mixtures at microwave frequencies", Journal of Food Science, vol. 37, pp. 199-204, 1972.

[102] R.V. Decareau, Microwaves in Food Processing Industry. Academic

Press, p. 29, 1985.

[103] The icing sugar was from Alberta Sugar Company, Canada and contained upto 5% starch.

[104] W.R. Tinga, and S.O. Nelson, "Dielectric properties of materials for microwave processing-tabulated, The Journal of Microwave Power, vol. 8, pp. 23-65, 1973.

[105] W.B. Westphall, Dielectric Constant and Loss Data. Laboratory for Insulation Research, MIT, Final Report AFML-TR-74-250, Part IV, December 1980.

[106] J.P. Poley, "Microwave dispersion of some polar liquids", Applied Science Research, vol. B4, pp. 337-387, 1955.

[107] . Grant, T.J. Buchanan and H.F. Cook, "Dielectric behavior of water at microwave frequencies", The Journal of Chemical Physics, vol. 26, pp. 156-161, 1957.

[108] R.J. Sheppard, B.P. Jordan and E.H. Grant, "Least square analysis of complex data with applications to permittivity measurements". Journal of Physics D: Applied Physics, vol. 3, pp. 1759-1764, 1970.

[109] R.J. Sheppard and E.H. Grant, "Alternative interpretations of dielectric measurements with particular reference to polar liquids". Advances in Molecular Relaxation Processes, vol. 6, pp. 61-67, 1974.

[110] J.B. Hasted, Aqueous Dielectrics. Chapman and Hall, London, pp. 40-50, 1973.

[111] H.P. Schwan, R.J. Sheppard, and E.H. Grant, "Complex permittivity of water at $25^{\circ}C$". The Journal of Chemical Physics, vol. 64, pp. 2257-2258, 1976.

[112]M.N. Afsar, and J.B. Hasted,"Measurements of the optical constants of liquid H_2O and D_2O between 6 and 450 cm^{-1}". Journal of Optical Society of America, vol. 67, pp. 902-904, 1977.

[113]E.H. Grant and R.J. Sheppard, "Dielectric relaxation in water in the neighbourhood of 4^0C". The Journal of Chemical Physics, vol. 60, pp. 1792-1796, 1974.

[114]C.H. Collie, J.B. Hasted and D.M. Ritson, "The dielectric properties of water and heavy water", The Proceedings of the Physical Society, London, vol. 60, pp. 145-160, 1948.

[115]J.A. Saxton and J.A. Lane "Dielectric dispersion in pure polar liquids at very high radio-frequencies. I. Measurement on water, methyl and ethyl alcohols", Proceedings of the Royal Society of London, Series A, vol. 213, pp. 400-408, 1952.

[116]H.F. Cook, "A comparison of the dielectric behavior of pure water and human blood at microwave frequencies", British Journal of Applied Physics, vol. 3, pp. 249-255, 1952.

[117]J.B. Hasted, and S.H.M. El Sabeh, "The dielectric properties of water in solutions", Transactions of the Faraday Society, vol. 49, pp. 1003-1011, 1953.

[118]T.J. Buchanan and E.H. Grant, "Phase and amplitude balance methods for permittivity measurements between 4 and 50cm", British Journal of Applied Physics, vol. 6, pp. 64-66, 1955.

[119]O. Sandus and B. Lurie, "Dielectric relaxation of aqueous glycine solutions at 3.2cm wave...", Journal of Physical Chemistry, vol. 65, pp. 881-885, 1961.

[120]J.B. Hasted, "Liquid water dielectric properties", The Physics and Physical Chemistry of Water. pp. 255-305, in Water, A

Comprehensive Tre____, vol. I, Ed. F. Franks, Plenum Press, New York, 1972.

[121]A. Stogryn, "_____ns for calculating the dielectric constant of saline water", IEEE Trans. MTT, vol. 19, pp. 733-736, 1971.

[122]J.L. Devore, Probability and Statistics for Engineering and the Sciences. Brooks/Cole Publishing Company, pp. 529-530, 1987.

[123] P.O. Risman, Personal communication regarding dielectric properties of water and NaCl solutions at 2.45 GHz, 1987.

[124]John R. Taylor, An Introduction to Error Analysis. University Science Books, Mill Valley, California, pp. 52-55, 1981.

[125]R. Paglione F. Sterzer, J. Mendeck, E. Friedenthal and C. Botstein, "27MHz ridged waveguide applicators for localized hyperthermia treatment of deep-seated malignant tumors", Microwave Journal, vol. 24, pp. 71-80, no. 2, 1981.

[126]"Time Domain Reflectometry", Hewlett-Packard Application Note 62, 1964.

[127]"Cable Testing With Time Domain Reflectometry", Hewlett-Packard Application Note 67, 1968.

[128]A. Sugget, "Microwave dielectric measurements using time domain spectroscopy: Note on recent technique advances", Journal of Physics E:Scientific Instruments, vol. 8, pp. 327-330, 1975.

[129]M.J.C. van Gemert, "High-Frequency time-domain methods in dielectric spectroscopy", Philips Research Reports 28, pp. 530-572, 1973.

[130]B. Gestblom and E. Noreland, "Transmission methods in dielectric time domain spectroscopy", The Journal of Physical Chemistry, vol. 81, pp. 782-788, 1977.

[131] H.W. Loeb, G.M. Young, P.A. Quickenden and A. Sugget, "New methods for measurement of complex permittivity up to 13 GHz and their applications to the study of dielectric relaxation of polar liquids including aqueous solutions", Berichte Der Bunsengesellschaft fur Physikalische Chemie", vol. 75, pp. 1155-1165, 1971.

[132] G.D. Cormack and J.O. Binder, "The EF-FFT (Extended Function Fast Fourier Transform)" submitted for publication in the IEEE Trans. IM., August, 1987.

[133] F. J. Harris, "On the use of windows for harmonic analysis with the discrete fourier transform", Proc. IEEE, vol. 66, pp. 51-83, 1978.

[134] S. M. Kay and S. L. Marple, "Spectrum analysis - a modern perspective", Proc. IEEE, vol. 69, pp. 1380-1419, 1981.

[135] H.A. Samulon, "Spectrum analysis of transient response curves", Proc. IRE, vol. 39, pp. 175-186, 1951.

[136] A.M. Nicholson, "Forming the Fast Fourier Transform of a step response in time-domain metrology", Electronics Letters, 12th July, vol. 9, pp. 317-318, 1973.

[137] J. Waldmeyer, "Fast Fourier Transform of steplike functions: the synthesis of three apparently different methods", IEEE Trans. IM, vol. 29, pp. 36-39, 1980.

[138] A.M. Shaarawi and S.M. Riad, "Computing the complete FFT of a step-like waveform", IEEE Trans. IM, vol. 35, pp. 91-92, 1986.

[139] R.W. Ramirez, The FFT Fundamentals and Concepts. Prentice-Hall, Inc., New Jersey, 1985.

[140] MACOM Catalogue on microwave coaxial connectors (1986-1987), pp.

73-74 and 165-166.

[141]J.F. White, Microwave Semiconductor Engineering. Van Nostrand Reinhold Company, New York, pp. 186-188, 1982.

[142]MathCAD^{TM} Software package of MathSoft, Inc., Cambridge, USA.

[143]"Fundamentals of the electronic counters", H.P. Application Note 200, p. 28, 1978.

[144]J. Peyrelasse, C. Boned et J.P. Le Petit, "Mise au point d'une manipulation de 'time domain spectroscopy'. Application a l'etude de la relaxation dielectrique des isomers du pentanol", J. Phys. E: Sci. Instrum., vol. 14, pp. 1002-1008, 1981.

[145]R.H. Cole, S. Mashimo, and P. Winsor, "Evaluation of dielectric behaviour by time domain spectroscopy; precision difference method", The Journal of Physical Chemistry, vol. 84, pp. 786-793, 1980.

[146]Ruth E. Baldwin, "Microwave cooking: an overview", Journal of Food Protection, vol. 46, no. 3, pp. 266-269, 1983.

[147]G.T. Ruck, Radar Cross Section Handbook. Plenum Press, New York, pp. 479-484, 1970.

[148]D.S. Jones, Acoustic and Electromagnetic Waves. Oxford University Press, New York, pp. 309-313, 1986.

[149]V.F. Fusco, Microwave Circuits Analysis and Computer Aided Design. Prentice-Hall International, New Jersey, pp. 226-232, 1987.

[150]S. Ramo, J.R. Whinnery and T. van Duzer, Fields and Waves in Communication Electronics. John Wiley and Sons, New York, pp. 295-296, 1986.

[151]H.K. Chaurasia, Ultra-thin films. Ph.D. Thesis, University of

Alberta, pp. 52-53, 1974.

[152]W.A.G. Voss and T. Greenwood-Madsen, "Microwave oven standards: effects of water load size and dispersion on heating power", A Technical Note to the IMPI Standards Committee, Washington, D.C., March 16, 1987.

[153]T.P. Labuza and M.K. Schmidl, "Advances in the control of browning reactions in foods", in Role of Chemistry in the Quality of Processsed Food, Ed. O.R. Fennema, Food and Nutrition Press, Westport, Connecticut, USA, pp. 65-95, 1986.

[154]A.S. Johnson and M.S. Peterson, Encyclopedia of Food Technology. The Avi Publishing Co., Inc., Connecticut, pp.136-139, 1974.

[155]D.A. Copson, Microwave Heating. Avi, Westport CT, pp. 293-295, 1975.

[156]Examples of field intensification devices can be found in the US Patents 2,450,036 , 3,271,552 , 3,591,751 , 3,857,009, 3,946,187 and 3,946,188.

[157]D.T. Llewellyn-Jones, R.J. Knight, P.H. Moffat, and H.A. Gebbie, "New method of measuring low values of dielectric loss in the near millimetre wavelength region using untuned cavities", Proc. IEE, vol. 127, Pt. A., pp. 535-540, 1980.

[158]F. Kremer and J.R. Izatt, "Millimeter-wave absorption measurements in low-loss dielectrics using an untuned cavity resonator", International Journal of Infrared and Millimeter Waves, vol. 2, pp. 675-694, 1981.

[159]O.P. Gandhi, Microwave Engineering and Applications. Pergamon Press, New York, pp. 11-97, 1981.

[160]E. Kreyszig, Advanced Engineering Mathematics. John Wiley and Sons, Inc., New York, p. 194, 1964.

APPENDIX I

A.1 Perturbation Equation for the TM_{012} Cavity

A.1.1 Field Equations for a TM_{012} Cavity

In this section, the field equations are derived for an ideal right circular cylindrical TM_{012} cavity of length 1 and radious b. In the following section (A.1.2), these equations are then used to derive the perturbation equation for an idealized version of the cavity used in this work.

The wave equation in cylindrical coordinates is

$$\nabla^2 \psi + k^2 \psi = 0 \qquad\qquad (A.1-1)$$

where

$$k^2 = \omega^2 \mu\epsilon \text{ , and}$$

$$\nabla^2 = \frac{1}{r}\frac{\partial}{\partial r}\left(r \frac{\partial}{\partial r}\right) + \frac{1}{r^2}\frac{\partial^2}{\partial \theta^2} - \frac{\partial^2 \psi}{\partial z^2}$$

For the TM wave propagating in z-direction, ψ represents the electric field, E_z, and r, θ, z represent the coordinates of an arbitrary point. All other symbols have their usual meanings. For obtaining the eigenfunctions of metallic enclosure, Equation A.1-1 is solved for the boundary conditions imposed by the geometry of that enclosure. For the propagating solutions varying as $e^{-j\beta z}$ (β is the phase constant), the solutions of Equation A.1-1 are [159],

$$\psi = D \, J_n(\gamma r) \cos(n \theta) \, e^{j(\omega t - \beta z)}. \tag{A.1-2}$$

In Equation A.1-2 $J_n(\gamma r)$ is the Bessel's function of order n and argument γr, where $\gamma = \sqrt{k^2 - \beta^2}$, n takes integral values from 0 to ∞, and $e^{j\omega t}$ represents the time variation of the field. Therefore, for a TM wave propagating in z-direction,

$$E_z = D \, J_n(\gamma r)\cos(n\theta) \, e^{j(\omega t - \beta z)} \tag{A.1-3}$$

For a metallic enclosure of radious b, $E_z = 0$ at $r = b$. This gives $J_n(\gamma b) = 0$. For each value of n, $J_n(\gamma b)$ has an infinite number of zeros; these are denoted as p_{nm}. In p_{nm} the first subscript n denotes the number of complete cycles of variation of the axial field component in θ-direction, for $0 \leq \theta \leq 2\pi$, and the second subscript m represents the number of zeros of the axial field in the radial direction, for $0 \leq r \leq b$. For TM_{012} mode, n=0 and m=1, which gives p_{nm} or, $p_{01} = 2.405$. Therefore,

$$\gamma = p_{01}/b. \tag{A.1-4}$$

Similarly, the boundary conditions in the z-direction require that $\beta \ell = p\pi$; where, p=0,1,2..., and ℓ is the length of the cavity. This gives

$$\beta = \frac{p\pi}{\ell} \tag{A.1-5}$$

Therefore, from Equations A.1-3, A.1-4 and A.1-5, E_z is given as

$$E_z = E_0 \, J_n(\, p_{01}r/b) \, \cos(n\theta) \, \cos(p \, \pi z/\ell) \, e^{j \omega t} \qquad \text{(A.1-6)}$$

In Equation A.1-6, D has been replaced with a new constant E_o. For TM_{012} mode, n=0, m=1 and p=2. Therefore, E_z is

$$E_z = E_0 \, J_0(p_{01}r/b) \, \cos(2 \pi z/\ell) \, e^{j\omega t} \qquad \text{(A.1-7)}$$

As only time harmonic fields are being considered, the term $e^{j\omega t}$ in Equation A.1-7 will be suppressed in the rest of the derivation. The other field components are [159],

$$E_r = - \frac{j\beta}{} \frac{\partial E_z}{\partial r} \qquad \text{(A.1-8)}$$

$$H_r = - \frac{\omega \epsilon}{} E_\theta \qquad \text{(A.1-9)}$$

$$H_\theta = \frac{\omega \epsilon}{} E_r \qquad \text{(A.1-10)}$$

From Equation A.1-2, it is seen that $-j\beta = \frac{\partial}{\partial z}$. Therefore,

$$E_r = \frac{1}{\gamma} \frac{\partial^2 E_z}{\partial z \partial r}$$

or, $\qquad E_r = \dfrac{E_o}{\gamma^2} \dfrac{\partial}{\partial z}\left[\gamma \overline{}'(\quad) \cdot \dfrac{2\pi z}{\ell})\right]$

or, $\qquad E_r = - \dfrac{E_o}{\ell} \cdot \dfrac{2\pi}{\ell} \cdot \overline{}_o'(\ \gamma r\ ) \ \sin \dfrac{2\pi z}{\ell}$

From Equation. A.1-8, E_r is given as

$$E_r = - \frac{E_o b}{P_{01}} \cdot \frac{\pi}{\ell} \cdot \overline{}'\ \frac{r}{b}\ \sin\ \frac{2\pi z}{\ell} \qquad (A.1-11)$$

and

$$E_\theta = - \frac{}{\gamma} \ \frac{\partial E_z}{\partial \theta} \qquad (A.1-12)$$

From Equation A.1-7, it is seen that E_z is constant with respect to a variation in θ , therefore $E_\theta = 0$. Since $E_{} = 0$, from Equation A.1-9 it is seen that $H_r=0$. From Equations A.1-8 and A.1-11, H_θ is given as

$$H_\theta = - \frac{\mu \varepsilon}{\beta}\ \frac{E_0 b}{P_{01}}\ \frac{2\pi}{\ell}\ J_0'(\ P_{01}\ r/b)\ \sin(2\pi z/\ell)$$

From Equation A.1-2, it can be seen that $\left(-1/j\beta\right)=\int$. Therefore,

$$H_\theta = - \frac{\mu \varepsilon E_o}{P_{01}} \quad \overline{}\ \overline{}'\left(\ \underline{}\ \ \underline{}\ \right)$$

or,

$$= \frac{j \omega \epsilon E_1 b}{p_{01}} \left(\frac{p_{01} \gamma}{b} \right) \cos \frac{2 \pi z}{\ell} \qquad (A.1-13)$$

Thus the electric and magnetic fields at a point inside the TM_{012} cavity are given by Equations A.1-7, A.1-11 and A.1-13. These equations are used in the next section to derive the perturbation equation for the cavity.

A.1.2 Perturbation equation for the TM_{012} cavity

In an unperturbed state, let the electric and magnetic fields for the TM_{012} mode of the cavity be

$$E = E_1 e^{j \omega t} \qquad (A.1-14(a))$$

$$H = H_1 e^{j \omega t} \qquad (A.1-14(b))$$

where E_1 and H_1 are functions of position in the cavity. When a parameter of the cavity is slightly modified, let the fields become

$$E' = (E_1 + E_2) \exp[j(\omega + \delta\omega)t] \qquad (A.1-15(a))$$

$$H' = (H_1 + H_2) \exp[j(\omega + \delta\omega)t] \qquad (A.1-15(b))$$

where it is assumed that the fields in the perturbed state can be represented as the sums of the unperturbed fields, E_1 and H_1, and additional fields, E_2 and H_2, with a small per cent change of the frequency. In general, ω and $\delta\omega$ are complex quantities. The parameters of the cavity whose modification produces the above

perturbation may be the dimensions of the cavity or the dielectric constant or relative permeability of the medium inside it. The perturbation should be small so that the total fields in Equations A.1-14 and A.1-15 have the same configurations; their magnitudes may be different. The smallness of the perturbation means a very small change in properties over a large volume, as when a cavity is filled with a ░░░░░░ dielectric constant is to be measured, or a large change in properties over a ░░░░░░ume, as when a small sample is introduced into a cavity for the purpose of measuring its dielectric or magnetic properties. For the case of a small sample, E_2 and H_2 of Equation A.1-15 will be small compared with E_1 and H_1 over most of the cavity volume, except in the vicinity of the sample [84]. The relative frequency shift of the cavity, ___ , can be obtained as [84],

$$\frac{\delta \omega}{\omega} = \ldots \qquad (A.1\text{-}16)$$

where V_c is the volume of the cavity, and the sign, '.', means dot product between two vectors. The rest of the symbols have their usual meanings. Equation A.1-16 is exact if the cavity walls are perfectly conducting. Next, an approximation is made of neglecting D_2 and B_2 in the denominator of Equation A.1-16 over most of the volume V_c. This is justified by the fact that $D_2 \ll D_1$ and $B_2 \ll B_1$. However, if D_2 and B_2 are comparable to D_1 and B_1, this will be true only over a very small part of

V_c, in the neighbourhood of a sample (or a small deformation of the cavity surface) and thus the contribution to the integral, in the denominator of Equation A.1-16, from this small volume is negligible. After neglecting D_2 and B_2 from the denominator of Equation A.1-16, ... is given by

$$\ldots \quad H_2 \cdot B_1 - \ldots_1 \cdot$$

$$(A.1-17)$$

In the TM_{012} cavity of Fig. ., the sample is placed concentric with the axis of the cavity where the magnetic field tends to zero (see Equation A.1-13). Substituting $H_1 = 0$, $H_2 = 0$ and $D_1 = \epsilon_0 E_1$, $D_2 = \epsilon_0 E_1 (\epsilon_r^* - 1)$ and $B_1 = \mu_0 H_1$, Equation A.1-17 becomes

$$\ldots E_2 \cdot \epsilon E_1 - \epsilon_0 \epsilon^* - 1 \, E_1 \cdot E_1 \ldots$$

$$(A.1-18)$$

$$E \cdot \epsilon_0 \quad - H \cdot \mu_0 \ldots$$

For a thin sample, the only electric field at the sample is the longitudinal component tangential to the sample (see Equations A.1-7 and A.1-11). Therefore, $E_1 = E_z$ and $E_2 = 0$. The integration in the numerator of Equation A.1-18 is done over the volume of the sample. Thus

$$\frac{\delta\omega}{\omega} = \left[\int \epsilon_r \left(1 - \right) E_1^2 \, dv \right] \frac{}{}$$

(A.1-19)

If ω is the complex frequency in Equation A.1-19,

$$= \frac{}{}$$

(A.1-20)

where ω_1 is the real frequency, is the shift in ω_1 due to the insertion of the sample into the cavity and $\frac{1}{Q_L}$ is the change in the loaded Q of the cavity. From Equations A.1-19 and A.1-20,

$$\frac{}{} =$$

(A.1-21(a))

and

$$=$$

(A.1-21(b))

where $\epsilon_r^* = \epsilon_r' - j\epsilon_r''$. Equation A.1-21 can be used to calculate ϵ_r' and ϵ_r'' of a sample after performing the integration given below. First the denominator of Equation A.1-21 is evaluated. If the denominator of this equation is denoted as "DEN",

$$DEN = \qquad \qquad \qquad \qquad \qquad \qquad dv \qquad \qquad (A.1\text{-}22)$$

In cylindrical coordinates, $dv=rdrd\theta dz$. Also there are two components of electric field in the cavity, E_r and E_z, therefore, total electric field, E_1, is given as

$$E_1^2 = E_r^2 + E_z^2 \qquad \text{.Therefore,}$$

$$DEN = \qquad \qquad \qquad \qquad \qquad \qquad (A.1\text{-}23)$$

where, a and b are the length and radius of cavity respectively. All the three terms of Equation A.1-23 are evaluated separately, as given below,

The standard result [160] given below is used to integrate the Bessel's function appearing in the above equation.

$$ \quad (A.1-25) $$

On integration and simplification,

$$ \quad (A. \quad) $$

Next the numerical values of various Bessel's functions appearing in the above equations are evaluated. From a table for Bessel's functions [160],

$$ J_1(2.4) = 0.5202 $$

and, $J_1(2.5) = 0.4971$.

Using linear interpolation,

$$ J_1(2.405) = 0.5202 - 0.0012 = \qquad (A. \quad) $$

For a rational number x, $J_1'(x) = $

for $x = p_{01} = 2.405$, $J_0(x) = 0$.

Therefore, $J_1'(p_{01}) = -1/2(J_2(p_{01}))$. Also,

$$ J_2(p_{01}) = $$

where $\lfloor 2$ means factorial of 2, And has a value of 2.

From the above power series expansion, $J_0(2.405) = 0.4314$. Therefore,

$$J_1'(2.405) = -1/2(J_2(2.405)) = -0.2157 \qquad (A.1-28)$$

Solving Equations A.1-26, A.1-27 and A.1-28,

or,

For the given cavity, $b/a = 0.896$. Therefore,

$$(A.1-29)$$

Next the integral of E_z is evaluated over the volume of the cavity,

From the trigonometric relation,

the above integral becomes

$$(A.1-30)$$

when integrated the second term of Equation A.1-30 turns out to be zero. Therefore,

$$\iiint_{/} E^{\cdot} \cdots = \int_0^b \int_0^{2\pi} \int_0^{\ell} \frac{E_0^2}{2} J \cdot \frac{p_{01} \gamma}{b} \quad \cdots \quad (A.1-31)$$

Solving Equation A.1-31 in the similar way as Equation A.1-24,

$$\iiint_{/} E^2 \, dv = \frac{E_0^2 \, b^2 \cdots}{2} \; J_1^2 \cdots$$

$$\iiint_{/} E_\gamma^2 \, dv = E_0^2 \, V_c \left(0.1347 \right).$$

$$(A.1-32)$$

Next the third term of Equation A.1-23 is evaluated

$$\int H_1^{\cdot} \cdots \cdots$$

$$= \left(- \frac{j \cdots \varepsilon_0}{b} \cdots \right) \int_0^b \int_0^{2\pi} \int \cdots \cdots \left(\frac{\cdots}{\cdots} \right) \cdots$$

$$\text{Let} \quad \left(\frac{\varepsilon_0 E}{b} \right) = C_2 \cdots$$

$$= - C_2 \int_0^b \gamma \cdot J_0' \left(\frac{p_{01} \gamma}{b} \right) \cdots \frac{1 + \cdots}{2} \cdots$$

On integration the second term of this equation becomes zero. Also using the relation $J_0'(p_{01}r/b) = J_1(p_{01}r/b)$, and $J_1(0) = 0$, the above integral becomes

$$= - \frac{C_2 \, 2\pi \ell \, b^2}{} \left[J_1'(p_{01})^2 + b^2\left(1 - \frac{1}{}\right) \pi^2 \right]$$

$$= - \frac{C_2 (\pi b^2 \ell)}{} \, (0.270)$$

Since $\pi b^2 \ell = V_c$, the above integral is

$$\frac{\mu_0 H_1^2}{V_c} = - \mu_0 \, \frac{}{b}$$

or,

$$\iiint_{V_c} \mu_0 H_1^2 \, dv = - 0 \ldots \ldots E_0^2 \qquad \text{(A.1-33)}$$

Thus from Equations A.1-29, A.1-32 and A.1-33, the "DEN" of

Equation A.1-22 is given as,

$$DEN = \epsilon_0 E_0^2 V_c (0.0671 + 0.1347 + 0.2026)$$

or, $DEN = 0.4182 \, \epsilon_0 E_0^2 V_c.$ (A.1-34)

The numerator of Equation A.1-19 is given as

NUM = −   (A.1-35)

where a is the radius of the sample, and the sample extends from d_1 to d_2 in z-direction. On integration Equation A.1-35 gives

If only the first four terms of the power series expansion of $J_0(0.1246)$ and $J_1(0.1246)$ are taken, $J_0(0.1246) = 0.9961$ and $J_1(0.1246) = 0.06216$. Thus, the numerator, NUM, of Equation A.1-19 is

$$NUM = \frac{E_0^2}{4}$$

$$\frac{NUM}{DEN} = -j \frac{E_o^2 V_s (0.9975 \quad - \quad)}{-0.4044 \quad V_c}$$ (A.1-35)

For the cavity and the sample holder used in this work, $V_s/V_c = 0.001432$. Therefore,

$$\frac{\delta\omega}{\omega} = -(\epsilon^* - 1)(0.0008520)$$ (A.1-36)

Equation A.1-36 is the perturbation equation for the idealized version of the TM_{012} cavity used in this work. After the separation of the real and imaginary parts this equation can be expressed as

$$\frac{\delta\omega_1}{\omega_1} = -(\epsilon' - 1)(0.0008520)$$ (A.1-37(a))

and,

$$\frac{1}{2} \delta(1/Q_L) = \epsilon'' (0.0008520)$$ (A.1-37(b))

Equation A.1-37(b) can also be written as

$$\frac{1}{2} (\frac{1}{Q_{LS}} - \frac{1}{Q_{LE}}) = 0.8520 \times 10^{-3}$$ (A.1-38)

where, Q_{LS} is the loaded Q factor of the cavity with the sample in the

sample holder and Q_{LE} is the Q factor of the cavity with an empty sample holder.

Equation A.1-37 was used to compute ϵ' and ϵ'' for four calibrating liquids of Table 3. A comparison between the computed values and the actual values (of Table 3) is shown in Table A.1.

Table A.1

ε^* for Calibration Liquids Computed from the Perturbation Equation

S.No.	Substance	ε'		ε''	
		Actual[a]	Computed[b]	Actual[a]	Computed[b]
1.	Methanol	22.0	39.33	13.0	23.5
2.	Distilled Water	78.0	80.39	11.0	12.73
3.	Methanol(60%) and Distilled Water (40%)	46.0	41.25	17.0	16.48
4.	Ethyl Acetate	6.40	10.48	0.34	0.81

[a] - From Table 3.

[b] - Computed from the perturbation equation (Equation A.1-37).

Appendix II

A.2.1   Reflection from a dielectric slab

According to the model given by van Gemert [129] reflection and transmission coefficients, R_1 and T_1, of a normally incident plane wave on a dielectric layer in free space are

$$R_1 = \rho \frac{[1-\exp(-2\gamma d)]}{[1-\rho^2 \exp(-2\gamma d)]} \qquad (A.2-1)$$

and

$$T_1 = \frac{(1-\rho^2)\exp(-\gamma d)}{[1-\rho^2 \exp(-2\gamma d)]} \qquad (A.2-2)$$

where

$$\rho = (1 - \sqrt{\varepsilon}^*)/(1 + \sqrt{\varepsilon}^*),$$

γ is the propagation constant and d is the layer depth. When a dielectric layer is on a metal reflector, the reflection coefficient, R_1, is given by

$$R_1 = \frac{\rho - \exp(-2\gamma d)}{1 - \rho \exp(-2\gamma d)}$$

where ρ is the reflection coefficient given above.

A.2.2 The Jones/Fuoss model [148,149]

The other model [148,149] is based on a matrix representation for each dielectric layer. In this model the tangential field components on two successive layers (e.g., free space and layer 1 in Figure 29) can be related by a matrix recursion relation:

$$
\begin{bmatrix} E_0 \\ H_0 \end{bmatrix} = M_1 \begin{bmatrix} E_1 \\ H_1 \end{bmatrix}
\tag{A.2-3}
$$

where

$$
M_1 = \begin{bmatrix} \cos\alpha_1 & j\,\eta_1\,\sin\alpha_1 \\ \dfrac{j\,\sin\alpha_1}{\eta_1} & \cos\alpha_1 \end{bmatrix} = \begin{bmatrix} a_{11} & a_{12} \\ a_{21} & a_{22} \end{bmatrix}
$$

M_1 is a (2x2) transformation matrix and characterizes layer 1. For normal incidence, $\alpha_1 = k_1 d_1$, where k_1 and d_1 are the complex wave number and thickness for layer 1, respectively. The reflection coefficient, R_1, when only one layer is present is:

$$
R_1 = \frac{Z - \eta_0}{Z + \eta_0}
\tag{A.2-4}
$$

where

$$
Z = \frac{(a_{11}\eta_2 + a_{12})}{(a_{21}\eta_2 + a_{22})}
$$

The transmission coefficient, T_{12}, from layer 1 to 2 is:

$$T_{12} = \frac{2Z_2}{a_{11}Z_2 + a_{12} + \eta_0(a_{21}Z_2 + a_{22})} \qquad (A.2-5)$$

where η_0 and η_1 are the intrinsic impedances of the free space and layer 1 respectively. Z_2 is the input impedance of the combination of to layers 2 and 3 of Fig. 29.

The computer programs, in Fortran 77, to solve Equations A.2-4 and A.2-5 are given at A.2.3, and that for Equation 4.4 is given at A.2.4. If these programs are executed with the given parameters, absorption vs. depth data at 20°C for Fig. 33 will result.

A.2.3   Computer program for solving Equations A.2-4 and A.2-5

```
C     PROGRAM FOR THE CALCULATION OF REFLECTION AND
C     ABSORPTON COEFFICIENTS OF A LAYERED DIELECTRIC
C     MEDIUM FOR A GIVEN INCIDENCE ANGLE
C     ....../.....................................
C     ..........................................
C     DIELECTRIC CONSTANT(EBS11-JEBS12),ETC , ARE CONSTANT IN
C     EACH LAYER  TOTAL 4 LAYERS
C     OUR OJECTIVE TO FIND THE ABSORPTION IN THE SECOND LAYER

      IMPLICIT COMPLEX*8(Z)
      DIMENSION  ZAK(6),ZMPARL(6),ZPM1(6),ZPM2(6),
     ZMPERP(6),ZALF(6),TL(6),ZEBS(6),ZR(6),ZPM3(6),
     ZAKS(6),ZK(6),ZN(6),ZAS(6),ZAM(6),ZPM4(6),ZT23(2)

C     ARRAY TL STORES LAYERS  THICKNESSES   IN THIS EXAMPLE LAYER 1
C     IS AIR AND ITS THICKNESS DOES NOT AFFECT THE RESULT
C     LAYER 2 IS LOSSY MATERIAL(WATER) WITH VARIABLE THICKNESS
C     THIRD LAYER IS A BOROSILICATE GLASS PLATE  FOURTH LAYER
C     IS A THICK METAL PLATE

C     THE THICKNESS OF THE SECOND LAYER(TL(2)) IS VARIED IN
C     DO LOOP 20  BELOW  TL(3) IS THE THICKNESS OF THE
C     BOROSILICATE GLASS TRAY  0 64 CM  TL(4) INITIALIZED
C     TO AN ARBITRARY VALUE BELOW DOES NOT AFFECT FINAL RESULT
C         TL 1  0
C              0
C            0 64
C              0

C     THE COMPLEX PERMETTIVITY ZEBS(I)  FOR EACH LAYER
C     DEFINE PERTINENT CONSTANTS  EBS14 AND EBS24
C     INITIALIZED TO ARBITRARY VALUES DO NOT AFFECT THE
C     FINAL RESULT AS THE IMPEDANCE OF THE FOURTH LAYER
C     IS SET EQUAL TO ZERO BELOW

      EBS12=77 4
      EBS22=9 7
      EBS13=4 05
      EBS23=0 0043
      EBS14=1 0
      EBS24=0 0

      EBS=8 854E-12

      ZEBS(1)=CMPLX(EBS 0 0)
      ZEBS(2)=EBS*CMPLX(EBS12 -EBS22)
      ZEBS(3)=EBS*CMPLX(EBS13 -EBS23)
      ZEBS(4)=EBS*CMPLX(EBS14 -EBS24)

      ZI=CMPLX(0 0 1 0)

      FREQ=2 45E+09
      PI=3 141593
      CWAVE=3 0E+08
      OMEGA=2 0*PI*FREQ
      ALAMDA=CWAVE/FREQ
      AMEU=PI*4 0E-07
C     ETA1 IS THE INTRINSIC IMPEDANCE OF THE FREE SPACE
      ETA1=120 0*PI
      PI8=PI/180 0

C     FIND COMPLEX PERMEABILITY  ZAMEU

      AMEU1=1 00
      TANMAG=0 0
      AMEU2=AMEU1*TANMAG
      ZAMEU=AMEU*CMPLX(AMEU1 -AMEU2)

C     LOOP FOR CALCULATION OF THE COMPLEX PROPOGATION CONSTANT
C     OF EACH LAYER  K(J)  DEFINED IN THE PROGRAM AS ZAK(J)

      DO 10 J=1 4 1
      ZR(J)=ZAMEU*ZEBS(J)
      ZAK(J)=OMEGA*CSQRT(ZR(J))

 10   CONTINUE

C     LOOP WHICH GOVERNS THE INCREMENTAL THICKNESS OF LAYER 2

      DO 20 P=0 001,0 060,0 001
      TL(2)=P
      J=1

C     LOOP FOR VARYING THE ANGLE OF INCIDENCE  THETA

      DO 19 JJ=1,J 1

C     DEFINE THETA AND CS  THE SINE**2 OF THAT ANGLE  THETAD
C     IS THE INCIDENCE ANGLE ON THE SECOND LAYER  IN DEGREES

      THETAD=0 0
      THETAD=THETAD+JJ*0 0
      THETA=THETAD*PI8
      TM=SIN(THETA)
      CS=TM**2

C     LOOP FOR CALCULATION OF THE PARALLEL AND PERPENDICULAR
C     COMPONENTS OF THE INPUT IMPEDANCES OF LAYERS 2 AND 3
C     ZMPARL(I) AND ZMPERP(I)  RESPECTIVELY
C     THE LOOP ALSO FINDS NECESSARY QUANTITIES FOR THE
C     CALCULATION OF THE TRANSFORMATION MATRIX WHICH IS
C     IMPORTANT IN FINDING T AND Z LATER

      DO 11 I=2,3,1
      ZAKS(I)=(ZAK(1)/ZAK(I))**2
      ZK(I)=CSQRT(1 0-ZAKS(I)*CS)
      ZN(I)=CSQRT(ZAMEU/ZEBS(I))
```

```
      ZMPERP(I)=ZM(I)/ZK(I)
      ZMPARL(I)=ZM(I)*ZK(I)

      ZALP(I)=ZAK(I)*TL(I)*ZK(I)
      ZAS(I)=CSIN(ZALP(I))
      ZAM(I)=CCOS(ZALP(I))
11    CONTINUE

C     PREPARE            FORMATON MATRIX FOR FOLLOWING CALCULATIONS
C     THIS IS          NTITY MATRIX

      ZBM1=CMPLX(1.0,0.0)
      ZBM2=CMPLX(0.0,0.0)
      ZBM3=ZBM2
      ZBM4=ZBM1

C     LOOP FOR DETERMINING THE TRANSFORMATION MATRIX
C     CORRESPONDING TO THE ENTIRE LAYER COMBINATION
C     THIS IS FOUND BY MULTIPLYING THE TRANSFORMATION
C     MATRICES OF LAYERS 2 AND 3 TOGETHER  LAYER 4 IS
C     NOT CONSIDERED BECAUSE ITS INPUT IMPEDANCE IS
C     ASSUMED TO BE  ZERO (PERFECTLY CONDUCTING METAL PLATE)

      DO 13  I=2,3,1

C     DEFINE THE TRANSFORMATION MATRIX FOR LAYER I
      ZAM1=ZAM(I)
      ZAM2=ZI*ZMPARL(I)*ZAS(I)
      ZAM3=ZI*ZAS(I)/ZMPARL(I)
      ZAM4=ZAM1

C     MULTIPLY THE CURRENT MATRIX BY THE PREVIOUS ONE
      ZFM1(I)=(ZBM1*ZAM1+ZBM2*ZAM3)
      ZFM2(I)=(ZBM1*ZAM2+ZBM2*ZAM4)
      ZFM3(I)=(ZBM3*ZAM1+ZBM4*ZAM3)
      ZFM4(I)=(ZBM3*ZAM2+ZBM4*ZAM4)

C     REINITIALIZE THE NEW MATRIX FOR THE NEXT  ITERATION
      ZBM1=ZFM1(I)
      ZBM2=ZFM2(I)
      ZBM3=ZFM3(I)
      ZBM4=ZFM4(I)

13    CONTINUE

C     FIND THE EFFECTIVE INPUT IMPEDANCE OF THE LAYER
C     COMBINATION  ZIMP
C     INPUT IMPEDANCE OF LAYER 4 IS ZERO (PERFECT CONDUCTOR)

      ZMPARL(4)=0.0
      ZMPERP(4)=0.0
      ZIMP1=ZFM1(3)*ZMPARL(4)+ZFM2(3)
      ZIMP2=ZFM4(3)*ZFM3(3)*ZMPARL(4)
      ZIMP=ZIMP1/ZIMP2

C     SET UP ANOTHER IDENTITY MATRIX FOR THE FOLLOWING
C     CALCULATONS

      ZKM1=CMPLX(1,0,0.0)
      ZKM2=CMPLX(0,0,0.0)
      ZKM3=ZKM2
      ZKM4=ZKM1

C     LOOP FOR CALCULATION OF THE INPUT IMPEDANCE LOOKING
C     INTO THE THIRD LAYER

      DO 27  I=3,3,1

C     DEFINE THE TRANSFORMATION MATRIX OF THE ITH LAYER
      ZRM1=ZAM(I)
      ZRM2=ZI*ZMPARL(I)*ZAS(I)
      ZRM3=ZI*ZAS(I)/ZMPARL(I)
      ZRM4=ZRM1

C     MULTIPLY THE CURRENT MATRIX BY THE PREVIOUS ONE
      ZSM1=(ZKM1*ZRM1+ZKM2*ZRM3)
      ZSM2=(ZKM1*ZRM2+ZKM2*ZRM4)
      ZSM3=(ZKM3*ZRM1+ZKM4*ZRM3)
      ZSM4=(ZKM3*ZRM2+ZKM4*ZRM4)

C     REINITIALIZE THE NEW MATRIX FOR THE NEXT ITERATION
      ZKM1=ZSM1
      ZKM2=ZSM2
      ZKM3=ZSM3
      ZKM4=ZSM4

27    CONTINUE

C     FIND Z200  THE EFFECTIVE INPUT IMPEDANCE LOOKING  INTO
C     THE THIRD LAYER

      Z91=ZSM1*0.0+ZSM2
      Z92=ZSM4+ZSM3*0.0
      Z200=Z91/Z92

C     RIN2 IS THE INPUT RESISTANCE LOOKING INTO LAYER 3
      RIN2=CABS(Z200)

C     INPUT IMPEDANCE OF AIR  THE FIRST LAYER  IS THE
C     INTRINSIC VALUE  120.0*PI
      ZMPARL(1)=376.7
      ZMPERP(1)=376.7

C     II GOES THROUGH TWO VALUES  FOR IIX1  RPARL AND ZT23PARL
C     ARE FOUND  FOR IIX2  RPERP AND ZT23PERP ARE FOUND
C     ZT23 IS THE COMPLEX COEFFICIENT REPRESENTING TRANSMISSION
C     FROM LAYER 2 TO LAYER 3

      DO 12 II=1,2,1
      ZR(II)=(ZIMP-ZMPARL(1))/(ZIMP+ZMPARL(1))
      ZT23N=2.0*Z200
      ZT23D=ZFM1(2)*Z200*ZFM2(2)+ETA1*(ZFM3(2)*Z200*ZFM4(2))
      ZT23(II)=ZT23N/ZT23D

C     INTERCHANGE ZMPARL AND ZMPERP FOR EACH LAYER SO THAT
C     ZR(2) WILL REPRESENT RPERP AND ZT23(2) WILL REPRESENT
C     ZT23PERP

      DO  14  MM=1,4,1
```

```
      IMPARL(MM)=IMPERP(MM)
 14   CONTINUE
 12   CONTINUE
C        DETERMINE THE ABSORPTION IN LAYER 2, A2, ON THE ASSUMPTION
C        THAT RAV=(RPAR(+RPERP) 2 AND THAT TAV=(TPERP+TPAR( ) 2

      R1=CABS(ZR(1))
      R2=CABS(ZR(2))
      RPAR(=R1**2
      RPERP=R2**2
      T1=CABS(ZT2)(1))
      T2=CABS(ZT2)(2))
      TPAR(=T1**2
      TPERP=T2**2
      RAV=(RPERP+RPAR()/2 0
      TAV=(TPERP+TPAR()/2 0
      I100=1 0/I700
      A2=1 0-RAV-TAV-(ETA1*REAL)/I100

C        THICK IS THE THICKNESS OF THE SECOND DIELECTRIC
C        LAYER IN MM

      THICK=(L /2)*1000 0

      WRITE(6,60) THETAD
      WRITE(6,70) THICK A2
      WRITE(6,80) RPERP RPAR
      WRITE(6,90) THICK RPAR

 60   FORMAT (1X THETAD= F )
 80   FORMAT (1X RPERP= F8 4 2X RPAR= F8 4
C 40  FORMAT (1X IMP= IF 2 2X THIN  F )
 70   FORMAT (1X F8 2 2X F8 4
 90   FORMAT (1X F8 2 2X F8 4

 18   CONTINUE
 2    CONTINUE

      STOP
      END
```

A.2.4   Computer program for solving Equation ... and for
         computing the absorption of a dielectric layer

```
C
C
C     THIS PROGRAM IS FOR THE CALCULATION OF ABSORPTION
C     IN ONE LAYER OF A 3 LAYERED MEDIUM  FOR EXAMPLE
C     IN A THIN LAYER OF A SUSCEPTOR OR A BROWNING
C     PASTE OVER A GIVEN FOOD PLACED ON A GLASS PLATE
C     HOWEVER  IN THE FOLLOWING EXAMPLE ABSORPTION IN A WATER
C     LAYER ON A BOROSILICATE GLASS TRAY IS COMPUTED
C
C     IEPS1 IS THE COMPLEX DIELECTRIC CONSTANT OF LAYER
C     ONE AND IEPS2 OF LAYER TWO ETC
C     IEPS1  IEPS2 ETC  ARE CONSTANT INSIDE EACH SWEEP
C     THICKNESS OF THE FIRST LAYER X D1 VARIABLE
C     THICKNESS OF BOROSILICATE GLASS TRAY X D2  0.44 M
C     SINCE WE ARE CONSIDERING TWO LAYERS THE
C     THICKNESS OF THE THIRD LAYER D3 X 0
C
      IMPLICIT COMPLEX X Z
      COMPLEX  Y0 ETA1 ETA2
      EPS1 X 77 8
      EPS1 2 X 12 04
      EPS2 X 5 5
      EPS2 2 X 0 085
      EPS3 X 1 0
      EPS3 2 X 0 0
      D2 X 0 44
      D3 X 0 0
      ZEPS1 X CMPLX EPS1   EPS1 2
      Z1 X 2 0 ZEPS1
      Z11 X CSQRT Z1
      ZEPS2 X CMPLX EPS2  EPS2 2
      Z2 X 2 0 ZEPS2
      Z22 X CSQRT Z2
      ZEPS3 X CMPLX EPS3  EPS3 2
      ZEPS1 IS DIELECTRIC CONSTANT OF WATER X 8
      ZEPS2 IS THE DIEL CONST OF GLASS
      Z3 X 2 0 ZEPS3
      Z33 X CSQRT Z3
      DO 100 PRO X 0    D1  0 01
      D1 X P
      FREQ X 2 45E 09
      P X 3 14159
      PI 2 X 2 0 P
      WAVE X 3 0E 08
      OMEGA X PI 2 FREC
      CON X ZO O P
      CON X OMEGA WAVE
      Z11 X CON Z1
      Z22 X CON Z2
      Z33 X CON Z3
      ETAO X CON
C
C     ETA1  ETA2 ETC   ARE THE INTRINSIC  IMPEDANCES
C     OF THE FIRST AND THE SECOND LAYER
C
      ETA1 X Z11
      ETA2 X Z22
      ETA3 X Z33
      Z45 X ZEPS1
      Z46 X ZEPS2
      Z44 X ZEPS3
      ZGAMA1 X CON2 CSQRT Z45
      ZGAMA2 X CON2 CSQRT Z46
      ZGAMA3 X CON2 CSQRT Z44
      Z17 X ZGAMA1 D1
      Z18 X ZGAMA2 D2
      Z19 X CEXP Z17
      Z20 X CEXP Z17
      Z21 X CEXP Z18
      Z22 X CEXP Z18
      ZNUM1 X Z19 Z20
      ZDEN1 X Z19 Z20
      ZTAN1 X ZNUM1 ZDEN1
      ZNUM2 X Z21 Z22
      ZDEN2 X Z21 Z22
      ZTAN2 X ZNUM2 ZDEN2
      Z45 X ZGAMA3 D3
      Z46 X CEXP Z45
      Z47 X CEXP Z45
      ZNUM3 X Z46 Z47
      ZDEN3 X Z46 Z47
      ZTAN3 X ZNUM3 ZDEN3
      Z48 X 0 0
      Z0 X CON
      Z3 X ETA3 Z4 ETA3 ZTAN3  ETA3 Z4 ZTAN3
      Z2 X ETA2 Z3 ETA2 ZTAN2  ETA2 Z3 ZTAN2
      Z1 X ETA1 Z2 ETA1 ZTAN1  ETA1 Z2 ZTAN1
      ZR X Z1 Z0  Z1 Z0
      AIN2 X CABS Z2
C
C     Z22 IS THE INPUT IMPEDANCE OF SECOND AND THIRD LAYER
C     OVER METAL SHEET
C
      RX X CABS ZR
      RX X 1 2
30    FORMAT 1X 5HRINZ X 2 17 4
40    FORMAT 1X F9   2X 3HA1X F9 4 6HT 2X F9 4 F9 4
C50   FORMAT 1X 3HZ1X 2F8   2X 3HZ2X 2F5   3H 33 2F5
C60   FORMAT 1X 3HD2X F7 2 2X 3HZ2X 2F9 2
C     WRITE 6 70  ZGAMA2 ZTAN2 Z11
      Z23 X 2 0 Z17
      Z24 X 2 0 Z18
      Z25 X   Z17 Z18
      Z31 X 2 0 ETA1 ETA1 Z0
      Z32 X 2 0 Z2 Z2 ETA1
      Z33 X Z0 ETA1 Z0 ETA1
      Z34 X Z2 ETA1 Z2 ETA1
      Z35 X ETA1 ETA2 ETA1 ETA2
      Z36 X Z3 ETA2 Z3 ETA2
```

```
ZP(I) = Z33+Z30*CEXP(Z22)
ZP(I) = Z30+Z30*CEXP(Z30)
ZP(I)=Z1*Z0
ZT(I)=Z3*Z30*Z30+Z30//Z0
Z1000 = O/Z3
Y=Y0*CABS(ZT(I))
T(I)=Y*Y1K*2
T(I)=YT(I)*ZETA0=REAL(Z100)
A(I)=0.0.T12
C    A IS POWER ABSORPTION IN FIRST LAYER  T12 IS THE
C    TRANSMISSION OF FIRST LAYER  R IS THE TOTAL REFLECTED
C    POWER FROM THE SYSTEM
Z7(I)=Z3*-Z33/Z0+CEXP(Z2)4
Y=CABS(ZT(I))
Y=Y1*2

C    THICK IS THE THICKNESS OF THE VARIABLE LAYER IN CM

     THICK=1000.0*D
     WRITE(4,40) THICK,A,T12,R
     WRITE(4,30) Z1K2
     WRITE(4,10) R,T,A
     WRITE(4,50) J,I,Z,I,J
99   CONTINUE
100  CONTINUE
1000 STOP
     END
```